CNIC-01844
CNDC-0037
INDC(CPR)-0061

COMMUNICATION OF NUCLEAR DATA PROGRESS

No. 30 (2006. 4)

China Nuclear Data Center
China Nuclear Information Center
Atomic Energy Press

COMMUNICATION OF NUCLEAR DATA PROGRESS

EDITORIAL NOTE

The editors hope that our readers and colleagues will not spare their comments in order to improve this publication. If you have any, please contact us by following address:

Mailing Address:
Prof. GE Zhigang
China Nuclear Data Center
China Institute of Atomic Energy
P.O. Box 275 (41), Beijing 102413
People's Republic of China
Telephone: 86-10-69357275
Facsimile: 86-10-69357008
E-mail: gezg @ iris.ciae.ac.cn

Abstract: This is the 30th issue of *Communication of Nuclear Data Progress* (CNDP), in which the progress and achievements in nuclear data field in China during 2004 are carried. It includes the evaluations and model calculations of neutron data for n + ^{31}P, ^{59}Co, $^{92\sim106}$Mo, $^{Nat\sim116}$Cd, ^{233}U and the covariance data evaluation of experimental data for ^{27}Al, update the decay data for radionuclide ^{7}B. Some results of studies for nuclear evaluation tool and model are also included in this issue, i.e. reaction mechanism studies of ^{5}He, a new method of evaluating the discrepant data, linear fit of correlative data by least squared method et al.

Communication of Nuclear Data Progress

No.30 (2006) Beijing

CONTENTS

1 Neutron Spectrum from ^{5}He Breakup Process in the Continuous Emission Region
ZHANG Jingshang

5 Pre-Formation Probability of ^{5}He Cluster in Pre-Equilibrium Mechanism
DUAN Junfeng et al.

10 Double-Differential Cross Section of ^{5}He Emission
YAN Yuliang et al.

16 A New Method of Processing the Discrepant Data
WANG Baosong et al.

20 Update the Decay Data for Radionuclide ^{7}Be Based on the Double Method
WANG Baosong et al.

23 Linear Fit of Correlative Data by Least Squared Method
LIU Tingjin et al.

29 Model Calculation of Neutron Reaction Data for ^{31}P in the Energy Range from 0.1 to 20 MeV
LI Jiangting et al.

34 n + $^{59}_{27}$Co ($E_n \leqslant 20$ MeV) Nuclear Data Calculation and Analysis
WANG Shunuan

40 Calculation and Recommendation of the Complete Sets of Nuclear Data for n + ^{92,94,96}Mo below 20 MeV
CAI Chonghai et al.

48 The Cross Section Calculation of ^{102,104,106}Mo below 20 MeV
LIANG Chuntai et al.

52 n + $^{106,108,110\sim114,Nat}$Cd ($E_n \leqslant 20$ MeV) Nuclear Data Calculation and Analysis
WANG Shunuan

58 Re-Evaluation of Complete Neutron Data for ^{233}U
YU Baosheng

63 Neutron Cross Section and Covariance Data Evaluation of Experimental Data for ^{27}Al
LI Chunjuan et al.

71 Evaluation of Production Cross Sections of γ-Rays from Thermal-Neutron Captures
ZHOU Chunmei et al.

CINDA INDEX

Neutron Spectrum from ^{5}He Breakup Process in the Continuous Emission Region

ZHANG Jingshang

China Nuclear Data Center, CIAE, P.O.Box 275(41), Beijing 102413, P.R.China

【**abstract**】*An unstable particle emission of ^{5}He has being included in the new version of LUNF code, as the evaluation tool and for interpreting experimental data. In order to describe the ^{5}He emission process, the formula on the double-differential cross sections of the neutron and the alpha-particle from $^5He \rightarrow n+\alpha$ was studied. Because of stronger recoil effect, the energy balance is strictly taken into account to meet the needs in nuclear engineering.*

Introduction

The possibility and the importance of ^{5}He emission in the neutron-induced reactions are elaborated [1,2]. Now ^{5}He emission has being included in the new version of LUNF code[3]. There is some new reaction mechanisms on ^{5}He emission process, one of which is the formulation on the double -differential cross sections of the neutron and the α-particle from the emitted ^{5}He breakup process. The formula of the double-differential cross sections of the neutron and the alpha-particle from the emitted ^{5}He breakup process to the discrete levels was obtained in Ref[1], while the formula of the double-differential cross sections of the neutron and the α-particle from the emitted ^{5}He breakup process to the continuous region is obtained in Section 1.

Meanwhile, it is proved that the energy balance is held exactly and given in Section 2. The conclusion remarks are given in the last section.

1 The Double-differential Cross Sections of the Neutron and α-particle from ^{5}He Separation in Continuous Region

In pre-equilibrium emission process, the emitted ^{5}He has forward angular distribution, so the neutron and the α-particle from ^{5}He two-body breakup process also has the same situation.

In this section the representation of the double-differential cross sections of the neutron and α-particle from ^{5}He breakup process in continuous region is given. The emitted ^{5}He in its ground state is assumed in the study, although ^{5}He has excited states.

Two motion systems are employed to set up the formulation, the physical quantities indicated by the superscript c and p are for center of mass system (CMS) and for emitted particle system (EPS), which is moving along with the emitted particle ^{5}He, respectively. Meanwhile, the physical quantities indicated by subscript 5 are for the emitted ^{5}He. The physical quantities indicated by subscripts n or α are for the neutron or the α-particle, respectively, from ^{5}He separation.

The double-differential cross section of emitted ^{5}He with the mass m_5 in CMS is represented in the standard form as

$$\frac{\mathrm{d}^2\sigma}{\mathrm{d}E_5^c \mathrm{d}\Omega_5^c} = \sum_l \frac{2l+1}{4\pi} f_l^c(E_5^c) P_l(\cos\theta_5^c) \qquad (1)$$

with normalization condition $\int_{E_{5,\min}^c}^{E_{5,\max}^c} f_0^c(E_5^c) dE_5^c = 1$ within energy region $E_{5,\min}^c \le E_5^c \le E_{5,\max}^c$. Then the emitted ^{5}He is separated into one neutron and one α-particle, spontaneously, with the Q-value of 0.894 MeV. The energy ε_n^p and ε_α^p carried by the outgoing neutron and the α-particle in EPS are given, respectively, by

$$\varepsilon_n^p = \frac{m_\alpha}{m_5} Q, \qquad \varepsilon_\alpha^p = \frac{m_n}{m_5} Q \qquad (2)$$

Based on the velocity composition relation, the velocities of the neutron and the α-particle in CMS can be obtained by $\vec{v}_n^c = \vec{V}_5 + \vec{v}_n^p$ and $\vec{v}_\alpha^c = \vec{V}_5 + \vec{v}_\alpha^p$, respectively. Therefore, the outgoing neutron energy region $\varepsilon_{n,\min}^c \le \varepsilon_n^c \le \varepsilon_{n,\max}^c$ is obtained by

$$\varepsilon^c_{n,\min}_{\max} = \frac{1}{2} m_n (v_n^p \mp V_{5,\min}_{\max})^2 = \varepsilon_n^p [1 \mp \gamma_n (E^c_{n,\min}_{\max})]^2 \quad (3)$$

With the same procedure, the energy region $\varepsilon^c_{\alpha,\min} \le \varepsilon^c_\alpha \le \varepsilon^c_{\alpha,\max}$ of the α-particle is obtained by

$$\varepsilon^c_{\alpha,\min}_{\max} = \frac{1}{2} m_\alpha (v_\alpha^p \mp V_{5,\min}_{\max})^2 = \varepsilon_\alpha^p [1 \mp \gamma_\alpha (E^c_{5,\min}_{\max})]^2 \quad (4)$$

The functions used in eqs.(3) and (4) are defined by

$$\gamma_n(E_5) = \sqrt{\frac{m_n E_5}{m_5 \varepsilon_n^p}}, \quad \gamma_\alpha(E_5) = \sqrt{\frac{m_\alpha E_5}{m_5 \varepsilon_\alpha^p}} \quad (5)$$

Based on the Jacobian relation, the solid angle in different motion system has the equation

$$\mathrm{d}\varepsilon_n^p \mathrm{d}\Omega_n^p = \sqrt{\frac{\varepsilon_n^c}{\varepsilon_n^p}} \mathrm{d}\varepsilon_n^c \mathrm{d}\Omega_n^c \quad (6)$$

and the double-differential cross section of the neutron is isotropic in EPS with definite value of energy

$$\frac{\mathrm{d}^2\sigma}{\mathrm{d}\varepsilon_n^p \mathrm{d}\Omega_n^p} = \frac{1}{4\pi} \frac{\mathrm{d}\sigma}{\mathrm{d}\varepsilon_n^p} = \frac{1}{4\pi} \delta\left(\varepsilon_n^p - \frac{m_\alpha}{m_5} Q \right) \quad (7)$$

The double-differential cross section of the emitted neutron can be obtained by averaging the double-differential cross section of emitted neutron over that of emitted ^{5}He.

$$\frac{\mathrm{d}^2\sigma}{\mathrm{d}\varepsilon_n^c \mathrm{d}\Omega_n^c} = \int \frac{\mathrm{d}^2\sigma}{\mathrm{d}E_5^c \mathrm{d}\Omega_5^c} \frac{\mathrm{d}^2\sigma}{\mathrm{d}\varepsilon_n^p \mathrm{d}\Omega_n^p} \sqrt{\frac{\varepsilon_n^c}{\varepsilon_n^p}} \mathrm{d}E_5^c \mathrm{d}\Omega_5^c \quad (8)$$

The normalized double-differential cross section of the neutron with the mass m_n in CMS is represented in the standard form as

$$\frac{\mathrm{d}^2\sigma}{\mathrm{d}\varepsilon_n^c \mathrm{d}\Omega_n^c} = \sum_l \frac{2l+1}{4\pi} f_l^c(\varepsilon_n^c) P_l(\cos\theta_n^c) \quad (9)$$

Substituting the representation of eq.(6) and eq.(7) into eq.(8), and using the orthogonal relation of Legendre polynomial, the Legendre coefficient of the outgoing neutron in eq.(9) can be obtained by

$$f_l^c(\varepsilon_n^c) = \int \frac{\mathrm{d}^2\sigma}{\mathrm{d}E_5^c d\Omega_5^c} \frac{\mathrm{d}^2\sigma}{\mathrm{d}\varepsilon_n^p \mathrm{d}\Omega_n^p} \sqrt{\frac{\varepsilon_n^c}{\varepsilon_n^p}} \mathrm{d}E_5^c \mathrm{d}\Omega_5^c P_l(\cos\theta_n^c) \mathrm{d}\Omega_n^c \quad (10)$$

Denoting Θ as the angle between $\vec{V}_5$ and $\vec{v}_n^{\,c}$, and using the useful expansion equation

$$P_L(\cos\theta_5^c) = \frac{4\pi}{2L+1} \sum_m Y^*_{Lm}(\Theta, \Phi) Y_{Lm}(\Omega_n^c) \quad (11)$$

In eq.(10) the solid angles have the explicit expression $\mathrm{d}\Omega_5^c \mathrm{d}\Omega_n^c = \mathrm{d}\cos\Theta \mathrm{d}\Phi \mathrm{d}\cos\theta_n^c \mathrm{d}\phi_n^c$, and carrying out the integration over $\mathrm{d}\cos\theta_n^c \mathrm{d}\Phi \mathrm{d}\phi_n^c$, the Legendre coefficient of the outgoing neutron is obtained by

$$f_l^c(\varepsilon_n^c) = \frac{1}{2} \int f_l^c(E_5^c) \frac{\mathrm{d}\sigma}{\mathrm{d}\varepsilon_n^p} \sqrt{\frac{\varepsilon_n^c}{\varepsilon_n^p}} P_l(\cos\Theta) \mathrm{d}E_5^c \mathrm{d}\cos\Theta \quad (12)$$

From the velocity relation $\vec{v}_n^{\,p} = \vec{v}_n^{\,c} - \vec{V}_5^{\,c}$, in energy scale, the energy relation reads

$$\varepsilon_n^p = \varepsilon_n^c + \frac{m_n}{m_5} E_5^c - 2\sqrt{\frac{m_n}{m_5} \varepsilon_n^c E_5^c} \cos\Theta \quad (13)$$

For a given ε_n^c we have

$$\mathrm{d}\cos\Theta = \frac{1}{2} \sqrt{\frac{m_5}{m_n \varepsilon_n^c E_5^c}} \mathrm{d}\varepsilon_n^p \quad (14)$$

Substituting eq.(7) and eq.(14) into eq.(12), and carrying out the integration over ε_n^p, the eq.(12) is reduced into the form as the following

$$f_l^c(\varepsilon_n^c) = \int \frac{m_5}{4\sqrt{m_n m_\alpha Q E_5^c}} f_l^c(E_5^c) f_l^c(E_5^c) P_l\left(\frac{\varepsilon_n^c + \frac{m_n}{m_5} E_5^c - \frac{m_\alpha}{m_5} Q}{2\sqrt{\frac{m_n}{m_5} \varepsilon_n^c E_5^c}} \right) \mathrm{d}E_5^c \quad (15)$$

Using $\gamma_n(E_5^c) = \sqrt{\frac{m_n E_5^c}{m_\alpha Q}} = \sqrt{\frac{m_n E_5^c}{m_5 \varepsilon_n^p}}$, the variable in Legendre polynomial of eq.(15) can be denoted by

$$\eta_n = \sqrt{\frac{\varepsilon_n^p}{\varepsilon_n^c}} \frac{\frac{\varepsilon_n^c}{\varepsilon_n^p} - 1 + \gamma_n^2(E_5^c)}{2\gamma_n(E_5^c)} \quad (16)$$

Hence eq.(15) becomes into the form as

$$f_l^c(\varepsilon_n^c) = \int_a^b \frac{f_l^c(E_5^c)}{4\varepsilon_n^p \gamma_n(E_5^c)} P_l(\eta_n) \mathrm{d}E_5^c \quad (17)$$

For a given value of the outgoing neutron ε_n^c, the integration limits of E_5^c can be given by

$$a = \max\left\{ E_{5,\min}, \frac{m_5}{m_n} \left(\sqrt{\varepsilon_n^c} - \sqrt{\varepsilon_n^p} \right)^2 \right\} \quad (18)$$

$$b = \min\left\{ E_{5,\max}, \frac{m_5}{m_n} \left(\sqrt{\varepsilon_n^c} + \sqrt{\varepsilon_n^p} \right)^2 \right\} \quad (19)$$

Obviously, from eq.(17) it can be seen that the forward tendency of the outgoing neutron is entirely determined by the forward tendency of ^{5}He emission.

With the same procedure, the Legendre coefficient of the outgoing α-particle can be obtained by ex-

changing m_n and m_α in the above formula.

2 Energy Balance

To meet the needs in engineering, the energy balance should be satisfied properly. In this section the energies carried by all kinds of particles, including the energies carried by the neutron and the α-particle from the ^{5}He breakup process, the energy carried by the residual nucleus as well as the gamma decay energy, are given analytically.

The energy carried by the neutron in CMS reads

$$E_n^c = \int \varepsilon_n^c f_0^c(\varepsilon_n^c)\mathrm{d}\varepsilon_n^c \tag{20}$$

Substituting the representation of eq.(16), and exchanging the integration order, then the integration region of ε_n^c for a given E_5^c is $\left(\sqrt{\varepsilon_n^p}-\sqrt{\frac{m_n}{m_5}E_5^c}\right)^2 \le \varepsilon_n^c \le \left(\sqrt{\varepsilon_n^p}+\sqrt{\frac{m_n}{m_5}E_5^c}\right)^2$. Therefore,

$$\begin{aligned} E_n^c &= \int_{E_{5,\min}^c}^{E_{5,\max}^c} \mathrm{d}E_5^c f_0^c(E_5^c)\left(\varepsilon_n^p + \frac{m_n}{m_5}E_5^c\right) \\ &= \varepsilon_n^p + \frac{m_n}{m_5}\int_{E_{5,\min}^c}^{E_{5,\max}^c} E_5^c f_0^c(E_5^c)\mathrm{d}E_5^c \end{aligned} \tag{21}$$

Analogously, The energy carried by the α-particle in CMS reads

$$E_\alpha^c = \varepsilon_\alpha^p + \frac{m_\alpha}{m_5}\int_{E_{5,\min}^c}^{E_{5,\max}^c} E_5^c f_0^c(E_5^c)\mathrm{d}E_5^c \tag{22}$$

The energy carried by residual nucleus after ^{5}He emission in CMS is given by

$$E_R^c = \frac{m_5}{M}\int_{E_{5,\min}^c}^{E_{5,\max}^c} E_5^c f_0^c(E_5^c)\mathrm{d}E_5^c \tag{23}$$

The residual excitation energy after ^{5}He emission is given by

$$E_R^* = E^* - B_5 - \left(1+\frac{m_5}{M}\right)E_5^c \tag{24}$$

Averaged by the double-differential cross section of ^{5}He emission, if the reaction channel is ended by gamma decay, the gamma decay energy can be obtained by.

$$E_\gamma = E^* - B_5 - \left(1+\frac{m_5}{M}\right)\int_{E_{5,\min}^c}^{E_{5,\max}^c} E_5^c f_0^c(E_5^c)\mathrm{d}E_5^c \tag{25}$$

where $E^* = \frac{M}{M_C}E_n + B_n$ is the excitation energy, E_n is the incident neutron energy, B_n , B_5 are the binding energy of neutron and emitted ^{5}He in the compound nucleus, respectively, M_C , M are the masses of compound nucleus and the residual nucleus, respectively,

Thus, the total released energy in CMS is given by

$$E_{total}^c = E_n^c + E_\alpha^c + E_R^c + E_\gamma = E^* - B_5 + Q \tag{26}$$

By means of the composition of velocities $\vec{v}^{\,l} = \vec{v}^{\,c} + \vec{V}_C$, where $\vec{V}_C$ is the velocity of the center of mass, and $V_C = \frac{\sqrt{2m_nE_n}}{M_C}$. So the energy of a particle with mass *m* in LS can be obtained by

$$E_m^l = \frac{m}{2}\int (v_m^l)^2 \frac{\mathrm{d}^2\sigma}{\mathrm{d}\varepsilon_m^c \mathrm{d}\Omega_m^c}\mathrm{d}\varepsilon_m^c \mathrm{d}\Omega_m^c \tag{27}$$

In laboratory system, the energy carried by the neutron can be obtained by

$$\begin{aligned} E_n^l &= \frac{m_n^2}{M_C^2}E_n + \int \varepsilon_n^c f_0^c(\varepsilon_n^c)\mathrm{d}\varepsilon_n^c + \\ &\frac{2m_n}{M_C}\int \sqrt{E_n\varepsilon_n^c}\, f_1^c(\varepsilon_n^c)\mathrm{d}\varepsilon_n^c \end{aligned} \tag{28}$$

Substituting the representation of the Legendre coefficients of eq.(17) in eq.(28), and carrying the integration over ε_n^c by exchanging the integration order, the eq.(28) is reduced into the form as follows

$$\begin{aligned} E_n^l &= \frac{m_n^2}{M_C^2}E_n + E_n^c + \\ &\frac{2m_n}{M_C}\sqrt{\frac{m_n}{m_5}E_n}\int_{E_{5,\min}^c}^{E_{5,\max}^c} \sqrt{E_5^c}\, f_1^c(E_5^c)\mathrm{d}E_5^c \end{aligned} \tag{29}$$

and for α-particle we have

$$\begin{aligned} E_\alpha^l &= \frac{m_n m_\alpha}{M_C^2}E_n + E_\alpha^c + \\ &\frac{2m_\alpha}{M_C}\sqrt{\frac{m_n}{m_5}E_n}\int_{E_{5,\min}^c}^{E_{5,\max}^c} \sqrt{E_5^c}\, f_1^c(E_5^c)\mathrm{d}E_5^c \end{aligned} \tag{30}$$

The derivation procedure of eqs.(29) and (30) is straightforward but tedious. Similarly, the energy carried by the recoil residual nucleus is obtained by

$$E_R^l = \frac{m_n M}{M_C^2}E_n + E_R^c -$$

$$\frac{2m_5}{M_C}\sqrt{\frac{m_n}{m_5}E_n}\int_{E^c_{5,\min}}^{E^c_{5,\max}}\sqrt{E^c_5}\,f^c_1(E^c_5)\mathrm{d}E^c_5 \qquad (31)$$

Thus, the total released energy in laboratory system is obtained by

$$\begin{aligned} E^l_{total} &= E^l_n + E^l_\alpha + E^l_R + E_\gamma \\ &= \frac{m_n}{M_C}E_n + E^c_{total} = E_n + B_n - B_5 + Q \end{aligned} \qquad (32)$$

It is proved that the energy balance is held exactly in the analytical form. From the eqs.(29~31) it can be found that the energies carried by the neutron and the α-particle increase with the increasing of the forward tendency of emitted ^{5}He. The partial wave $l=1$ plays an important role in the energies carried by different kinds of emitted particles. The larger of $f^c_1(E^c_5)$, the more energies carried by the neutron and the α-particle. Meanwhile, the spectrum shape of $f^c_0(E^c_5)$ can also influence the energy distributions between the emitted particles, the residual nucleus and de-excitation γ energy. The harder of the spectrum, the more energies carried by the emitted particles, while the energies carried by the residual nucleus and de-excitation γ particle are reduced.

3 Conclusion Remarks

The formulation of the neutron and α-particle from ^{5}He separation in the continuous emission region has been obtained. Together with that in discrete level emissions [2], the ^{5}He emission process can be described with full energy balance. The energy balance is not only to meet the needs in nuclear engineering, but also could give the reasonable shape of the outgoing particles spectra. So far only the stable clusters, like d, t, ^{3}He, and α, have been included in the present widely used statistical model codes, now the ^{5}He emission, as an unstable cluster emission is added in the new code. It will be able to make the improvement to reproduce the experimental data.

^{5}He emission is a new reaction mechanism in both equilibrium and pre-equilibrium emission processes. The formula aforementioned will be employed in the new version of LUNF code.

References

[1] ZHANG Jingshang, CNDP No: 28 (2002) 3.

[2] ZHANG Jingshang, Science in China G 47 (2004) 137-145.

[3] ZHANG Jingshang, UNF code for Fast Neutron Reaction Data Calculations, Nucl. Sci.Eng., 133 (1999) 218.

Pre-Formation Probability of ^{5}He Cluster in Pre-Equilibrium Mechanism

DUAN Junfeng YAN Yuliang ZHANG Jingshang

China Nuclear Data Center, CIAE, P.O.Box 275(41), Beijing 102413, P.R.China

【**abstract**】 *The ^{5}He cluster is apt to be emitted than ^{3}He from point of view on the threshold energy. In terms of Iwamoto-Harada model, the theoretical formula of pre-formation probability of ^{5}He cluster including 1p shell nucleon in pre-equilibrium mechanism has been established and calculated. In the case of low incident energies, the configuration of [1,m] for ^{5}He cluster is the dominant part in the nuclear reaction. The calculated results indicate that pre-formation probability of configuration [1,m] for the unstable ^{5}He cluster is much smaller than that of d,t,^{3}He, and ^{4}He light stable composite particles, which is consisted of only 1s shell nucleons. However, it is propitious to the emission of ^{5}He from the point of view on threshold energies, since the binding energies of ^{5}He are generally lower than that of ^{3}He in compound system. The corresponding model formula has been given in this paper for describing pre-formation probability of ^{5}He cluster in pre-equilibrium mechanism.*

Introduction

In recent years, the total outgoing neutron double -differential cross sections for neutron induced light nuclear reaction have been calculated by using the unitive Haser-feshbach theory and exciton model, which can reproduce the experimental measured data nicely[1~4]. The total outgoing neutron double -differential cross sections consist of the neutrons emitted from various reaction channels to discrete level of residual nucleus, which strongly differ from each other. It is shown that ^{5}He emission should be taken into account for fitting the experimental data. Otherwise, it will appear obvious deficiency at low energy part of neutron emission angle-energy spectra, which can be reparative when ^{5}He emission channel has been considered[5].

In addition, it is shown that the composite particle emissions mainly come from the pre-equilibrium reaction processes in light nuclear reaction. The angular momentum dependent exciton model is able to describe the pre-equilibrium reaction successfully[6]. In the exciton model the pre -formation probabilities of all kinds of composite particles in compound system are the important factors to describe composite particle emissions, which should be given by theory. The Iwamoto -Harada model has been proposed to give the pre-formation probabilities of d, t, ^{3}He, and ^{4}He reasonably, which only include 1s shell nucleons for pre-equilibrium emission mechanism[7,8]. The basic physical idea of this model is that the pick-up mechanism in pre-equilibrium processes of composite particles emission is employed, namely, the emitted single nucleon picks up other nucleons to form composite particle before emitting. The nucleon inside nucleus can be described by wave function of shell model, and the associate condition of momentum and position of every degree of freedom can be given by the shell model. Then the pre -formation probability of each kind of configuration for a composite particle could be obtained by means of the volume of the phase space occupied by the composite particles.

Based on the idea of Iwamoto-Harada model, and extending to the composite particle of ^{5}He cluster including 1p shell nucleon, the formulation of the pre-formation probability in compound nucleus for ^{5}He has been established and calculated. Compared with the results of pre-formation probabilities for other composite particles, the calculated results for ^{5}He cluster is reasonable. The theoretical formula of pre-formation probability for ^{5}He cluster are given in section II. The calculated results and discussion are given in the last section.

1 The Formula of Pre-formation Probability for ^{5}He Cluster

The model has been used to calculate pre-formation probability of light composite particles, which only consist of 1s state nucleons described by using the harmonic oscillator model[9,10]. The coordinate $\vec{R}$ of the center of mass for a cluster including N nucleons is given by

$$\vec{R}=\frac{1}{N}\sum_{i=1}^{N}\vec{r}_i \tag{1}$$

where $\vec{r}_i$ stands for the coordinate of the i_{th} nucleon. The total wave function of composite particle is constructed by

$$\psi=\prod_{i=1}^{N}\phi(r_i)=\Phi(R)\varphi_{\text{int}} \tag{2}$$

It can be divided into two parts, $\Phi(R)$ is movement wave function of the motion of the center of mass, and φ_{int} is intrinsic wave function. The normalized $\Phi(R)$ and the single particle wave function for 1s shell nucleons are given by the harmonic oscillator model as follows

$$\Phi(R)=\left(\frac{N\beta}{\pi}\right)^{3/4}e^{-\frac{\beta}{2}NR^2} \tag{3}$$

$$\varphi(\vec{r}_i)=\left(\frac{\beta}{\pi}\right)^{3/4}e^{-\frac{\beta}{2}r_i^2} \tag{4}$$

The configuration of composite particle with N nucleons is denoted by [λ,m], namely, λ and m are the particle numbers above and below the Fermi surface respectively, and $\lambda+m=N$. The parameter β in the wave functions can be determined by harmonic oscillator parameter $\hbar\omega$.

Thus the conditions of the momentum for each nucleon is given by

$$\left.\begin{aligned}|\vec{p}_i|>p_f \qquad i=1,2,\cdots,\lambda\\ |\vec{p}_j|<p_f \qquad j=1,2,\cdots,m\end{aligned}\right\} \tag{5}$$

The intrinsic relative coordinates of ^{5}He cluster can be defined as follows

$$\left.\begin{aligned}&\vec{r}=\vec{r}_1-\vec{r}_2\\ &\vec{r}'=\vec{r}_3-\vec{r}_4\\ &\vec{r}''=\frac{1}{2}(\vec{r}_1+\vec{r}_2)-\frac{1}{2}(\vec{r}_3+\vec{r}_4)\\ &\vec{r}'''=\frac{1}{4}(\vec{r}_1+\vec{r}_2+\vec{r}_3+\vec{r}_4)-\vec{r}_5\\ &\mathrm{d}\vec{r}_1\mathrm{d}\vec{r}_2\mathrm{d}\vec{r}_3\mathrm{d}\vec{r}_4\mathrm{d}\vec{r}_5=\mathrm{d}\vec{R}\mathrm{d}\vec{r}\mathrm{d}\vec{r}'\mathrm{d}\vec{r}''\mathrm{d}\vec{r}'''\end{aligned}\right\} \tag{6}$$

where the $\vec{r},\vec{r}',\vec{r}''$ are the intrinsic relative coordinates of an α cluster, while the fourth relative coordinates $\vec{r}'''$ stand for the intrinsic coordinate between the fifth nucleon and the α cluster in ^{5}He nucleus. Hence the corresponding intrinsic momentum coordinates can be obtained as the following

$$\left.\begin{aligned}&\vec{p}_r=\frac{1}{2}(\vec{p}_1-\vec{p}_2)\\ &\vec{p}_{r'}=\frac{1}{2}(\vec{p}_3-\vec{p}_4)\\ &\vec{p}_{r''}=\frac{1}{2}(\vec{p}_1+\vec{p}_2)-\frac{1}{2}(\vec{p}_3+\vec{p}_4)\\ &\vec{p}_{r'''}=\frac{1}{5}(\vec{p}_1+\vec{p}_2+\vec{p}_3+\vec{p}_4)-\frac{4}{5}\vec{p}_5\\ &\mathrm{d}\vec{p}_1\mathrm{d}\vec{p}_2\mathrm{d}\vec{p}_3\mathrm{d}\vec{p}_4\mathrm{d}\vec{p}_5=\mathrm{d}\vec{p}\mathrm{d}\vec{p}_r\mathrm{d}\vec{p}_{r'}\mathrm{d}\vec{p}_{r''}\mathrm{d}\vec{p}_{r'''}\end{aligned}\right\} \tag{7}$$

The momentum of ^{5}He cluster is given by

$$\vec{p}=\sum_{i=1}^{5}\vec{p}_i \tag{8}$$

The construction of ^{5}He cluster is different from d,t,^{3}He and α. The latter only include 1s shell nucleons. While for ^{5}He, besides the 1s shell nucleons the 1p shell nucleon is involved, in which the former forth nucleons are described by 1s shell wave function and the fifth nucleon is described by 1p shell wave function as

$$\varphi_{\text{int}}=R_{01}(r)Y_{1m}(\Omega) \tag{9}$$

where $R_{01}(r)$ stands for normalized radial wave function of 1p shell nucleon.

$$R_{01}=\beta\left(\frac{64\beta}{9\pi}\right)^{\frac{1}{4}}e^{-\frac{1}{2}\beta r^2} \tag{10}$$

here $Y_{1m}(\Omega)$ is spherical harmonic function.

According to the knowledge of the shell model, for each intrinsic degree of freedom the occupied energy is $\frac{3}{2}\hbar\omega$ for 1s shell nucleons, but it is $\frac{5}{2}\hbar\omega$ for 1p shell nucleons inside ^{5}He cluster. The kinetic

energy and potential energy for each degree of freedom satisfy the equation obtained by the shell model as

$$\begin{aligned}
&\frac{p_r^2}{m}+\frac{1}{4}m\omega_5^2 r^2=\frac{3}{2}\hbar\omega_5\\
&\frac{p_{r'}^2}{m}+\frac{1}{4}m\omega_5^2 r'^2=\frac{3}{2}\hbar\omega_5\\
&\frac{p_{r''}^2}{2m}+\frac{1}{2}m\omega_5^2 r''^2=\frac{3}{2}\hbar\omega_5\\
&\frac{5p_{r'''}^2}{8m}+\frac{2}{5}m\omega_5^2 r'''^2=\frac{5}{2}\hbar\omega_5
\end{aligned} \tag{11}$$

Based on the physical idea of Iwamoto-Harada model, the volume in phase space occupied by the ^{5}He cluster with the configuration $[\lambda,m]$ constrained by conditions of eq.(11) is given in the following form

$$\begin{aligned}
&F_{[\lambda,m]}(\varepsilon_5)\\
&=\frac{C}{(2\pi\hbar)^{12}}\int_{P-fixed[\lambda,m]}\mathrm{d}\vec{r}\mathrm{d}\vec{r}'\mathrm{d}\vec{r}''\mathrm{d}\vec{r}'''\mathrm{d}\vec{p}_r\mathrm{d}\vec{p}_{r'}\mathrm{d}\vec{p}_{r''}\mathrm{d}\vec{p}_{r'''}
\end{aligned} \tag{12}$$

The normalized coefficient C in eq.(12) is determined with the normalized condition

$$\sum_{lm}F_{lm}(\varepsilon_5)=1 \tag{13}$$

Since the former three intrinsic relative coordinates and relative momentum are designed as the coordinates of the α cluster. The integrated analytical results were obtained in reference [8], which can be employed in eq.(12). By using the last condition in eq.(11), and carrying out the integration over the relative coordinate $\vec{r}'''$ and the relative coordinate $\vec{p}_{r'''}$ with the constrain condition of the configuration $[\lambda,m]$, the integrated analytical expression of configuration [5,0], [4,1], [3,2], [2,3], [1,4], [0,5] can be obtained.

Denoting

$$B=\left[\frac{1}{25}p^2+p_{r'''}^2-p_f^2\right]\Big/\frac{2}{5}pp_{r'''} \tag{14}$$

here p_f is the Fermi momentum.

The expression of relative momentum coordinates between the fifth nucleon and the α cluster by using eq.(11) for a given total momentum $\vec{p}$ of ^{5}He is obtained by

$$\vec{p}_5=\frac{1}{5}\vec{p}+\vec{p}_{r'''} \tag{15}$$

Based on the conditions mentioned above, the representation of the pre-formation probability of ^{5}He cluster can be obtained with two mathematical cases.

---

(1) If $p<5p_f$ we have

$$\begin{aligned}
F_{50}(p)&=\int_{p_f-\frac{1}{5}p}^{\sqrt{5\mu\hbar\omega_5}}\mathrm{d}p'T(p')\int_{-1}^{B}\mathrm{d}\cos\beta F_{40}(\vec{p})\\
F_{41}(p)&=\int_{0}^{p_f-\frac{1}{5}p}\mathrm{d}p'T(p')\int_{-1}^{1}\mathrm{d}\cos\beta F_{40}(\vec{p})+\int_{p_f-\frac{1}{5}p}^{\sqrt{5\mu\hbar\omega_5}}\mathrm{d}p'T(p')\left[\int_{-1}^{B}\mathrm{d}\cos\beta F_{31}(\vec{p})+\int_{B}^{1}\mathrm{d}\cos\beta F_{40}(\vec{p})\right]\\
F_{32}(p)&=\int_{0}^{p_f-\frac{1}{5}p}\mathrm{d}p'T(p')\int_{-1}^{1}\mathrm{d}\cos\beta F_{31}(\vec{p})+\int_{p_f-\frac{1}{5}p}^{\sqrt{5\mu\hbar\omega_5}}\mathrm{d}p'T(p')\left[\int_{-1}^{B}\mathrm{d}\cos\beta F_{22}(\vec{p})+\int_{B}^{1}\mathrm{d}\cos\beta F_{31}(\vec{p})\right]\\
F_{23}(p)&=\int_{0}^{p_f-\frac{1}{5}p}\mathrm{d}p'T(p')\int_{-1}^{1}\mathrm{d}\cos\beta F_{22}(\vec{p})+\int_{p_f-\frac{1}{5}p}^{\sqrt{5\mu\hbar\omega_5}}\mathrm{d}p'T(p')\left[\int_{-1}^{B}\mathrm{d}\cos\beta F_{13}(\vec{p})+\int_{B}^{1}\mathrm{d}\cos\beta F_{22}(\vec{p})\right]\\
F_{14}(p)&=\int_{0}^{p_f-\frac{1}{5}p}\mathrm{d}p'T(p')\int_{-1}^{1}\mathrm{d}\cos\beta F_{13}(\vec{p})+\int_{p_f-\frac{1}{5}p}^{\sqrt{5\mu\hbar\omega_5}}\mathrm{d}p'T(p')\left[\int_{-1}^{B}\mathrm{d}\cos\beta F_{04}(\vec{p})+\int_{B}^{1}\mathrm{d}\cos\beta F_{13}(\vec{p})\right]\\
F_{05}(p)&=\int_{0}^{p_f-\frac{1}{5}p}\mathrm{d}p'T(p')\int_{-1}^{1}\mathrm{d}\cos\beta F_{04}(\vec{p})+\int_{p_f-\frac{1}{5}p}^{\sqrt{5\mu\hbar\omega_5}}\mathrm{d}p'T(p')\left[\int_{B}^{1}\mathrm{d}\cos\beta F_{04}(\vec{p})\right]
\end{aligned} \tag{16}$$

(2) If $p > 5p_f$ we have

$$
\begin{aligned}
F_{50}(p) &= \int_0^{\frac{1}{5}p-p_f} \mathrm{d}p'T(p')\int_{-1}^{1}\mathrm{d}\cos\beta F_{40}(\vec{p}) + \int_{\frac{1}{5}p-p_f}^{\sqrt{5\mu\hbar\omega_5}} \mathrm{d}p'T(p')\int_{-1}^{B}\mathrm{d}\cos\beta F_{40}(\vec{p}) \\
F_{41}(p) &= \int_0^{\frac{1}{5}p-p_f} \mathrm{d}p'T(p')\int_{-1}^{1}\mathrm{d}\cos\beta F_{31}(\vec{p}) + \int_{\frac{1}{5}p-p_f}^{\sqrt{5\mu\hbar\omega_5}} \mathrm{d}p'T(p')\left[\int_{-1}^{B}\mathrm{d}\cos\beta F_{31}(\vec{p}) + \int_{B}^{1}\mathrm{d}\cos\beta F_{40}(\vec{p})\right] \\
F_{23}(p) &= \int_0^{\frac{1}{5}p-p_f} \mathrm{d}p'T(p')\int_{-1}^{1}\mathrm{d}\cos\beta F_{13}(\vec{p}) + \int_{\frac{1}{5}p-p_f}^{\sqrt{5\mu\hbar\omega_5}} \mathrm{d}p'T(p')\left[\int_{-1}^{B}\mathrm{d}\cos\beta F_{13}(\vec{p}) + \int_{B}^{1}\mathrm{d}\cos\beta F_{22}(\vec{p})\right] \\
F_{14}(p) &= \int_0^{\frac{1}{5}p-p_f} \mathrm{d}p'T(p')\int_{-1}^{1}\mathrm{d}\cos\beta F_{04}(\vec{p}) + \int_{\frac{1}{5}p-p_f}^{\sqrt{5\mu\hbar\omega_5}} \mathrm{d}p'T(p')\left[\int_{-1}^{B}\mathrm{d}\cos\beta F_{04}(\vec{p}) + \int_{B}^{1}\mathrm{d}\cos\beta F_{13}(\vec{p})\right] \\
F_{05}(p) &= \int_{\frac{1}{5}p-p_f}^{\sqrt{5\mu\hbar\omega_5}} \mathrm{d}p'T(p')\int_{B}^{1}\mathrm{d}\cos\beta F_{04}(\vec{p})
\end{aligned}
\qquad (17)
$$

where $\mu = \frac{4}{5}m$ is the reduced mass between the fifth nucleon and the α cluster, and

$$T(p) = \frac{16}{27\pi(\mu\hbar\omega_5)^3}(3\mu\hbar\omega_5 - p^2)^{\frac{3}{2}}p^2 \qquad (18)$$

Summing over all of the configurations, one can prove that the normalization condition of ^{5}He cluster is held analytically.

2 The Calculated Results and Discussion

Based on the idea of Iwamoto-Harada model, the formulation of the pre-formation probabilities of ^{5}He cluster with various configurations are established and calculated. The results are shown in Fig.1.

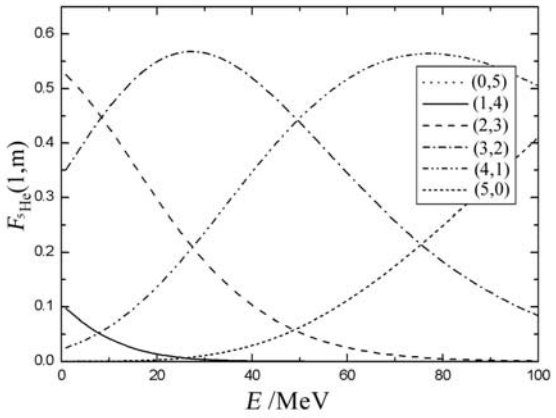

Fig.1 Pre-formation probability of ^{5}He cluster,

where ε_b is the observational energy of outgoing composite particle and B_b is the binding energy.

From Fig.1, the pre-formation probability of [2,3], [3,2], [4,1], [5,0] are larger than that of [1,4] with the observational energy of outgoing composite particle increasing. But when incident neutron energies are below 20 MeV, the configuration of [λ=1,m] is the dominant part, and other configurations can be ignored. On the other hand, in the emission rate the two terms are always occurred simultaneous, then the following inequality

$$
\begin{aligned}
&F_{b[\lambda=1,m]}(\varepsilon)Q_{b[\lambda=1,m]}\omega(n-1,E') \\
&> F_{b[\lambda=2,m]}(\varepsilon)Q_{b[\lambda=2,m]}\omega(n-2,E')
\end{aligned}
\qquad (19)
$$

is always held, because the exciton state densities reduce rapidly with the decreasing of the exciton number. This is the reason that the configuration of [λ=1,m] is only considered in low energy nuclear reaction.

The comparison of pre-formation probabilities for configuration of [λ=1,m] in composite particle emissions, such as d, t, ^{3}He, α, as well as ^{5}He cluster is shown in Fig.2.

From Fig.2 one can see that the formation probability of configuration of [λ=1,m] for ^{5}He cluster is obviously less than that of d, t, ^{3}He and α.

The calculated results indicate that the pre-formation probability of unstable ^{5}He cluster is much less than that of the stable composite particle clusters. In general, the binding energies of ^{5}He are smaller than that of ^{3}He clearly[5], and the ^{5}He cluster is apt to be emitted than ^{3}He. However, combining with optical model potential, the values of cross section for ^{5}He cluster emission should be taken into account synthetically. The theoretical model formulation for describing the pre-equilibrium emission of ^{5}He has been given in this paper, which can be used in the statistical model calculations for neutron induced reactions.

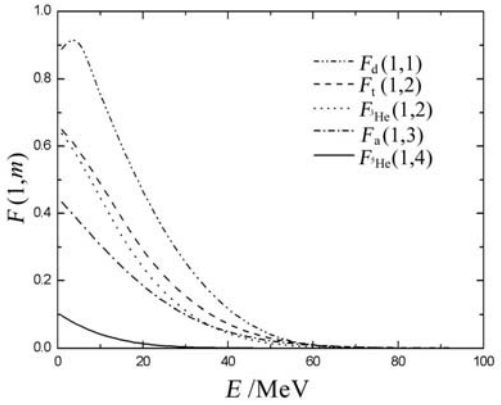

Fig.2 Comparison of pre-formation probabilities with configuration [1,m] for d,t,^{3}He,α,^{5}He

References

[1] ZHANG J. S., HAN Y. L., Cao L. G.. "Model Calculation of n+^{12}C Reactions from 4.8 to 20 MeV". Nucl. Sci. Eng., 133（1999）218-234.

[2] ZHANG J. S., HAN Y. L., Fan X. L., "Theoretical analysis of the neutron double differential cross section of n+^{16}O at E_n=14.1 MeV". Commun. Theor. Phys. (Beijing, China), 35 (2001) 579-584.

[3] ZHANG J. S., "Theoretical analysis of the neutron double differential cross section of n+^{11}B at E_n=14.2 MeV". Commun. Theor. Phys. (Beijing, China), 39 (2003) 83-88.

[4] ZHANG J. S., "Theoretical analysis of the neutron double differential cross section of n+^{10}B at E_n=14.2 MeV". Commun. Theor. Phys. (Beijing, China), 39 (2003) 433-438.

[5] ZHANG J. S., "Possibility of ^{5}He emission in Neutron induced Reactions" Science in China 47-2（2004）(to be published)

[6] ZHANG J. S., "UNF Code for Fast Neutron Reaction Data Calculations", Nucl Sci Eng, 142 (2002) 207-219

[7] Iwamoto A. and Harada K.,"Mechanism of cluster emission in ucleon-induced pre-equilibrium reactions". Phys. Rev., C26, (1982) 1821.

[8] Sato. K., Iwamoto A. and Harada K., "Pre-equilibrium emission of light omposite particles in the framework of the exciton model". Phys. Rev., C28, (1983) 1527.

[9] ZHANG J. S., YAN S. W., Wang C. L., "The Pick-up Mechanism in Composite Particle Emission Processes". Z. Phys. A 344 (1993) 251-258.

[10] ZHANG J. S., WEN Y. Q., Wang S. N., Shi X. J., "Formation and emission of light particles in fast neutron induced reaction-a united compound pre-equilibrium model". Commun. Theor. Phys (Beijing, China). 10（1988）33-44.

Double-Differential Cross Section of ^{5}He Emission

YAN Yuliang DUAN Junfeng ZHANG Jingshang

China Nuclear Data Center, CIAE, P.O.Box 275(41), Beijing 102413, P.R.China

【**abstract**】 *The probability of ^{5}He particle emission has been affirmed theoretically. In order to describe the ^{5}He emission, the theoretical formula of the double-differential cross section of emitted ^{5}He is to be established. Based on the pick-up mechanism, used for calculating the formula of d,t,^{3}He, α emissions, the theoretical formula of double-differential cross section of ^{5}He is obtained, which is expressed in the form of Legendre coefficients. The calculated result indicates that the forward peaked angular distribution of the composite particle emission is weaker than that of the emitted single nucleon due to pick-up nucleon from the Fermi sea. As an example, the reactions of n+^{14}N weren calculated, and the Legendre coefficients of d,t,^{3}He,α,^{5}He emissions were obtained respectively. The results show that the forward tendency is decided by the average momentum per nucleon in the emitted composite particles. The larger of the average momentum, the stronger of the forward tendency.*

Introduction

In recent years, the total outgoing neutron double-differential cross section of neutron induced light nuclear reaction has been calculated by using a new nuclear reaction model. In this model the ^{5}He emission is involved[1]. When the ^{5}He emission is taken into account, the calculated result can reproduce the experimental data successfully[2~5].

There are very few measurements on the double-differential cross section of composite particle emissions at present. Internationality, the Kalbach systematic formula[6] has been employed to set up the neutron data libraries. This formula is very useful for the middle and heavy nuclei, while it's imperfect to the 1p shell light nuclei. The model for describing the double-differential cross section of composite particle emissions of d, t, ^{3}He, α emissions has been proposed, which can reproduce the double-differential measurements of deuterium and alpha particle emissions nicely[7,8], and has been employed in the UNF code[9]. Now, extending this method for ^{5}He emission, the theoretical formula of the double-differential cross section of ^{5}He emission is established.

The composite particle emissions are mainly from pre-equilibrium reaction processes, which could be described successfully by the angular momentum dependent exciton model[9]. The pre-formation probability of ^{5}He in pre-equilibrium mechanism has been obtained[10]. The method for calculating the angular factor of ^{5}He emission in pre-equilibrium reaction processes is introduced in Sec.2, and the theoretical formulae of double-differential cross section of composite particle emission are given. As an example, the angular factor of d, t, ^{3}He, α, as well as ^{5}He of n+^{14}N reaction are calculated at incident neutron energies of 15, 20 MeV, respectively, meanwhile the angular distribution of single nucleon, α and ^{5}He particle are also calculated, the results and discussion are given in Sec.2. The summary is given in Sec.3.

1 The Angular Factor of ^{5}He in Pre-equilibrium Emission Process

The basic idea of the model for describing the double-differential cross section of composite particle emission is as follows:

(1) If the outgoing single nucleon picks up other nucleons in compound nucleus formed a composite particle during the emission process, then the composite particle emission would be occurred, otherwise only single particle emission would be happen.

(2) The double-differential cross section of single particle emission is obtained by the linear momentum dependent exciton model[11,12], in which the Fermi motion and the Pauli exclusion effects are taken into account.

(3) The Fermi gas model is employed for the compound nucleus system.

(4) The momentum of the composite particle is the summation over the outgoing single nucleon and the picked-up nucleons with the momentum conserving.
(5) The pre-formation probability is determined by the pick-up mechanism.

Based on the idea mentioned above, the normalized angular factor of composite particle *b* at the exciton state *n* with the emitted energy ε and the outgoing direction Ω is proposed by [9,13]

$$A(n,\varepsilon,\Omega)=\frac{1}{N}\int_{[lm]}\mathrm{d}\vec{p}_1\cdots\mathrm{d}\vec{p}_{A_b}\delta(\vec{P}-\sum_{i=1}^{A_b}\vec{p}_i)\tau(n,\Omega_1) \quad (1)$$

where N is the normalization factor, A_b is mass number of the composite particle.

For ^{5}He, the angular factor reads

$$A(n,\varepsilon,\Omega)=\frac{1}{N}\int_{[lm]}\mathrm{d}\vec{p}_1\mathrm{d}\vec{p}_2\mathrm{d}\vec{p}_3\mathrm{d}\vec{p}_4\mathrm{d}\vec{p}_5\delta$$
$$(\vec{P}-\vec{p}_1-\vec{p}_2-\vec{p}_3-\vec{p}_4-\vec{p}_5)\tau(n,\Omega_1) \quad (2)$$

where $\vec{P}$ is the momentum of ^{5}He, $\vec{p}_i$, i=1, 2, 3, 4, 5 are the momenta of the nucleons formed ^{5}He, and the outgoing single nucleon is denoted by i=1. τ (n,Ω_1) stands for the lifetime of the n exciton state with the direction Ω_1. The δ function in eq.(2) implies the momentum conservation.

In the case of low incident energies, the configuration [1,m] is the dominant part in the pre-equilibrium emission mechanism[9,10], which means that the outgoing single nucleon picked up four nucleons below the Fermi surface for ^{5}He emission. When the value of $\vec{P}$ is given, and the nucleon 1 is forward-peaked angular distribution in the pre-equilibrium emission process, then the probability of ^{5}He emission in direction Ω is determined by the integrated momentum space volume occupied by the other four picked up nucleons restricted by the δ function for momentum conserving.

Except nucleon 1, the other four picked-up nucleons corresponds to a α-particle, their relative intrinsic momenta are defined by

$$\vec{p}_{23}=\vec{p}_2+\vec{p}_3 \qquad \vec{p}_r=\frac{1}{2}(\vec{p}_2-\vec{p}_3)$$
$$\vec{p}_{45}=\vec{p}_4+\vec{p}_5 \qquad \vec{p}_{r'}=\frac{1}{2}(\vec{p}_4-\vec{p}_5) \quad (3)$$

then $\mathrm{d}\vec{p}_2\mathrm{d}\vec{p}_3\mathrm{d}\vec{p}_4\mathrm{d}\vec{p}_5=\mathrm{d}\vec{p}_{23}\mathrm{d}\vec{p}_r\mathrm{d}\vec{p}_{45}\mathrm{d}\vec{p}_{r'}$ is held. Thus, the angular factor of ^{5}He becomes

$$A(n,\varepsilon,\Omega)=\frac{1}{N}\int_{[lm]}\mathrm{d}\vec{p}_1\mathrm{d}\vec{p}_{23}\mathrm{d}\vec{p}_r\mathrm{d}\vec{p}_{45}\mathrm{d}\vec{p}_{r'}\delta$$
$$(\vec{P}-\vec{p}_1-\vec{p}_{23}-\vec{p}_{45})\tau(n,\Omega_1) \quad (4)$$

When $\vec{P}$ and $\vec{p}_1$ are given, then the value of $\vec{p}_\alpha$ is definite due to $\vec{p}_\alpha=\vec{p}_{23}+\vec{p}_{45}$, so the relationship of $\vec{p}_{23}$ and $\vec{p}_{45}$ can be obtained. The observable emitted energy ε of ^{5}He is obtained by

$$\varepsilon=\frac{P^2}{10m}+\frac{7}{2}\hbar\omega_5-5\varepsilon_f-B_5$$

where $\varepsilon_f=p_f^2/2m$ is the Fermi energy, p_f refers to the Fermi momentum and B_5 stands for the binding energy of ^{5}He in compound nucleus. So the inequality $P^2>16P_f^2$ could be reduced into

$$9\varepsilon_f>5\left(\frac{7}{2}\hbar\omega_5-\varepsilon-B_5\right)$$

which is always holds since B_5, ε are always less than 20 MeV, and ε_f≈30 MeV, $\hbar\omega_5\approx 7.63$ MeV. Therefore, the inequality $P>4p_f$ is always holds. Meanwhile, p_1 satisfies $p_1^2/2m\le E^*+\varepsilon_f$, where E^* is the excitation energy. In the case of low energies, if $E^*<\varepsilon_f$, then $p_1<2p_f$, and by using the momentum relation $\vec{P}=\vec{p}_1+\vec{p}_\alpha$, one has $|\vec{P}-\vec{p}_1|\equiv\vec{p}_\alpha>2p_f$.

The configuration [1,4] hints that $p_2\le p_f$, $p_3\le p_f$. Since $\vec{p}_r$ and $\vec{p}_{r'}$ do not appear in the δ function of eq.(4), so we ought to carry out the integration over them in advance. At first, for the integration $\int\mathrm{d}\vec{p}_{23}\mathrm{d}\vec{p}_r$, once $\vec{p}_{23}$ is given, the integration limits of $\vec{p}_r$ can be confirmed. The relationship of $\vec{p}_2$, $\vec{p}_3$ and their relative momenta $\vec{p}_{23}$, $\vec{p}_r$ is shown in Fig.1, where θ_r is the angle between $\vec{p}_{23}$ and $\vec{p}_r$, then we have

$$p_2^2=\frac{1}{4}p_{23}^2+p_r^2-p_{23}p_r\cos\theta_r\le p_f^2$$
$$p_3^2=\frac{1}{4}p_{23}^2+p_r^2+p_{23}p_r\cos\theta_r\le p_f^2 \quad (5)$$

Hence, the integration limits over θ_r satisfy the inequality $-\beta\le\cos\theta_r\le\beta$.

Where

$$\beta=\frac{p_f^2-\frac{1}{4}p_{23}^2-p_r^2}{p_{23}p_r} \quad (6)$$

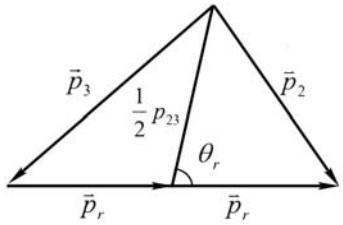

Fig.1 The relations of $\vec{p}_2, \vec{p}_3$ and $\vec{p}_{23}, \vec{p}_r$

The condition for the integration existence needs $\beta \geq 0$, which gives

$$p_r \leq \sqrt{p_f^2 - \frac{1}{4}p_{23}^2}$$

In addition, from the condition of $\beta \leq 1$, one gets

$$p_r \leq p_f - \frac{1}{2}p_{23}$$

Then the integration $\int \mathrm{d}\vec{p}_{23}\mathrm{d}\vec{p}_r$ can be written explicitly as

$$\int \mathrm{d}\vec{p}_{23}\mathrm{d}\vec{p}_r = \int \mathrm{d}\vec{p}_{23}\left\{\int_0^{p_r-\frac{1}{2}p_{23}} p_r^2\mathrm{d}p_r \int_{-1}^{1}\mathrm{d}\cos\theta_r \int_0^{2\pi}\mathrm{d}\varphi_r + \int_{p_r-\frac{1}{2}p_{23}}^{\sqrt{p_r^2-\frac{1}{4}p_{23}^2}} p_r^2\mathrm{d}p_r \int_{-\beta}^{\beta}\mathrm{d}\cos\theta_r \int_0^{2\pi}\mathrm{d}\varphi_r\right\} \quad (7)$$

Carrying out the integration over $\vec{p}_r$, the result is

$$\int \mathrm{d}\vec{P}_r = \frac{\pi}{12}\left(16p_f^3 - 12p_f^2 p_{23} + p_{23}^3\right) \quad (8)$$

With the same procedure for the integration over $\vec{p}_{r'}$, one can get

$$\int \mathrm{d}\vec{P}_r = \frac{\pi}{12}\left(16p_f^3 - 12p_f^2 p_{45} + p_{45}^3\right) \quad (9)$$

Thus the eq.(4) is reduced into the form as follows

$$A(n,\varepsilon) = \frac{\pi^2}{144N}\iiint_{[1,4]}\mathrm{d}\vec{p}_1\mathrm{d}\vec{p}_{23}\mathrm{d}\vec{p}_{45}\delta (\vec{P} - \vec{p}_1 - \vec{p}_{23} - \vec{p}_{45}) (16p_f^3 - 12p_f^2 p_{23} + p_{23}^3) (16p_f^3 - 12p_f^2 p_{45} + p_{45}^3)\tau(n,\Omega_1) \quad (10)$$

Since $\vec{p}_\alpha = \vec{p}_{23} + \vec{p}_{45}$, and θ is the angular between $\vec{p}_\alpha$ and $\vec{p}_{23}$.

$$p_{45} = \sqrt{p_\alpha^2 + p_{23}^2 - 2p_\alpha p_{23}\cos\theta} \leq 2p_f \quad (11)$$

The integration limits of θ satisfy the inequality as

$$\cos\theta \geq \frac{p_\alpha^2 + p_{23}^2 - 4p_f^2}{2p_\alpha p_{23}} \equiv \gamma \quad (12)$$

If $\gamma \leq -1$ were held, one could get $p_\alpha + p_{23} \leq 2p_f$, which is contradictory with the condition $p_\alpha > 2p_f$, so $\gamma \leq -1$ is impossible. Thus the integration limits of θ are given by $\gamma \leq \cos\theta \leq 1$. The condition $\gamma < 1$ needs $p_{23} \geq p_\alpha - 2p_f$. Therefore, the integration over $\vec{p}_{23}$ is obtained explicitly by

$$\int p_{23} = \int_{p_\alpha - 2p_f}^{2p_f} p_{23}^2\mathrm{d}p_{23}\int_\gamma^1 \mathrm{d}\cos\theta \quad (13)$$

For convenience the dimensionless quantities are introduced as follows

$$\vec{x}_b \equiv \frac{\vec{P}}{p_f},\quad \vec{x}_1 \equiv \frac{\vec{P}_1}{p_f},\quad \vec{x}_{23} \equiv \frac{\vec{P}_{23}}{p_f}$$

$$\vec{x}_{45} \equiv \frac{\vec{P}_{45}}{p_f},\quad \vec{y} \equiv \frac{\vec{P}_\alpha}{p_f},\quad t \equiv \cos\theta$$

In spite of the constant factor, and inserting the factor $\int \mathrm{d}\vec{y}\delta(\vec{y} - \vec{x}_{23} - \vec{x}_{45})$ in eq.(10), then it is rewritten by

$$A(n,\varepsilon,\Omega) = \iiint_{[1,4]}\mathrm{d}\vec{x}_1\mathrm{d}\vec{y}\mathrm{d}\vec{x}_{23} \mathrm{d}\vec{x}_{45}\delta(\vec{x}_b - \vec{x}_1 - \vec{y})\delta(\vec{y} - \vec{x}_{23} - \vec{x}_{45}) (16 - 12x_{23} + x_{23}^3)(16 - 12x_{45} + x_{45}^3)\tau(n,\Omega) \quad (14)$$

Using the second δ function in eq.(14), $\vec{x}_{45}$ can be replaced by $\vec{x}_{23}$ and $\vec{y}$.

Carrying out the integrating over *t*, and x_{23}, the angular factor is reduced into the form as

$$A(n,\varepsilon,\Omega) = \iiint_{[1,4]}\mathrm{d}\vec{x}_1\mathrm{d}\vec{y}\delta(\vec{x}_b - \vec{x}_1 - \vec{y})Z_b(y)\tau(n,\Omega_1) \quad (15)$$

The function $Z_b(y)$ in eq.(15), as used for the other composite particles [7,8,10], reads

$$Z_b(y) = \frac{(y-4)^6}{y}(-144 + 224y + 156y^2 + 24y^3 + y^4) \quad (16)$$

Using the δ function in eq.(15), the integration is reduced only over $\mathrm{d}\vec{y}$, where *y* can be expressed by $\vec{x}_b$ and $\vec{x}_1$ as

$$y = \sqrt{x_b^2 + x_1^2 - 2x_b x_1\cos\Theta} \leq 4$$

or

$$\cos\Theta = \frac{x_b^2 + x_1^2 - y^2}{2x_b x_1} \tag{17}$$

where Θ is the angular between $\vec{P}$ and $\vec{p}_1$. The particle 1 is always above the Fermi surface, so the integration limits of $\vec{p}_1$ satisfies

$$\max\{x_f, x_b - 4x_f\} \le x_1 \le x_f\sqrt{1+\frac{E^*}{\varepsilon_f}} \tag{18}$$

In terms eq.(17), the integration limits of Θ is obtained by

$$b_5 \le \cos\Theta \le 1 \tag{19}$$

where

$$b_5 = \frac{P^2 + p_1^2 - 16p_f^2}{2Pp_1} = \frac{x_b^2 + x_1^2 - 16}{2x_b x_1} \tag{20}$$

By using the composition formula between θ_1 and Θ, Ω

$$P_l(\cos\theta_1) = \frac{4\pi}{2L+1}\sum_m Y_{lm}^*(\Theta\Phi)Y_{lm}(\Omega) \tag{21}$$

where θ_1 is the outgoing angle of the particle 1. Thus, the integration over $\vec{p}_1$ could be replaced by $\mathrm{d}\vec{x}_1 = x_1^2\mathrm{d}x_1\mathrm{d}\cos\Theta\mathrm{d}\Phi$. Carrying out the integration over Φ, the lifetime of n exciton states can be given in the Legendre expansion form as [12].

$$\tau(n,\Omega_1) = \sum_l \tau_l(n)P_l(\cos\Theta)P_l(\cos\theta) \tag{22}$$

Finally, the normalized angular factor in the form of Legendre polynomials [9,13] is obtained by

$$A(n,\varepsilon,\Omega) = \frac{1}{4\pi}\sum_l \frac{G_l(\varepsilon,n)}{G_0(\varepsilon,n)}\frac{\tau_l(n)}{\tau_0(n)}P_l(\cos\theta) \tag{23}$$

In this equation the lifetime partial waves can be obtained by solving the generalized master equation[12]. Moreover, the geometrical factors $G_l(\varepsilon)$ is obtained by the pick-up nucleons below the Fermi surface, and reads

$$G_l(\varepsilon) = \frac{1}{x_b}\int_{\max\{1,x_b-4\}}^{\sqrt{1+\frac{E^*}{e_f}}} x_1\mathrm{d}x_1 \int_{x_5-x_1}^{4} Z_5(y)P_l(\cos\Theta)\mathrm{d}y \tag{24}$$

The double-differential cross section of composite particle emission is given by [11]

$$\frac{\mathrm{d}^2\sigma}{\mathrm{d}\varepsilon\mathrm{d}\Omega} = \sum_n \frac{\mathrm{d}\sigma(n)}{\mathrm{d}\varepsilon}A(n,\varepsilon,\Omega) \tag{25}$$

where $\mathrm{d}\sigma(n)/\mathrm{d}\varepsilon$ is the normalized energy spectrum of n exciton state, which is obtained by the pre-equilibrium statistical theory [12].

2 Calculated Results and Discussions

The angular factors of ^{5}He, as well as d, t, ^{3}He, α emissions in the reaction n+^{14}N, as an example, are calculated at 15, 20 MeV, respectively. The common form of $Z_b(y)$ functions are given by[12]

$$Z_b(y) = \begin{cases} 1 & b = d \\ (1-\frac{1}{2}y)^2(4+y) & b = t, {}^3\mathrm{He} \\ \frac{(3-y)^4}{y}\left[210-126(3-y)+21(3-y)^2-(3-y)^3\right] & b = \alpha \\ \frac{(y-4)^6}{y}(-144+224y+156y^2+24y^3+y^4) & b = {}^5He \end{cases} \tag{26}$$

In our case the outgoing energy ε_b is a constant due to emissions are from the compound nucleus to the ground states of their residual nuclei. In this case the double differential cross section is reduced to the angular distributions. The partial wave $G_l^b(\varepsilon_b)$ of the composite particle b in the common form reads

$$G_l^b(\varepsilon_b) = \frac{1}{x_b}\int_{\max(1,x_b-A_b+1)}^{\sqrt{1+\frac{E^*}{e_f}}} x_1\mathrm{d}x_1 \int_{x_b-x_1}^{A_b-1}\mathrm{d}y Z_b(y)\,p_l(\cos\Theta) \tag{27}$$

where A_b is mass number of the composite particle b. The values of the parameters used in the calculation are given in Table.1, and ε_f=30 MeV, B_n=10.833 MeV.

The values of $G_l(\varepsilon_b)/G_0(\varepsilon_b)$ calculated by using eq.(28) are given in the Table 2

Using the method introduced in reference [12] and UNF[9] code, the lifetime partial wave factors $\tau_l(n)/\tau_0(n)$ are calculated with n=3 exciton state at E_n=15, 20 MeV. The result are given in Table 3

The results in Table 3 indicate that for a composite particle, the higher of the incident energy is, the stronger of the forward tendency is. Since the motion of the nucleons in the Fermi sea is isotropic, the picked-up particles should counteract the forward tendency of the outgoing single particle, as shown in Table.2. All of the values of the geometrical factors $G_l(\varepsilon_b)/G_0(\varepsilon_b)$ are always less than 1. It should be pointed out that the forward tendency of ^{5}He is stronger than that of α particle. This fact implies that the forward tendency is dependent on the average momentum per nucleon of the emitted composite particle, which is denoted by p_b/A_b in Table.2. Because the average momentum of the nucleons consisted ^{5}He is higher than α-particle's, so the forward tendency of ^{5}He emission is stronger than that of the α-particle. To show this fact the angular distributions of n, ^{5}He as well as α-particle in n+^{14}N reaction at E_n=15MeV are shown in Fig.2.

Table.1 The parameters used in n+^{14}N reaction

Particle *b*	d	^{3}He	t	α	^{5}He
B_b	16.160	28.199	14.849	10.991	23.339
$\hbar\omega$	8.1	11.7	14.4	18.2	7.63

All the quantities are in unit of MeV.

Table.2 The values of $G_l(\varepsilon_b)/G_0(\varepsilon_b)$ in n+^{14}N reaction

E_n	*b*	P_b/A_b	*l*=1	*l*=2	*l*=3	*l*=4
15	d	1.137	0.991 7	0.975 3	0.951 1	0.919 4
	^{3}He	1.043	0.979 6	0.939 7	0.882 5	0.810 6
	t	1.007	0.968 8	0.908 9	0.824 7	0.722 5
	α	0.914	0.943 2	0.838 0	0.699 4	0.545 7
	^{5}He	0.992	0.974 8	0.926 1	0.857 2	0.772 4
20	d	1.167	0.992 5	0.977 5	0.955 4	0.926 6
	^{3}He	1.063	0.981 0	0.943 9	0.890 4	0.823 0
	t	1.027	0.971 1	0.915 5	0.836 9	0.740 9
	α	0.929	0.947 1	0.848 5	0.717 5	0.570 3
	^{5}He	1.002	0.975 8	0.929 1	0.862 7	0.780 9

Table.3 The results of τ_l(n=*3*) / τ_0(n=*3*) in n+^{14}N reaction

E_n(MeV)	*l*=1	*l*=2	*l*=3	*l*=4
15	0.511 0	0.126 6	0.051 7	0.058 3
20	0.529 7	0.133 8	0.032 2	0.037 4

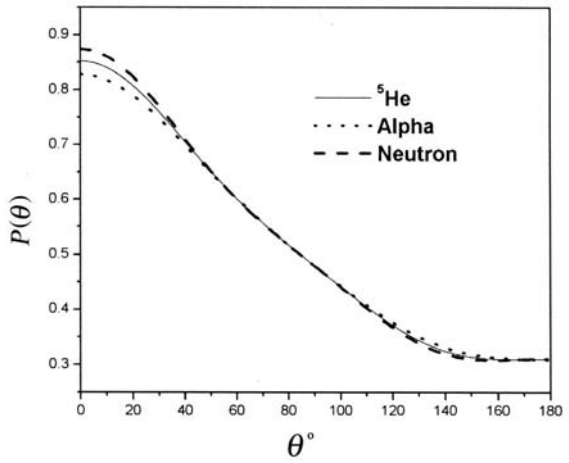

Fig.2 The angular distributions of n,α and ^{5}He from n+^{14}N reaction with incident neutron energy E_n=15 MeV

3 Summary

In this paper the theoretical formula of the double-differential cross section of ^{5}He emission is established to complete the description on the double-differential cross section of composite particle emissions.

Being unstable, ^{5}He will be separated into one neutron and one α-particle spontaneously, using the formula in reference [1], the double-differential cross section in the center of mass system of the outgoing neutron and the α-particle can be calculated. Their energy ranges of the outgoing neutron and the α-particle spectra are shown in Table.4

The results in Table.4 indicate that the energy spectrum of neutron is located in low energy region. Since only the ground states are taken into account in this calculation, if the residual nuclei are in their excited levels, the emitted energies become small, and the energy spectrum ranges will be located at even low area.

Table.4 The energy ranges of n and α from ^{5}He separation in n+^{14}N reaction

E_n	$\varepsilon_{^5\mathrm{He}}$	$\varepsilon_{n-\min}$	$\varepsilon_{n-\max}$	$\varepsilon_{\alpha-\min}$	$\varepsilon_{\alpha-\max}$
15	4.279	0.006	3.137	2.037	5.168
20	7.601	0.150	4.323	4.173	8.346

All the quantities are in unit of MeV.

References

[1] ZHANG J.S., Science in China G, 47 (2004) 137-145.

[2] ZHANG J. S., HAN Y. L., CAO L. G.. Nucl. Sci. Eng., 133 （1999）218-234.

[3] ZHANG J. S., HAN Y. L., FAN X. L., Commun. Theor. Phys. (Beijing, China), 35 (2001) 579-584.

[4] ZHANG J. S., Commun. Theor. Phys. (Beijing, China), 39 (2003) 83-88.

[5] ZHANG J. S., Commun. Theor. Phys. (Beijing, China), 39 (2003) 433-438.

[6] Kalbach C., Phys. Rev. C, 37 (1988) 2350.

[7] ZHANG J. S., Chin. J. of Nucl, Phys. 15 (1993) 347-351.

[8] ZHANG J. S., Nucl Sci Eng, 116 (2002) 35-41.

[9] ZHANG J. S., Nucl Sci Eng, 142 (2002) 207-219.

[10] DUAN J. F., YAN Y. L., ZHANG J. S., Commun. Theor. Phys. (Beijing, China), (to be published)

[11] Chadwick M. B. Phys. Rev. C 44 (1991).R1740.

[12] SUN Z. Y., WANG S. N., ZHANG J. S., ZHOU Y. Z., Z. Phys. A, 305(1982) 61.

[13] DIN Dazhao et al.，“Neutron Physics”, p361, Published by Atomic Energy Press, 2001.

A New Method of Processing the Discrepant Data

WANG Baosong[1,2] FAN Sheng[1] HUANG Xiaolong[1]

[1]*China Nuclear Data Center, CIAE, P.O.Box 275(41), Beijing 102413, P.R.China*

[2]*Department of Physics, Shanghai University, Shanghai 201800, P.R.China*

【**abstract**】*Several methods of evaluating the discrepant data are introduced and compared briefly. On the basis of these analysis and comparison, a new method, i.e. double-mean method, of evaluating the discrepant data was proposed. The application is given for half-life of ^{137}Cs as an example. The half-life evaluated by this method is 10981±11 days for ^{137}Cs.*

Introduction

The nuclear data evaluators often encounter discrepant set of data. They must decide, which ones are more doubtful, and to determine the "best" method for deriving a "best" value and its standard deviation from the discrepant set of data. In order to solve this problem, many data evaluation procedures have been proposed by several authors in recent years. These proposed methods assume that the incorrect uncertaintaies are responsible for the data discrepancy and usually modify them by a common factor by keeping unchanged the measured values.

In present paper several methods of evaluating the discrepant data are introduced and compared briefly. The advantage and disadvantage of these methods are outlined. On the basis of these analysis and comparison, a new method, i.e. double-mean method of evaluating the discrepant data is proposed. The application is given for half-life of ^{137}Cs as an example.

1 Data Processing Methods

In the following discussion, x_i and σ_i refer to individual data and their associated uncertainties respectively and N refer to the number of measurements. The processing method. Evaluating with statistical techniques in the discrepant decay data sets are summarized as follows.

1.1 Arithmetical Mean (UWM)

The arithmetical mean for N measurements is given by

$$x_u = \frac{\sum x_i}{N} \tag{1}$$

with associated uncertainty

$$\sigma_u = \sqrt{\frac{\sum (x_i - x_u)^2}{N(N-1)}} \tag{2}$$

1.2 Weighted Mean (WM)

The weight associated with measurement i is given by

$$w_i = 1/\sigma_i^2 \tag{3}$$

and the total weight is given by

$$W = \sum_{i=1}^{N} w_i \tag{4}$$

The weighted mean is then given by

$$x_w = \frac{\sum w_i x_i}{W} \tag{5}$$

with the internal error

$$\sigma_w = \sqrt{1/W} \tag{6}$$

and external error

$$\sigma_e = \sqrt{\frac{\sum (x_i - x_w)^2/\sigma_i^2}{N-1}}\sigma_w \tag{7}$$

1.3 Limitation of Relative Statistical Weights (LRSW)[1,2]

A relative statistical weight is defined as w_i/W. To avoid any single datum having too much influence in

determining the weighted mean, LRSW prescribed that no single datum should have a relative statistical weight greater than 0.50 when determining the weighted mean of a data set. The uncertainty of any datum should be increased until its relative statistical weight is reduced to 0.50. Then the result is compared with arithmetical mean. If they meet the relation.

$$\left|x_u - x_w\right| \le \sigma_u + \sigma_w \tag{8}$$

the weighted mean could be adopted. If not, the data are inconsistent and it would be safer to use the unweighted mean. In either case the uncertainty is increased, if necessary, to cover the most precise value in the data set.

1.4 Normalized Residuals (NR)

The normalized residuals method was introduced by James et al. [3], in which the uncertainties of only the discrepant data are adjusted. Such discrepant data are identified on the basis of the normalized residual R_i which is defined as:

$$R_i = \sqrt{\frac{w_i W}{W - w_i}}\left(x_i - w_w\right) \tag{9}$$

A limiting value of the normalized residual R_0 for a set of N values is defined as:

$$R_0 = \sqrt{1.8 \ln N + 2.6} \qquad \text{for } 2 \le N \ge 100 \tag{10}$$

If any value in the data set has $|R_i| > R_0$, the weight of the value with the largest R_i is reduced until the normalized residual is reduced to R_0. This procedure is repeated until no normalized residual is greater than R_0. The weighted mean is then recalculated with the adjusted weights.

1.5 Rajeval (RA)

Rajput and MacMahon[4] proposed a method in 1992. This method shares the same basic principle as the normalized residuals method where the uncertainties of only the more discrepant data are adjusted. The method comprises of three stages:

(1) Outliers in the data set are detected by calculating the quantity y_i

$$y_i = \frac{x_i - x_{ui}}{\sqrt{\sigma_i^2 + \sigma_{ui}^2}} \tag{11}$$

where x_{ui} is the unweighted mean of all the data set excluding x_i, and σ_{ui} is the standard deviation associated with x_{ui}. The critical value of $|y_i|$ is 1.96 at 5% significance level for a two-tailed test. Measurements with $|y_i| > 3 \times 1.96$ are considered to be outliers and may be excluded from further stages in the processing.

(2) Inconsistent measurements that remain in the data set after the population test are revealed by calculating a standardized deviation Z_i:

$$Z_i = \frac{x_i - x_w}{\sqrt{\sigma_i^2 - \sigma_w^2}} \tag{12}$$

for each Z_i the probability integral

$$P(z) = \int_{-\infty}^{z} \frac{1}{\sqrt{2\pi}} \exp\left(\frac{-t^2}{2}\right) dt \tag{13}$$

is determined. The absolute difference between $P(z)$ and 0.5 is a measure of the central deviation (CD). A critical value of the central deviation (cv) can be determined by the following expression:

$$\text{cv} = [(0.5)^{N/(N-1)}] \qquad \text{for } N > 1 \tag{14}$$

(3) If the central deviation of any value is greater than the critical value, that value is regarded as inconsistent. The uncertainties of the inconsistent values are adjusted to σ_i':

$$\sigma_i' = \sqrt{\sigma_i^2 + \sigma_w^2} \tag{15}$$

An iteration procedure is adopted in which σ_w is recalculated each time and added in quadrature to the uncertainties of those values with CD>cv. The iteration process is terminated when all CD<cv.

1.6 Modified Bayesian Technique (MBAYS)[5,6]

A Bayesian data processing technique was proposed by Gray et al.[5]. Nothing is assumed to be known about the extent to which the experimentalists estimated their uncertainties incorrectly, and therefore an uninformative prior density is used as an error probability density function. The recommended value is the weighted mean with a standard deviation given by[6]

$$\sigma_b = \sqrt{\frac{\sum \left(x_i - x_w\right)^2 / \sigma_i^2}{N - 2}}\,\sigma_w \tag{16}$$

1.7 Double Mean (DM)

The arithmetical mean (UWM) is influenced by outliers in the data and takes no account of the fact that different authors made measurements with different precision, so some of the measurement information are lost and therefore to be avoided if possible.

The weighted mean (WM) can be heavily influenced by discrepant data with small quoted uncertainties, and would only be acceptable where the reduced chi-squared is close to unity. If the value of chi-squared is very high, indicating inconsistencies

in the data.

The Limitation of Relative Statistical Weights (LRSW) still chooses the weighted mean but inflates its associated uncertainty to cover the most precise value. In this case, therefore, both the LRSW value and its associated uncertainty are heavily influenced by the most precise value of the data set.

The Normalized Residuals (NR) and Rajeval techniques(RA) have been developed to address the problems of the other techniques and to maximize the use of all the experimental information available. They use different statistical techniques to reach the same objective: that is to identify discrepant data and to increase the uncertainties of only such data to reduce their influence on the final weighted mean. In general the Rajeval Technique makes larger adjustments to the uncertainties of discrepant data than does the Normalised Residuals Technique, and has a lower final uncertainty.

The modified Bayesian(MBAYS) method use the weighted mean as the recommended value and alter only the magnitude of the recommended uncertainty. Compared to the NR and RA method, MBAYS can derive the more reliable uncertainty [6] because both NR and RA method sometimes underestimate uncertainties and sometimes overestimate them.

On the basis of the above analysis and comparison, a new method of evaluating the discrepant data was proposed in present work, i.e. the double-mean method (DM). The DM procedure compares the Modified Bayesian Technique (MBAYS) mean with the Normalized Residuals (NR) mean. If their uncertainties overlap, i.e.

$$\left|\chi_N - \chi_{MB}\right| \le \sigma_N + \sigma_{MB} \tag{17}$$

the mean of the MBAYS, NR and RA with the larger of the three uncertainties should be adopted. If their uncertainties did not overlap, the mean of the NR and RA with the larger of the two uncertainties should be adopted.

2 Application

All the measured values and their uncertainties of the half-life of ^{137}Cs are collected and listed in Table 1 with the chronological order of their publication. In Table 1 it also listed the results of applying each of the above method as each new data point is added to the set. Fig. 1 shows the data of Table 1.

Fig.1 is to demonstrate how the various methods of evaluating discrepant data converge as the number of points in the data set increases. It shows that there are significant differences in the ways the evaluation techniques behave with small numbers of discrepant data and the Normalized Residuals and Rajeval techniques converge much more quickly than the other techniques.

From Table 1 it is easy to get:

χ_B=10 988, σ_B=11, χ_N=10 985, σ_N=10; $\chi_N - \chi_B$ =3; $\sigma_B + \sigma_N$ =21

$$|\chi_N - \chi_B| < \sigma_B + \sigma_N \tag{18}$$

According to the DM method, A value of 10 981±11 days can be adopted as the current best estimate of the half-life of ^{137}Cs.

3 Conclusion

Several methods of evaluating the discrepant decay data are introduced and compared briefly. The advantage and disadvantage of these methods are outlined. On the basis of these analysis and comparison, a new method of evaluating the discrepant data was proposed in present work, -i.e. the double-mean method (DM).

The DM procedure compares the the Modified Bayesian Technique (MBAYS) mean with the Normalized Residuals (NR) mean. If their uncertainties overlap, the mean of the MBAYS, NR and RA with the larger of the three uncertainties should be adopted. If their uncertainties did not overlap, the mean of the NR and RA with the larger of the two uncertainties should be adopted.

Table 1 Comparision of the measurement and evaluation by several evaluation methods of the half-life of ^{137}Cs (all data in days)

Authors	Measurement	WM	LRSW	NR	RA	MBAYS	DM
Wiles et al. (1955)[7]	9 715 146	9 715 146	9 715 146	9 715 146	9 715 146	9 715 146	9 715 146
Brown et al. (1955)[8]	10 957 146	10 336 621	10 336 621	10 891 279	10 336 103	10 336 621	10 521 621
Farrar et al. (1961)[9]	11 103 146	10 592 440	10 592 511	10 993 102	11 045 113	10 592 623	10 877 623
Fleishman (1962)[10]	10 994 256	10 631 348	10 631 472	10 989 94	11 025 96	10 631 427	10 882 427
Gorbics et al. (1963)[11]	10 840 18	10 830 70	10 936 220	10 845 27	10 904 68	10 830 81	10 860 81
Rider et al. (1963)[12]	10 665 110	10 826 63	10 741 161	10 840 28	10 841 18	10 826 70	10 836 70
Lewis et al. (1965)[13]	11 220 47	10 873 75	10 930 120	10 891 93	11 031 74	10 873 82	10 932 93
Flynn et al. (1965a)[14]	10 921 183	10 873 69	10 928 109	10 892 82	11 006 68	10 873 75	10 924 82
Flynn et al. (1965b)[14]	11 286 256	10 875 65	10 931 102	10 909 80	11 041 62	10 875 70	10 942 80

Cont. Table 1

Authors	Measurement		WM		LRSW		NR		RA		MBAYS		DM	
Harbottle (1970)[15]	11 191	157	10 878	62	10 936	96	10 944	77	11 073	55	10 878	66	10 965	77
Emery et al. (1972)[16]	11 023	37	10 901	57	10 934	94	11 011	45	11 030	30	10 901	60	11 021	45
Dietz et al. (1973)[17]	11 020.8	41	11 012	17	10 961	60	11 020	7	11 021	4	11 012	18	11 018	18
Corbett (1973)[18]	11 034	29	11 012	16	10 975	46	11 021	7	11 021	4	11 012	17	11 018	17
Gries et al.(1978)[19]	10 906	33	11 011	16	10 973	48	11 020	7	11 021	4	11 011	17	11 017	17
Houtermans (1980)[20]	11 009	11	11 011	14	10 996	25	11 018	6	11 019	4	11 011	15	11 016	15
Martin et al.(1990)[21]	10 967.8	45	10 994	12	10 994	27	10 987	13	10 996	10	10 994	13	10 992	13
Gostely (1992)[22]	10 940.8	69	10 986	12	10 986	35	11 008	10	10 969	4	10 986	12	10 988	12
Unterweger (2002)[23]	11 018.3	95	10 988	11	10 988	32	10 988	11	11 007	7	10 988	12	10 994	12
Schrader (2004)[24]	10 970	20	10 988	11	10 988	33	10 985	10	10 970	4	10 988	11	10 981	11

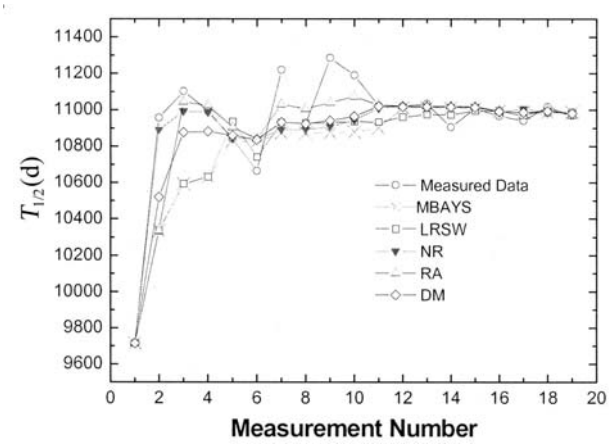

Fig.1 Comparisn of the measurement and evaluation by several evaluation methods of the half-life of ^{137}Cs

References

[1] W.L.Zijp, ECN-179, 1985.
[2] M.J.Woods, A.S.Munster, NPL Report RS(EXT)95, 1988.
[3] M.F.James et al., AEA-RS-1082, 1992.
[4] M.U.Rajput et al., Nucl. Instrum. Methods A 312, 289 (1992).
[5] P.W.Gray et al., Nucl. Instrum. Methods A 286, 569 (1990).
[6] S.I.Kafala et al., Nucl. Instrum. Methods A 339, 151 (1994).
[7] D.M.Wiles et al., Phys. Rev. 99,188(1955).
[8] F.Brown, et al., J. Inrog. Nucl.Chem. 1, 241(1955).
[9] H.Farrar et al., H., Can.J.Chem.39, 681(1961).
[10] D.G.Fleishman et al., Sov. J. At. Energy 13,1244(1962).
[11] S.G.Gorbics et al., Nucleonics 21, 63(1963).
[12] B.E.Rider et al., Nucl. Sci. Eng. 15,284(1963).
[13] R.E.Lewis et al., R.E., Trans. Am. Nucl. Soc. 8,79 (1965).
[14] K.F.Flynn, et al. J.Inorg.Nucl.Chem. 27, 21(1965).
[15] G.Harbottle et al., Radiochim.Acta 13,132(1970).
[16] J.F.Emery et al., Nucl.Sci. Eng. 48,319(1972).
[17] L.A.Diez et al., J.Inorg.Nucl.Chem.35, 1769(1973).
[18] J.A.Corbett et al., Nucl.Eng.Int 18,715(1973).
[19] W.H.Gries et al., Nucl.Instrum. Methods 152, 495 (1978).
[20] H.Houtermans et al., Int. J. Appl. Radiat. Isot. 31, 153 (1980).
[21] R.H.Martin et al., Nucl. Instrum. Methods 286,507 (1990).
[22] J.J.Gostely et al., Appl. Radiat.Isot. 31,153(1992).
[23] M.P.Unterweger et al., Appl. Radiat.Isot. 56, 125(2002).
[24] H.Schrader, Appl. Radiat. Isot., 58, 1016(2004).

Update the Decay Data for Radionuclide ^{7}Be Based on the Double Method

WANG Baosong[1,2] HUANG Xiaolong[1]

[1]*China Nuclear Data Center, CIAE, P.O.Box 275(41), Beijing 102413, P.R.China*

[2]*Department of Physics, Shanghai University, Shanghai 201800, P.R.China*

【**abstract**】 *The decay data of ^{7}Be were re-evaluated based on the new measured data and by using a new evaluation method. The half-life and γ emission probability of ^{7}Be are recommended to be $T_{1/2}$=53.282±0.012 days and P_{γ}=10.45±0.04%, respectively.*

Introduction

^{7}Be is a radionuclide of ε decay. It's very useful as standard source of γ-ray detector calibration. Therefore its half-life and γ emission probability need to be known with good accuracy. Before 2001 several evaluations were finished[1~4]. Recently there are some new measurements, so it is necessary to update them.

1 Half-life

All measured data and their uncertainties of the half-life of ^{7}Be were collected and were listed in Table 1 in the chronological order of their publication. In Table 1 are also listed the results of processing with different evaluation methods (WM, weighted mean; LRSW[5,6], limitation of relative statistical weights; MBAYS[7,8], modified Bayesian technique; NR[9], normalised residuals; RA, Rajeval[10]; DM[11], double mean) as each new datum is added to the set. The data of Table 1 are shown in Fig.1.

In Fig.1 it is demonstrated how the evaluated data with different evaluation methods are converged as the number of the points in the data set increases. It shows that there are significant differences in the ways the evaluation techniques behave with small numbers of discrepant data. Meantime the Normalized Residuals and Rajeval techniques recover much more quickly than the other techniques.

From Table 1 it is easy to get:

χ_B=53.292, σ_B=0.012, χ_N=53.282, σ_N=0.006;

$\chi_N - \chi_B$ =0.01, $\sigma_B + \sigma_N$ =0.018,

$|\chi_N - \chi_B| < \sigma_B + \sigma_N$

According to the DM method, a value of 53.282±0.012 days can be adopted as the current best estimate of the half-life of ^{7}Be.

2 γ-emission Probability

^{7}Be is ε decay to ground state and the first excited state (477.621 0 keV) of ^{7}Li. Only 477.603 5 keV γ-ray can be emitted. The measured values and their uncertainties were collected and listed in Table 1 with the chronological order of their publication. Fig. 2 shows the data of Table 2.

From Table 2 it is easy to get:

χ_B=10.449, σ_B=0.041, χ_N=10.449, σ_N=0.044;

$\chi_N - \chi_B$ =0； $\sigma_B + \sigma_N$ =0.085;

$|\chi_N - \chi_B| < \sigma_B + \sigma_N$

According to the DM method, a value of 10.45±0.04 days can be adopted as the current best estimate of the γ emission probability P_{γ}(477.6 keV) for ^{7}Be.

Table 1 Comparison of the measured data and evaluated data by different evaluation methods of the half-life of ^{7}Be(all data in days)

Authors	Measurement	WM	LRSW	NR	RA	MBAYS	DM
E.Segre et al. (1949,1951)[12]	52.93 22	52.93 22	52.93 22	52.93 22	52.93 22	52.93 22	52.93 22
J.J.Kraushaar et al. (1953)[13]	53.61 17	53.356 329	53.270 340	53.311 200	53.311 200	53.356 329	53.326 339

Cont. Table 1

Authors	Measurement		WM		LRSW		NR		RA		MBAYS		DM	
R.Bouchez et al.. (1956)[14]	53.0	4	53.320	233	53.278	332	53.209	153	53.126	281	53.320	330	53.218	330
H.W.Wright et al.. (1957) [15]	53.5	2	53.372	167	53.372	238	53.372	108	53.471	119	53.372	205	53.405	205
J.B.A.Eugland (1965) [16]	53.1	3	53.341	143	53.341	269	53.341	101	53.354	121	53.341	165	53.345	165
R.Vaninbroukx et al. (1966) [17]	53.20	55	53.336	126	53.336	274	53.336	100	53.363	112	53.336	141	53.345	141
J.S.Merritt(1969) [18]	53.284	6	53.284	7	53.310	82	53.284	6	53.284	6	53.284	8	53.284	8
H.W.Johlige et al. (1970) [19]	53.52	10	53.285	8	53.356	72	53.285	6	53.326	47	53.285	9	53.299	47
P.J.Cressy(1974) [20]	53.0	3	53.285	8	53.345	62	53.285	6	53.284	6	53.285	9	53.285	9
F.Lagoutiue et al. (1975) [21]	53.17	17	53.285	8	53.328	57	53.285	6	53.284	6	53.285	8	53.285	8
A.R.Rutledge et al.(1982) [22]	53.284	4	53.284	4	53.284	5	53.284	3	53.284	3	53.284	4	53.284	4
M.Jaeger et al. (1996) [23]	53.12	7	53.284	5	53.284	6	53.284	5	53.284	3	53.284	5	53.284	5
C.A.Huh et al. (2000) [24]	53.42	1	53.297	12	53.302	18	53.285	8	53.335	32	53.297	13	53.306	32
E.B.Norman et al.(2001a) [25]	53.107	22	53.294	14	53.232	52	53.284	8	53.242	36	53.294	15	53.273	36
E.B.Norman et al.(2001b) [25]	53.174	37	53.293	14	53.228	56	53.283	7	53.204	24	53.293	14	53.260	24
E.B.Norman et al.(2001c) [25]	53.195	52	53.292	13	53.226	58	53.282	7	53.204	21	53.292	14	53.259	21
E.B.Norman et al. (2001d) [25]	53.311	42	53.292	13	53.231	53	53.282	7	53.238	18	53.292	13	53.271	18
Z.Y.Liu et al. (2003a)[26]	53.270	19	53.292	12	53.233	51	53.282	6	53.267	12	53.292	13	53.280	13
Z.Y.Liu et al. (2003b)[26]	53.275	25	53.292	12	53.235	49	53.282	6	53.271	10	53.292	12	53.282	12

Table 2 Comparison of the measured data and evaluated data by different evaluation methods of γ emission probability P_γ(477.6 keV)for ^{7}Be

Authors	Measurement		WM		LRSW		NR		RA		MBAYS		DM	
Tayor et al. (1962)[27]	10.32	16	10.32	16	10.32	16	10.32	16	10.32	16	10.32	16	10.32	16
Poenitz et al. (1973)[28]	10.42	18	10.364	120	10.370	127	10.364	120	10.364	120	10.364	120	10.364	120
Goodier et al. (1974)[29]	10.35	8	10.354	66	10.357	85	10.354	66	10.354	66	10.354	28	10.354	66
Balamuth et al. (1983)[30]	10.10	45	10.349	66	10.348	82	10.349	66	10.349	66	10.349	32	10.349	66
Davids et al. (1983) [31]	10.61	23	10.369	63	10.375	73	10.369	63	10.369	63	10.369	47	10.369	63
Donoghue et al.(1983)[32]	10.60	50	10.372	63	10.379	72	10.372	63	10.372	63	10.372	43	10.372	63
Donald et al. (1983) [33]	10.90	50	10.380	62	10.389	70	10.380	62	10.380	62	10.380	48	10.380	62
Mathews et al. (1983)[34]	10.70	20	10.409	59	10.416	66	10.409	59	10.409	59	10.409	56	10.409	59
Norman et al. (1983) [35]	9.80	50	10.400	59	10.405	62	10.400	59	10.400	59	10.400	58	10.400	59
Evans et al. (1984) [36]	10.40	70	10.400	59	10.405	61	10.400	59	10.400	59	10.400	54	10.400	59
Fisher et al. (1984)[37]	10.61	17	10.423	56	10.423	73	10.423	56	10.423	56	10.423	53	10.423	56
Skelten et al. (1984) [38]	10.49	7	10.449	44	10.449	44	10.449	44	10.449	44	10.449	41	10.449	44

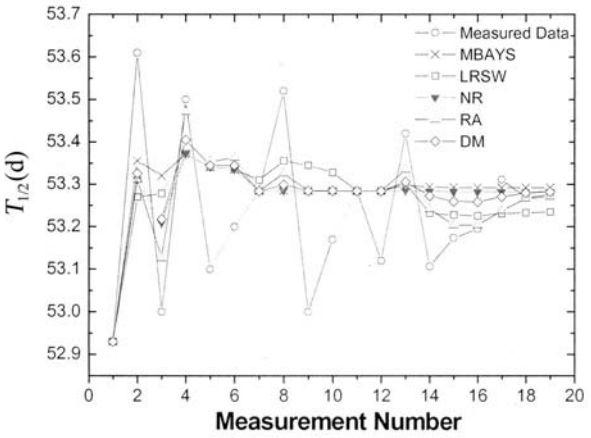

Fig.1 Comparison of the measured data and evaluated data by different evaluation methods for the half-life of ^{7}Be

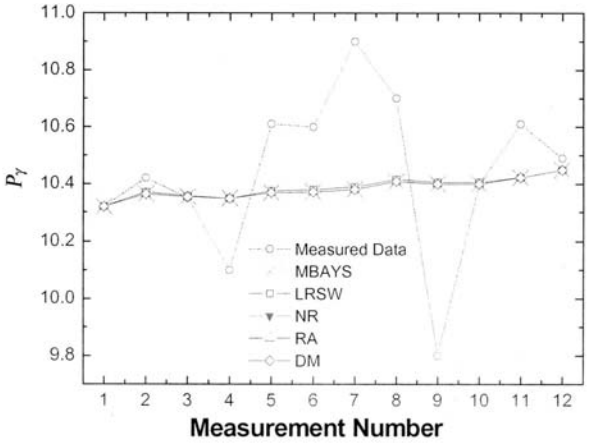

Fig.2 Comparison of the measured data and evaluated data by different evaluation methods for P_γ(477.6 keV) of ^{7}Be

3 Decay Scheme

The decay scheme of ^{7}Be is shown in Fig.3.

The decay energy Q_{ε}=861.89±0.07 keV[39]. The ε branching ratios P_{ε}(to ground state of ^{7}Li)=89.55± 0.04 and P_{ε}(to 477.6 keV state of ^{7}Li)=10.45±0.05 are deduced from %ε=100 of ^{7}Be and P_{γ}(477.6 keV γ-ray)=10.45±0.04%. The *logft* values are calculated by LOGFT code.

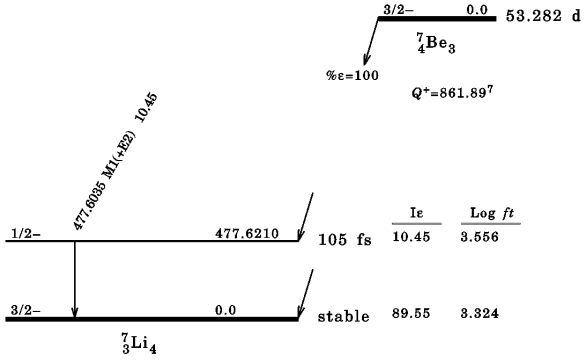

Fig. 3 The Decay scheme of ^{7}Be radionuclide

4 Comparison with other evaluations

The present evaluated half-life and γ emission probability are compared with other evaluations and listed in Table 3.

Table 3 Comparison of the evaluated half-life and γ remission probability for ^{7}Be radionuclide

$T_{1/2}$, days	P_{γ}(477.6 keV γ-ray)/ %	References
53.282±0.012	10.45±0.04	Present work
53.22±0.06	10.44±0.04	E.Browne et al.[1]
53.26±0.05	10.45±0.05	ZHOU Chunmei et al.[2]
53.29±0.07	10.52±0.06	R.B.Firestone et al.[3]
53.23±0.06	10.60±0.20	T.Horiguchi et al.[4]

5 Conclusion

Several evaluation methods were applied in evaluating the half-life and γ emission probability of ^{7}Be. On the basis of the new measurements, the half-life and γ emission probability of ^{7}Be are deduced using DM method (Double Mean method) and recommended to be $T_{1/2}$=53.282±0.012 days and P_{γ}=10.45±0.04%, respectively.

References

[1] E.Browne et al., CEA-R-5990, 2001.
[2] ZHOU Chunmei, Huang Xiaolong, INDC(CPR)-043/L, 62(1997).
[3] R.B.Firestone et al., Table of Isotopes, Vol. I, 1996.
[4] T.Horiguchi et al., Chart of Nuclides, 1992.
[5] W.L.Zijp, ECN-179, 1985.
[6] M.J.Woods, A.S.Munster, NPL Report RS(EXT)95, 1988.
[7] P.W.Gray et al., Nucl. Instrum. Methods A 286, 569(1990).
[8] S.I.Kafala et al., Nucl. Instrum. Methods A 339, 151(1994).
[9] M.F.James et al., AEA-RS-1082, 1992.
[10] M.U.Rajput et al., Nucl. Instrum. Methods A 312, 289(1992).
[11] Wang Baosong et al., to be published in 2004.
[12] E.Segre et al., Phys. Rev., 75, 39(1949); Phys. Rev., 81, 284(1951).
[13] J.J.Kraushaar et al., Phys. Rev., 90, 610(1953).
[14] R.Bouchez et al., J. Phys. Radium, 17, 363(1956).
[15] H.W.Wright et al., Nucl. Sci. Eng., 2, 427(1957).
[16] J.B.A.Eugland, Nucl. Phys., 72, 449(1965).
[17] R.Vaninbroukx et al.,Int.J.Appl.Radiat.Isotop. 17, 41 (1966)
[18] J.S.Merritt, AECL-3512, 30(1969).
[19] H.W.Johlige et al.,Phys.Rev. C2, 1616(1970)
[20] P.J.Cressy, Nucl. Sci. Eng., 55, 450(1974).
[21] F.Lagoutiue et al., Int. J. Appl. Radio. Isotopes, 26, 131(1975).
[22] A.R.Rutledge et al., NBS-SP=626, 1982.
[23] M.Jaeger et al., Phys. Rev. C54, 423(1996).
[24] C.A.Huh et al., J.Radioanal.Nucl.Chem. 246, 229 (2000).
[25] E.B.Norman et al., Phys.Lett. 519B, 15 (2001).
[26] Z.Y.Liu et al.,Chin.Phys.Lett. 20, 829 (2003).
[27] Tayor and Merritl, Can. J. Phys., 40, 926(1962).
[28] Poenitz and Devopl, Int. J. Appl. Radio. Isotopes, 24, 471(1973).
[29] Goodier, Mekepeace and Williams, Int. J. Appl. Radio. Isotopes, 25, 373(1974).
[30] Balamuth et al., Phys. Rev., C27, 1724(1983).
[31] Davids et al., Phys. Rev., C28, 885(1983).
[32] Donoghue et al., Phys. Rev., C28, 875(1983).
[33] Knapp Mc Donald et al., Nucl. Phys., A411, 195(1983).
[34] Mathews et al., Phys. Rev., C28, 879(1983).
[35] Norman et al., Phys. Rev., C27, 1728(1983).
[36] Evans et al. Can. J. Phys, 62, 1139(1984).
[37] Fisher and Hershbergen, Nucl. Phys., A423, 121(1984).
[38] Skelten and Kavanagh, Nucl. Phys. A414, 141(1984).
[39] G.Audi et al., Nucl. Phys. A729, 337(2003)

Linear Fit of Correlative Data by Least Squared Method

LIU Tingjin SUN Zhengjun

China Nuclear Data Center, CIAE, P.O.Box 275(41), Beijing 102413, P.R.China

【**abstract**】 *On base of the least-square method, the formulas for linear fitting the correlative data were deduced and a program for linear fitting multi sets of correlative experimental data was developed. With the code, the fit values and their covariance matrices in different formats can be calculated. The correctness of the code was tested in different ways. The code has been practically used for the evaluation of fission yield data and reasonable results have been obtained. There are many of features for the linear fitting of correlative data, which should be paid attention to and studied thoroughly. The fit values are changed with the correlation increasing degree of the input data, and outside of a reasonable region in the case that the input data are statistically inconsistent and strong correlation. The error of the fit value is increased with the increasing of the input data correlation. The correlation of the fit values is not only transformed from the correlation of the input data, but also produced in the fitting.*

Introduction

As well known, the linear fit of the experimental data by least squared method is often faced, where the fit coefficients a, b and their error can be calculated in the conditions that the reduced χ^2 is minimum[1]. But in tradition, the data to be fitted are supposed to be statistically independent with each other, e.g. only the error itself is but the correlation between the data is not considered. This suppose is not held in many practical case, for example, for the fission yield data measured at different energy points, the error is comes from statistical count, fission rate, detector efficiency, decay data used and etc. Only the statistical count is statistically independent for the data at different energy points, while the error of fission rate, decay data used, detector efficiency is long or middle range one, which make the data at different energy points correlation and usually they are quite larger than statistical one. As discussed in section 3, comparing the traditionally statistically independent linear fit, there are many new important features for the correlative linear fit, which is not familiar with and even not paid attention to.

In this paper, physical and mathematics model for the fitting is given in Section 1, based on which the program was developed. The program and its test are presented in Section 2. The features of the correlative data fitting is given in section 3. The practical application of the code is presented in Section 4. And at last, there are some conclusion remarks in Section 5.

1 Physical and Mathematics Model of Correlative Linear Fitting

1.1 Linear-Linear Fit

Let express the measured data assembly with $\{x_i,y_i\}$ i=1, 2,⋯ , N, namely $\{X,Y\}$ and the covariance matrix of Y is V_Y. The vector $\boldsymbol{Y}$ should be a linear function of vector $\boldsymbol{X}$, or the vector $\boldsymbol{Y}$ can be fitted with a linear function of vector $\boldsymbol{X}$, namely should be $Y=aX+b=c_1X+c_2$, and the parameter vector $C^{\mathrm{T}}=(c_1,c_2)$. According to the least squared method, making the reduced

$$\chi^2=(Y-\hat{Y})^T V_Y (Y-\hat{Y})/(N-2)=\text{minimum}$$

Then, the optimum value of the parameter vector

$$\hat{C}=(F^T V_Y^{-1} F)^{-1} F^T V_Y^{-1} Y \tag{1}$$

The covariance matrix of the fit parameters

$$V_{\hat{C}}=(F^T V_Y^{-1} F)^{-1} \tag{2}$$

The fit values

$$\hat{Y}=F\hat{C} \tag{3}$$

The covariance of fit values

$$V_{\hat{Y}}=FV_{\hat{C}}F^T \tag{4}$$

Where

$$F^T = \begin{bmatrix} x_1 & x_2 \cdots x_N \\ 1 & 1 \cdots 1 \end{bmatrix} \quad (5)$$

1.2 Logarithm-Linear Fit

If the data can be fitted with function $y' = b'e^{a'x}$, make a transformation

$$y = \ln y' = \ln b' + a'x = b + ax$$

where $b = \ln b'$, $a = a'$ and

$$\Delta y = \Delta \ln y' = \Delta y' / y' = \Delta y'_R$$

Namely $V_Y = V^R_{Y'}$, where $\Delta y'_R$ is the relative error of measured data y', and $V^R_{Y'}$ is the relative covariance matrix of vector $\boldsymbol{Y}'$.

For vector $\boldsymbol{Y}$ and its covariance matrix V_Y, the formulas given above can be used to calculate the optimum parameters $\hat{C}$, fit values $\hat{Y}$ and their covariance matrices $V_{\hat{C}}$, $V_{\hat{Y}}$.

For the calculated quantities, make a transformation again

$$y'_i = e^{x_i}, \quad V'_{ij} = V_{ij} y'_i y'_j$$

From which, the quantities required, namely fit values Y' and their covariance matrix $V_{Y'}$, can be obtained.

2 Program and its Test

According to the formulas given above, a program was developed. Using the code, the fit coefficients $\hat{C}$, fit values $\hat{Y}$ and their covariance matrices $V_{\hat{C}}$, $V_{\hat{Y}}$ can be calculated. Also the reduced $\chi^2_1 = (Y-\hat{Y})^T V_Y (Y-\hat{Y}) / (N-2)$ and $\chi^2_2 = \sum_{i=1}^{N} \left[(y_i - \hat{y}_i)^2 / \Delta y_i^2 \right]$ are given to know what level of the fitting is reached. For the convenience of using, the calculated covariance matrix is given in different forms, including absolute covariance matrix V^A, relative covariance matrix V^R and correlation coefficient matrix. V^ρ. The relationships between them are

$$V^R_{ij} = V^A_{ij} / y_i y_j, \quad V^\rho_{ij} = V^A_{ij} / V_{ii} V_{jj}$$

The input data include multi sets of measured values $\{x_i, y_i\}_j$ i=1, 2, ···, N_i, namely $\{\boldsymbol{X}, \boldsymbol{Y}\}_j$ j=1, 2,···, J, and the covariance matrix of Y_j is V_{Yj}. There are altogether J sets of data and N_i data points for ith set of data. For the convenience of using, the input covariance matrices are allowed in different formats for each set of data: absolute covariance matrix V^A, relative covariance matrix V^R and correlation coefficient matrix. V^ρ which is indicated by a flag number in the input file. Also there is an option for linear-linear or logarithm-linear fitting in the input file.

There are three output files: one(fort.3) is for reduced χ^2, fit coefficients and its covariance. The other one(fort.4) for fit values at the given points and their covariance V^A, V^R and V^ρ. The multi sets of data and their covariance matrices for each set of data are merged into one large vector and one absolute covariance matrix for calculation by using formulas given in Section 1. The merged vector and its covariance matrix are given in the third output file(fort.9).

The correctness of the code was tested in the following different ways.

1) If only input one set of no-correlation data, namely the input covariance matrix is diagonal, the fitting is reduced into usual linear fitting, which also can do with our another code LIFIT[1]. Some examples show that the results from two codes are the same.

2) Take the input data to be fitted y as 1.0 and the error of y as 0.05 for all x from 1 to 20 in a step by 1.0. Fitting the data, the result is shown in Fig. 1. It can be seen that the fit values are 1.0 for all x. The errors of the fit values are symmetrical around the middle point of x=10, and are considerably reduced, which is dependent on the input data point number. At the middle, the error is reduced by about $1/\sqrt{20}$, here 20 is the point number of the input data, and at the two ends, the errors are reduced by about $1/\sqrt{5}$. All of these results are reasonable from the physical and statistical point of view.

3) Take another example, in which the all of y are the same as x for all x from 1 to 20 in a step by 1, and the error of y are 5.0 for all y. Fitting the data, the result is shown in Fig.2. It can be seen that the fit curve is a straight line with a slope of 45° relative to the abscissa. And the errors of the fit values are also symmetrical around the middle point of x=10, and reduced by about $1/\sqrt{20}$ at the middle and about $1/\sqrt{5}$ at the two ends. The results are reasonable and respected.

3 The Features of the Correlative Data Fitting

3.1 The Fit Value

The fit values are changed with the correlation degree of the input data, which can be expressed by the correlation coefficient intuitively, but the change magnitude depends on the statistical agreement degree of the data to be fitted. If the input data are a straight line exactly, the fit values are not changed with their correlation coefficient. If the input data are in statistically consistence, the fit values are changed with their correlation coefficient in a reasonable region. If the input data are not in statistical consistence, the fit values can be changed outside of a reasonable region, so called the PPP[2] problem happens. The more statistically inconsistent and more correlative the input data are, the more changed and the more unreasonable the fit values are. An example is given in Fig.3. It can be seen from the figure that the input data are quite discrepant, and the fit values are changed with the correlation coefficient ρ_0 of input data considerably. When the ρ_0=0.95, the fit values are all smaller than the all input experimental data due to the relatively small errors of the data with smaller values of input data. If the errors of the second and fifth points of the input data are changed smaller by about half and make the same fit, then the fit values are all larger than all input experimental data (Fig.4) due to the relatively small errors of the data with larger values of input data. If delete the second and fifth points of the input data, the fit values are reasonable and PPP problem is disappeared(Fig.4) due to the input data are statistically consistent.

3.2 The Errors of the Fit Values

In Fig. 5 is shown that the errors of the fit values are how to change with the errors of the input data in the case of the correlation coefficient ρ_0=0.0 of the input data. When the errors of the input data are all 0.05, the errors of the fit values are symmetrical around the middle point, as pointed in the item 3 of Section 2. If the input error at middle point is changed to 0.01 and the others are still remained as 0.05, the errors of all fit values are reduced considerably. The smallest one is at middle and smaller than 0.01. If the error of last input data is changed to 0.01(others are remained as 0.05), the errors of the second half of the fit values (in x range from 10 to 20) are reduced considerably, but the smallest one is not exactly at, only near this last point. If do the same but changed to 0.01 at last second point, the same result is obtained, only the curve is shifted to the left somewhat. From above, it can be deduced that the smallest error of the input data, even only one data point, effect the errors of the all fit values, especially the data points nearby considerably, and the smallest one of the fit values must be smaller than this one. This is easily understandable from statistics point of view.

The error of the fit value is changed with the increasing degree of the input data correlation. The more correlation of the input data, the larger the error of the fit value. When the correlation coefficient is close to one, the error of the fit value is close to the input one. In Fig. 6 is shown an example, where the errors are 0.05, the same for all input data. It can be seen that the errors of fit values are increased with increasing of the correlation coefficient of the input data. And also the error curves become flat with the correlation increasing. When the correlation coefficient ρ_0=0.0 of the input data, the curve is symmetrical and the minimum at the middle point x=10. When the correlation coefficient ρ_0=0.95 of the input data, the curve goes near to a straight line and close to 0.05, the error of the input data.

3.3 The Correlation of the Fit Values

The Correlation of the fit values depends on the correlation of the input data. In Fig.7 is shown as an example that the correlation between the data point at 1 MeV and other data points of fit values for different correlation coefficients ρ_0 of input data. It can be seen that the correlations between the data points nearby 1 MeV of the fit values are always very strong (the correlation coefficients ρ are almost 1.0), no matter how much ρ_0 is. But the correlations between the data point at 1 MeV and other data points far from 1 MeV are increased considerably with increasing the correlation of the input data. When the correlation of the input data is small, e.g. ρ_0=0.1, the correlation coefficients are very small, even become negative. With increasing the correlations of the input data, the correlation coefficients go near to 1.0. It can be deduced from the results mentioned above that the correlation of the fit values is not only transformed from the correlation of the input data, but also produced in the fitting, so even there is no correlation of the input data (ρ_0=0.0), there is still correlation for fit value and even quite strong for the data points nearby. In Fig.8 is shown the correlation coefficients of the data at different data points with others in the case that the correlation coefficient of the input data is 0.0. It can be seen that the correlations between the data points nearby are quite strong and become weak for the data points far away. Also the curves are changed regularly for different data points.

4 Practical Application

The code has been practically used for the fission yield data evaluation of important fission products from ^{235}U[3] and ^{238}U[4]. The multi sets of evaluated experimental data were fitted with the code taking into the correlation for each set of data. Here, a set of data is processed as that their correlation comes from

same sources, no matter they were measured by same author or not. In fact, if the yield data were measured by same author for one product nuclide at different energy points, the errors of the detector efficiency, decay data used and maybe the fission rate are long range one and contribute to the correlation of the data. If the yield data were measured by different author for same product nuclide at different energy points, the errors of the decay data used are also long range one and contribute to the correlation of the data too. So in the later case, for convenience of processing, that kind of data is taken as one set of data in the fitting. In Figs.9 and 10 are shown two practical examples of the evaluation results for ^{235}U and ^{238}U respectively. It can be seen that the errors of fit values for ^{144}Ce from ^{235}U fission are quite small for all data points and although the experimental data points are not so many, this is because that there are two data points with very small errors (less that 3%) at 1.95 and 14.8 MeV, as pointed out above, by which the errors of all fit values were effected. The errors of fit values for ^{99}Mo from ^{238}U fission are not small for all data points and even the experimental data points are quite more, this is because that the errors of all data points are quite large and no data with very small error. As an example, the correlations of the fit values are shown in Fig.11 for ^{144}Ce from ^{235}U fission. It can be seen that the correlation between the data points nearby are quite strong and the correlations between the data at different energy points with others are changed regularly.

5 Conclusion Remarks

On base of the least-square method, the formulas for linear fitting the correlative data were deduced and a program for linear fitting multi sets of correlative experimental data was developed. Using the code, the fit values and their absolute, relative covariance matrix and correlation coefficient matrix can be calculated. The correctness of the code was tested in different ways. The code has been practically used for the evaluation of fission yield data and reasonable results have been obtained.

Comparing with the traditional linear fitting, where the correlation of the data to be fitted is not considered, there are many of features for the linear fitting of correlative data, which are not familiar with, should be paid attention to and studied thoroughly. The fit values are changed with the correlation increasing of the input data, and outside of a reasonable region in the case that the input data are statistically inconsistent and strong correlation, so called the PPP problem happens. The error of the fit value is increased with the increasing of the input data correlation. The correlation of the fit values is not only transformed from the correlation of the input data, but also produced in the fitting.

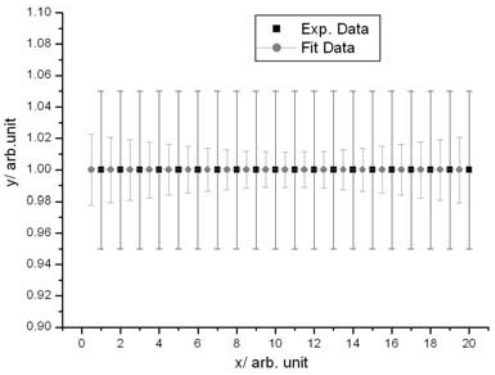

Fig.1 The correlative data fitting for a horizontal line

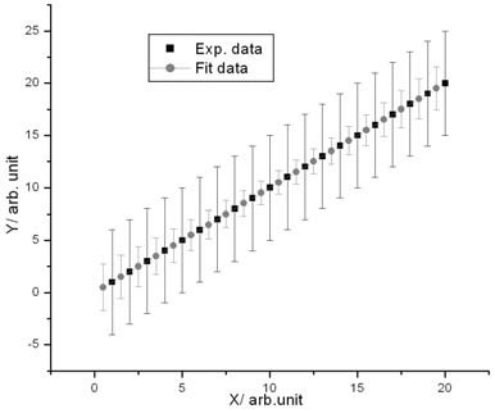

Fig.2 Correlative data fitting for a straight line with a slope 45° relative to the abscissa

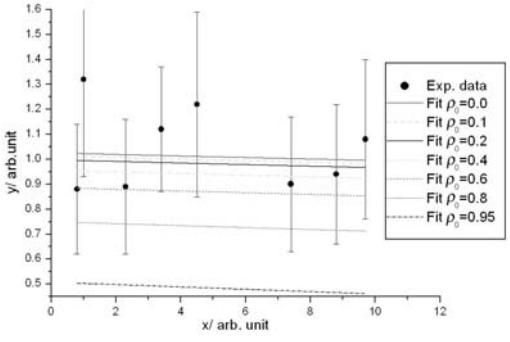

Fig.3 The dependence of fit values on input coefficient ρ_0

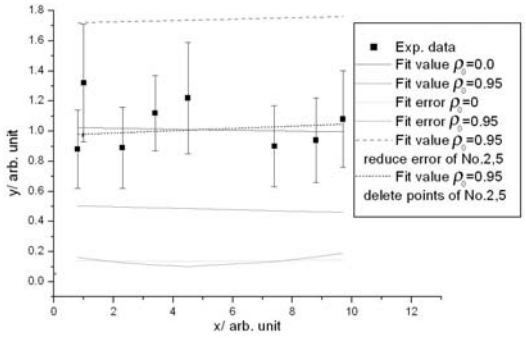

Fig.4 Exploring on PPP problem

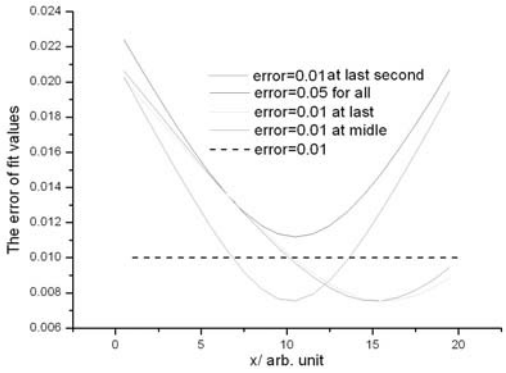

Fig.5 The error dependence of fit values on input ones

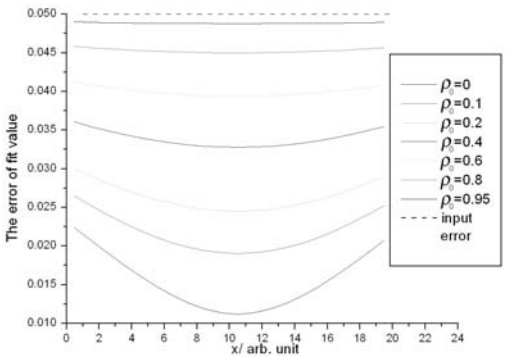

Fig.6 The dependence of the fit values's error on the correlation coefficient ρ_0 of the input data

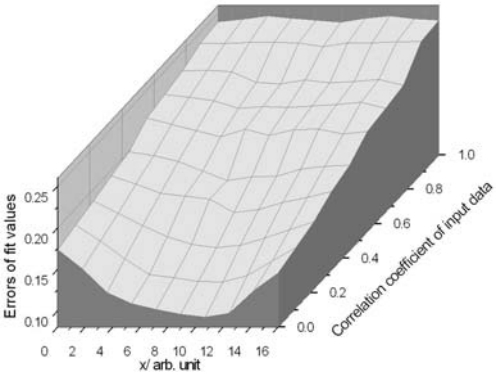

Fig.7 The dependence of the error of fit values on correlation coefficient of input data and energy

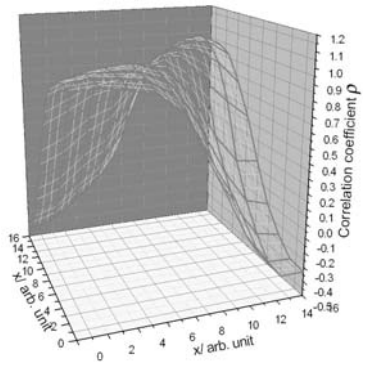

Fig.8 The CC(correlation coefficient) ρ matrix of fit values(CC of input data ρ_0=0.0)

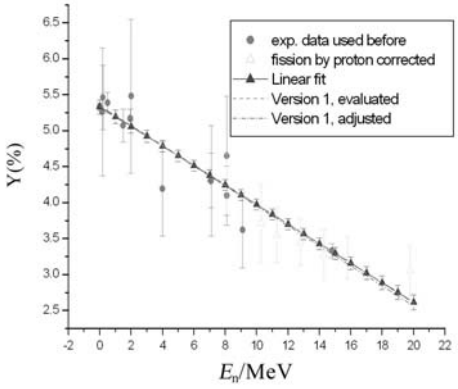

Fig.9 ^{144}Ce yield from ^{235}U fission as function of energy

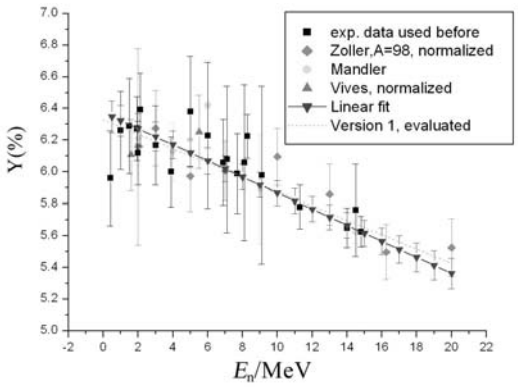

Fig.10 ^{99}Mo yield from ^{238}U fission

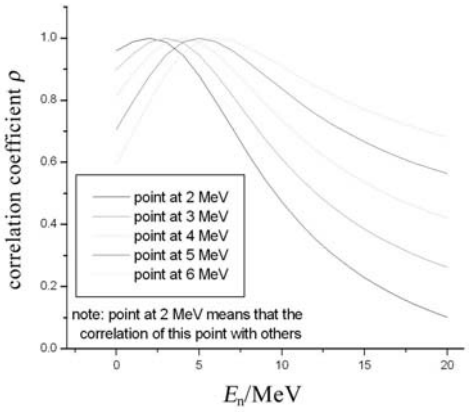

Fig.11 The correlation between the linear values for ^{144}Ce from ^{235}U fission

References

[1] LIU Tingjin, et al. CNDP, 19,103 (1998)
[2] P. Peelle. Private communication (1987)
[3] LIU Tingjin, et al. Internal report, to be published (2003)
[4] LIU Tingjin, et al. Internal report, to be published (2003)

Model Calculation of Neutron Reaction Data for ^{31}P in the Energy Range from 0.1 to 20 MeV

LI Jiangting[1] GE Zhigang[2] SUN Xiuquan[3]

[1]*Physics Department, Northwest University, Xi'an 710069 P.R.China*

[2]*China Nuclear Data Center, CIAE, P.O.Box 275(41), Beijing 102413, P.R.China*

[3]*Engineering and Technology Department, Shenzhen University, Shenzhen 518000, P.R.China*

【abstract】 *The neutron data calculation of ^{31}P in the energy range from 0.1 to 20 MeV was carried out. The neutron optical potential parameters for ^{31}P in energy range from 0.1 to 20 MeV were obtained, based on the fitting of the available neutron experimental data with the code APOM94. The DWUCK4 code was used to investigate the cross section for neutron direct inelastic scattering. The re-evaluated neutron data is based on the available measured data by using the UNF code. The theoretical results reproduce the experimental data well, and the results were given in ENDF/B-6 format.*

Introduction

^{31}P is the only stable isotope of element phosphorus. There are some evaluated files for ^{31}P, such as in ENDF/B-6 and JENDL3.3 . The evaluation of ^{31}P was done for ENDF/B-6 in 1997 and for JENDL3.3 in 2001, which still needs to be improved. Based on the newer and more reliable experimental data, the model calculation of n+^{31}P was performed to improve the neutron reaction data. The experimental data of ^{31}P from neutron-induced reaction with energy lower than 20 MeV were collected from EXFOR and current publications. According to the experimental data and using UNF code, the neutron data were calculated, compared with the data of ENDF/B-6, JENDL3.3 and available experimental data.

1 Model Calculations and Parameters

The code APOM94[1] is used to get the neutron optical potential parameters with energy region from 0.1 to 20 MeV based on the available measured data, such as total cross section, non-elastic scattering cross section and elastic angular distributions.

From fitting the total, non-elastic scattering cross section and elastic angular distributions, the parameters of neutron optical potential were determined by the code APOM94, which are shown in Table 1. In this work the spherical optical potential is employed to calculate cross sections mentioned above. The phenomenological optical potential includes the following parts:

The total optical potential is given as follows

$$V_{op}(r) = V_R(r) + i[W_s(r) + W_v(r)] + V_{so} + V_c$$

The parameters of the neutron optical potential are also employed as input data for the DWUCK4 code in order to get the cross sections for neutron direct inelastic scattering.

The UNF code[3] written in FORTRAN-90 is developed for calculating fast neutron reaction data of structure materials with incident energies from about 1 keV up to 20 MeV. The code consists of the spherical optical model, the unified Hauser-Feshbach and exciton model. The theoretical improvements have been made.

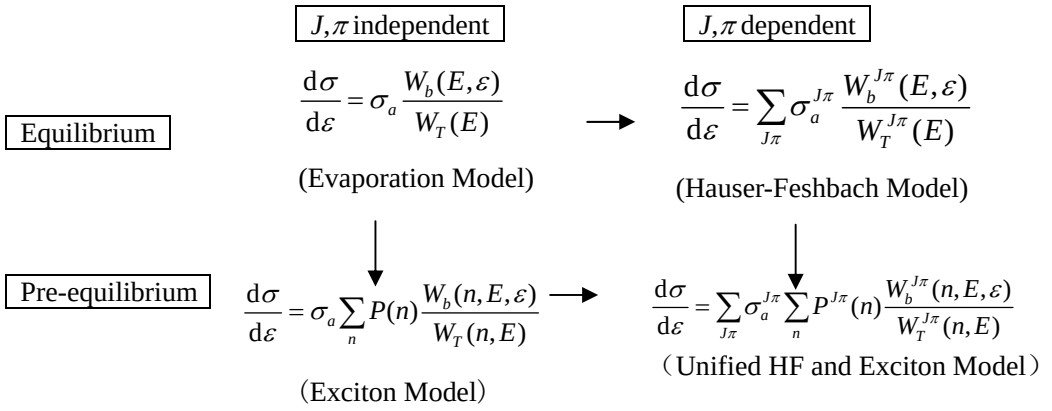

Table 1 Optical Potential Parameters

	unit	n	p	α	^{3}He	d	t
A_R	fm	0.720 711 71	0.5	0.72	0.72	0.81	0.75
A_S	fm	0.554 884 20	0.51	0.60	0.88	0.68	0.75
A_V	fm	0.473 661 93	0.51	0.60	0.88	0.68	0.75
A_{So}	fm	0.720 711 71	0.5	0.72	0.72	0.81	0.75
X_R	fm	1.140 862 46	1.13	1.2	1.2	1.15	1.2
X_S	fm	1.210 889 22	1.13	1.20	1.20	1.34	1.20
X_V	fm	1.231 324 20	1.13	1.20	1.20	1.34	1.20
X_{So}	fm	1.140 862 46	1.13	1.20	1.20	1.15	1.30
X_C	fm	1.250 000 00	1.25	1.30	1.30	1.15	1.30
U_0	MeV	–0.514 118 67	–2.7	0.0	0.0	0.0	0.0
U_1	MeV	–0.190 003 38	0.22	0.0	0.0	0.0	0.0
U_2	MeV	–0.000 055 17	0.0	0.0	0.0	0.0	0.0
V_0	MeV	57.913 665 77	54.0	151.9	151.9	81.00	165.0
V_1	MeV	–0.676 995 34	–0.32	–0.17	–0.17	–0.22	–0.17
V_2	MeV	0.000 098 42	0.0	0.0	0.0	0.0	0.0
V_3	MeV	–24.000 000 00	24.0	50.0	50.0	0.0	–6.4
V_4	MeV	0.000 000 00	0.4	0.0	0.0	2.0	0.0
V_{So}	MeV	6.199 999 81	6.2	2.5	2.5	7.0	2.5
W_0	MeV	11.910 427 09	11.8	41.7	41.7	14.4	46.0
W_1	MeV	–0.117 478 94	–0.25	–0.33	–0.33	0.24	–0.33
W_2	MeV	–12.000 000 00	12.0	44.0	44.0	0.0	–110.0

A_{2S}=0.7 fm, A_{2V}=0.7 fm

The angular momentum conservation is considered in whole reaction processes for both equilibrium and pre-equilibrium mechanism. The recoil effects in varied emission processes are taken into account strictly, so the energy balance can be held exactly. A method for calculating double-differential cross section of composite particles is proposed and is used in UNF code. The parameters of density level, giant dipole resonance, the nuclear level scheme, pair corrections were taken from RIPL[4].

2 Calculated Results

The cross sections have some complicated structure in the energy range below 5 MeV, so there are obvious resonance structures. The resonance parameters were directly taken from ENDF/B-6 in the resonance energy region. Fig.1 shows our results for fitting the experimental data on total cross section and the comparison with the ENDF/B-6 and JENDL3.3. It can be seen that they are in agreement basically, the deviation with ENDF/B-6 is shown at energy around 15~20 MeV. The data of ENDF/B-6 is lower than the measured data from 15 MeV to 20 MeV.

Fig.2 gives the comparisons of the calculated results with the experimental data of ^{31}P for elastic differential cross section at 4.8, 5.95, 7.79 and 9.05 MeV. It is clear that the UNF calculated elastic differential cross section are in good accordance with the experimental data given by J.D. Brandenberger[5] at 9.05 MeV. The deviation is shown at energies of 4.8, 5.95 and 7.79 MeV around 100 degree. From the Fig.2, in which the data given by K.T Sukada[6], J. Martin[7] and J.D. Brandenberger, JENDL3.3 is apparently higher than the experimental data and our calculated values are in good agreement with the experimental data.

Fig.3 shows the cross section of (n,γ) for ^{31}P calculated with the UNF code. Based on the data given by Csikai[8] in 1968 we got calculated (n,γ) reaction cross sections of ^{31}P. One can see that the calculated (n, γ) reaction cross section of ^{31}P are in good accordance with the experimental data, while JENDL3.3 is apparently lower than the experimental data around 14 MeV.

Fig.4 gives the calculated and experimental ^{31}P(n,2n) reaction cross section and the comparison with the ENDF/B-6 and JENDL3.3. The experimental data was measured by M. Bormann[9] in energies from 13.2 to 19.7 MeV, T.Katoh[10] in energies from 13.4 to 14.9 MeV, J.M.Ferguson[11] in energies from 14.7 to 18 MeV, J.E.Strain[12] at 14 MeV, R.A. Sigg[13] at 14.6 MeV, etc. The calculated (n,2n) cross section is in good accordance with the experimental data, the curves pass through the experimental data within error bars and the ENDF/B-6 and JENDL3.3 are higher than the experimental data.

The cross section of ^{31}P(n,α) was evaluated carefully in neutron energy range from 0.1 to 20 MeV and compared with experimental data, as well as ENDF/B-6 and JENDL3.3. The experimental data was measured by P. Cuzzocrea[14] in energies from 3 to 5.09 MeV, F.Gabbard[15] in energies from 13.0 to 16.6 MeV, E.Zupranska[16] in energies from 13.0 to 17.8 MeV, M.Bormann[17] in energies from 13.2 to 19.7 MeV, A.Fessler[18] in energies from 16.0 to 20 MeV, etc. Fig.5 shows the result fitting for the experimental data on (n,α) cross section and the comparison with the ENDF/B-6 and JENDL3.3.

The comparison of calculated results with ENDF/B-6, JENDL3.3 and experimental data for ^{31}P (n,p) reaction cross sections are given in Fig.6. The calculated results are in good agreement with the experimental data and the curves pass through the experimental data smoothly.

There are no measured data for cross sections of (n,d) and (n,t) reactions, and the two reaction data are not included in ENDF/B-6.The evaluated data were taken from UNF code calculation. It seems that our calculated values are reasonable in physics.

The experimental data of ^{31}P(n,el) reaction were measured by K. Tsukada[19] in energy region from 3.5 to 4.8 MeV, L.Ya.Kazakova[20] at 2 MeV, Th. Schweitzer[21] at 3.4 MeV, B.Ramstein[22] at 6.4 MeV and G.C.Bonazzola[23] at 14.2 MeV. From the Fig .7 we can see that the curve passes through the average of data by K. Tsukada in energy region from 3.5 to 4.8 MeV. The non-elastic cross section was obtained by summing all the reaction cross sections.

3 Conclusion

The neutron data for ^{31}P were evaluated and recommended in energy range from 0.1 to 20 MeV by fitting the experimental data and UNF calculations. The theoretically calculated results were in good accordance with the experimental data. Our calculated values are both reasonable in shapes and in physics. The model calculation of n+^{31}P improved the neutron reaction data, in comparisons with ENDF/B-6, JENDL3.3. The theoretical results of ^{31}P with experimental data are given in figures of this paper.

Thanks to ZHANG Zhengjun, CHEN Guochang, SUN Zhengjun and ZHANG Jingshang for their explanation on the theory of the model calculation.

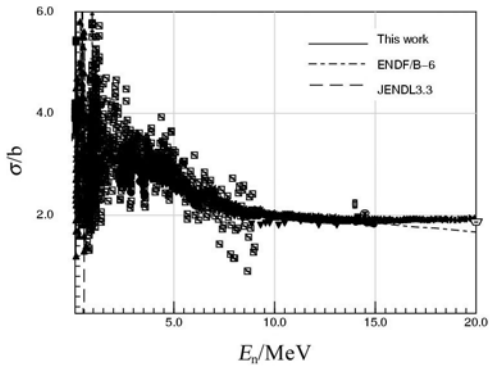

Fig.1 Comparison of neutron total cross section

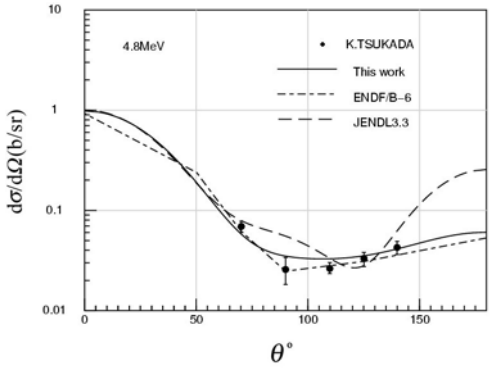

Fig.2(a) ^{31}P elastic differential cross section at 4.8MeV

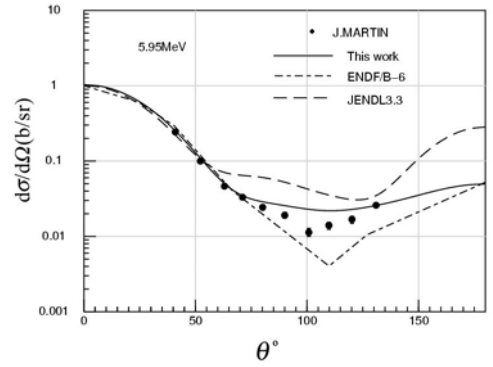

Fig.2(b) ^{31}P elastic differential cross section at 5.95MeV

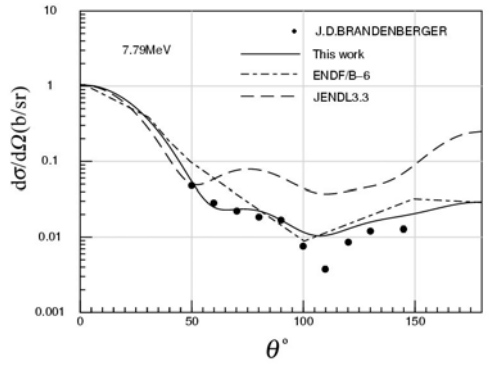

Fig.2(c) ^{31}P elastic differential cross section at 7.79MeV

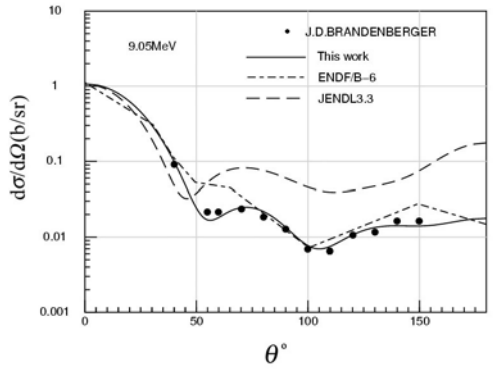

Fig.2(d) ^{31}P elastic differential cross section at 9.05MeV

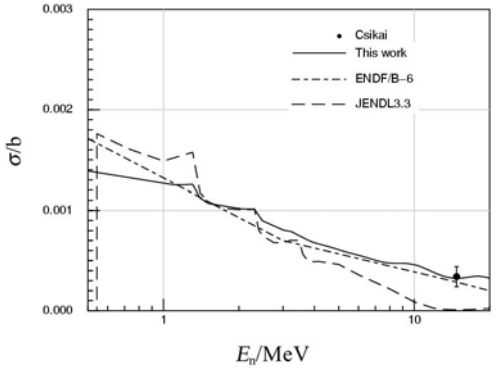

Fig.3 The cross section of (n,γ) for ^{31}P

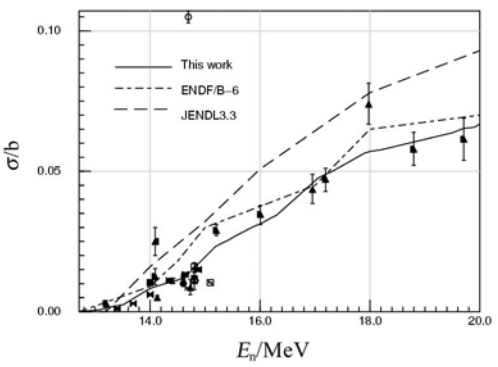

Fig.4 The cross section of (n,2n) for ^{31}P

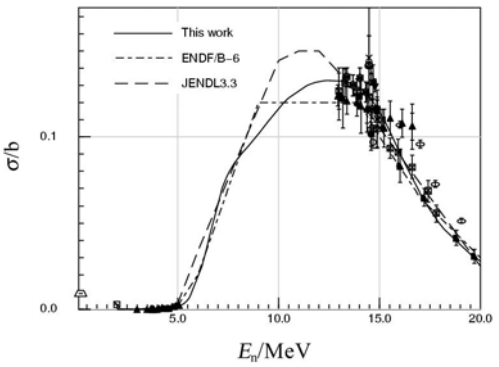

Fig.5 The cross section of (n, α) for ^{31}P

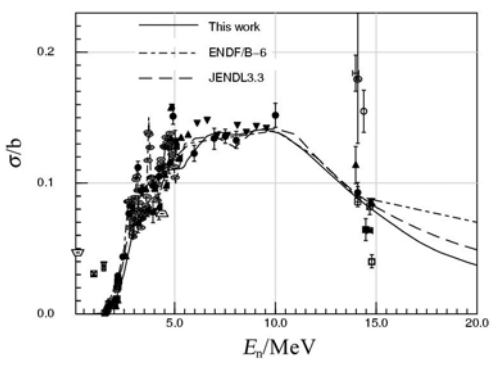

Fig.6 The cross section of (n, p) for ^{31}P

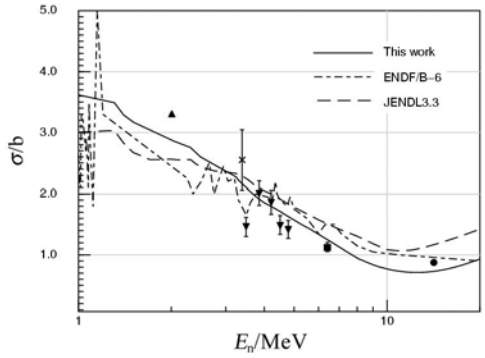

Fig.7 The elastic cross section of n+ ^{31}P reaction

References

[1] SHEN Qingbiao, CNDP, 7, 43, 1992
[2] P.D.Kunz, A DWBA Code DWUCK4, University of Colorado, USA (unpublished)
[3] ZHANG Jingshang, "User Manual of UNF Code", CNIC-01616, CNDC-0032, China institute of Atomic Energy, December 3, 2001
[4] P Oblozinsky et al., IAEA-TECDOC-1034, 1998
[5] J.D.Brandenberger, J,NP/A,196,65,7211
[6] K.Tsukada, C,61VIENNA,1,75,6108
[7] J.Martin, J,NP/A,113,564,6806
[8] J.Csikai, J,NP/A,95,229,6703
[9] M.Bormann, J,ZP,174,1,6302
[10] T.Katoh, R,JAERI-M-89-083,89
[11] J.M.Ferguson, J,PR,118,228,6004
[12] J.E.Strain, R,ORNL-3672,196501
[13] R.A.Sigg, T,SIGG,76
[14] P.Cuzzocrea, J,NP,48,686,6311
[15] F.Gabbard, J,PR,128,1276,62
[16] E.Zupranska, J,APP/B,11,853,8011
[17] M.Bormann, J,ZP,174,1,6302
[18] Fessler, J,NSE,134,(2),171,2000
[19] K.Tsukada, C,61VIENNA,1,75(18/12),6108
[20] L.Ya.Kazakova, S,EANDC-50,200,6507
[21] Th.Schweitzer, W,SEELIGER,781116
[22] B.Ramstein, J,JPR,37,6,651,7606
[23] G.C.Bonazzola, J,NP,68,369,6506

n+$^{59}_{27}$Co($E_n \leqslant 20$ MeV) Nuclear Data Calculation and Analysis

WANG Shunuan

China Nuclear Data Center, CIAE, P.O.Box 275(41), Beijing 102413, P.R.China

Introduction

Whole set of nuclear data calculation in ENDF/B-6 format for n+$^{59}_{27}$Co ($E_n \leqslant 20$ MeV) has been finished by using spherical optical model, coupled channel optical model, pre-equilibrium exciton model and Hauser-Fashbach equilibrium statistical model. The calculated cross sections, angular distributions, spectrum and double differential cross sections by using codes of APOM[1], ECIS95[2] and UNF[3] are compared with all existing experimental data for n+$^{59}_{27}$Co ($E_n \leqslant 20$ MeV) taken from EXFOR. The calculated results are analyzed from point of view of theoretical model and model parameters used. The work is for CENDL-3.

1 Brief Review of Exist ENDF/B-6, JENDL-3 and CENDL-2

There is only one element of Co with half-life $T_{1/2} \geq 5\times10^8$ a. CENDL-2 was finished in Sep.1985, in which the direct reaction calculation was not taken into account. ENDF/B-6 was finished in July-1989 and reviewed in Jun-1992. JENDL-3.3 was finished in Aug-1988 and reviewed in Apr-1994. The direct reaction contributions were taken into account properly for ten levels using DWUCK-4 code[4] in JENDL-3 evaluation.

2 Spherical Optical Model Calculation

All the n+$^{59}_{27}$Co ($E_n \leqslant 20$ MeV) existing experimental data for total cross section σ_t and non-elastic cross section σ_{non} as well as angular distributions of elastic cross sections $\sigma_{el}(\theta)$ at different energy points taken from EXFOR have been reviewed. According to all the existing experimental data of σ_t, σ_{non} and $\sigma_{el}(\theta)$ after 1970, with running code APOM by using n+$^{55}_{25}$Mn ($E_n \leqslant 20$ MeV)(because $^{55}_{25}$Mn, $^{59}_{27}$Co both are neighboring odd-odd nuclides) spherical optical model 21 parameters[5] as the initialed input data of the code, the whole set of optimum spherical optical model 21 parameters for n+$^{59}_{27}$Co ($E_n \leqslant 20$ MeV) has been obtained by automatically searching for main 14 parameters among 21 parameters based on the formula described in Ref.[3]. The 21 parameters searched and used in UNF code are shown in Table 1.

The calculated total cross section, elastic cross section and its angular distributions at different energies of 5, 5.44, 6.44, 7.55, 8.56, 1.8, 2.8, 3.8, 8.97, 11.01, 1.57, 2.07, 2.48, 3.04, 3.55, 3.88, 4.5, 5.5, 5.9, 6.5, 7.14, 7.5, 8.03, 8.4, 9.06, 9.5, 9.9, 3.4, 14.7 MeV contributed by different Labs, non-elastic cross section are compared with all experiments data and also with CENDL-2, ENDF/B-6 and JENDL-3. A satisfied agreement is obtained in general view, see Figs. 1~9.

3 Coupled Channel Optical Model ECIS95 Calculations

The direct inelastic scattering cross section and angular distributions for two excited discrete levels of $^{59}_{27}$Co have been calculated by coupled channel optical model codes of ECIS95[2] and PRECIS[6] using spherical optical model parameters obtained in the present work as mentioned above with deformed parameters of β_2=0.2 and β_4=0.02.

Table 1 Spherical optical model optimum 21 parameters for n+ $^{59}_{27}$Co ($E_n \leqslant 20$ MeV)

AR	0.64884752	AS	0.43459845	AVV	0.29399756	ASO	0.64884752
XR	1.24858582	XS	1.39492249	XV	1.33691561	XSO	1.24858582
XC	1.25						(in fm)
U0	–0.19159417	U1	0.18993407	U2	0.00082281	V0	55.37618256
V1	–0.59999192	V2	–0.01551631	V3	–24.0	V4	0.0
VSO	6.2	W0	11.14011288	W1	–0.28809050	W2	–1.2
							(in MeV)

4 Cross Sections, Spectrum, Double Differential Cross Sections of Pre-equilibrium and Hauser -Feshbach Equilibrium Statistical Model Calculation

In spectrum, double differential cross sections of pre-equilibrium exciton model calculations, the free parameter *K*-value of the square of the average two-body residual interaction matrix element formulated by C.Kalbach et al.[7] was taken as K=190 MeV^3. This consideration is referenced to our previous papers[8~11]. This value taken mentioned above means that in the calculation the pre-equilibrium contribution is considered very sufficiently. The calculated $\sigma(n,\gamma)$, $\sigma(n,inl)$, $\sigma(n,2n)$, $\sigma(n,p)$, $\sigma(n,t)$, $\sigma(n,\alpha)$ cross sections are compared with all existential measured data and also with CENDL-2, ENDF/B-6 and JENDL-3 as shown in Figs.10~15, respectively. There are no any experimental data for other reaction channels. From Fig.11 it can be seen clearly that the results of CENDL-2 and JENDL-3 are much lower than the experimental data at low energy range of 2~4 MeV in comparison with ENDF/B-6 specially with the newest data of Lashuk (1994 41186014). From this point of view, the present work presents best fitting with data not only in this energy range, but also in energy range of 9~15 MeV (also seeing the rather new data of ZHOU Hongyu (1988 30927004)). The results of the present work are a little higher than the data of Smithkov (1992 41155010) at energy range of 5~8 MeV. They may have some discrepancy between the two rather new data of Lashuk and Smithkov in energy range below 8 MeV. It is shown that the calculated $\sigma(n,2n)$, $\sigma(n,p)$, $\sigma(n,t)$, $\sigma(n,\alpha)$ cross sections are compared with existing experimental data [after 1970 for $\sigma(n,2n)$] and also with CENDL-2, ENDF/B-6 and JENDL-3 in Fig. 12~15 respectively. The results are reasonable and satisfied. We have calculated spectrum, double differential cross sections for n+ $^{59}_{27}$Co (n,inl) and compared with experimental data. In the present paper we only show the calculated double differential cross sections for n+ $^{59}_{27}$Co (n,inl) at 9.1 MeV with 30°, 60°, 90°, 120°, 150° compared with experimental data in Figs.16~20, respectively. The result looks perfectly nice.

In summary, the whole set of nuclear data calculation in ENDF-6 format for n+ $^{59}_{27}$Co ($E_n \leqslant 20$ MeV) has been carried out. From the agreement of the comparison between theoretical results and available experimental data it can be concluded that the model and its parameters used in the present work are rather suitable.

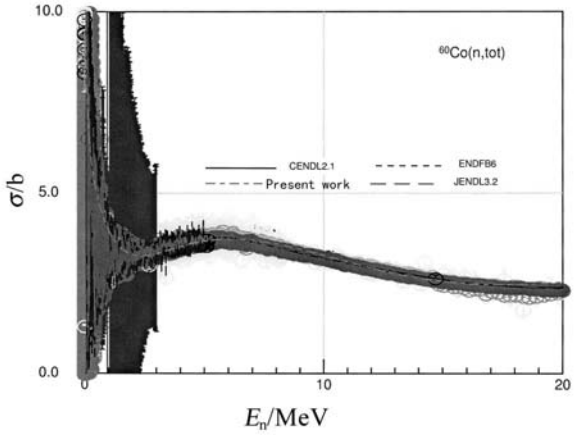

Fig.1 Calculated σ_t of n+ $^{59}_{27}$Co ($E_n \leqslant 20$ MeV) and compared with exp. data and ENDF/B-6, JENDL3, CENDL2

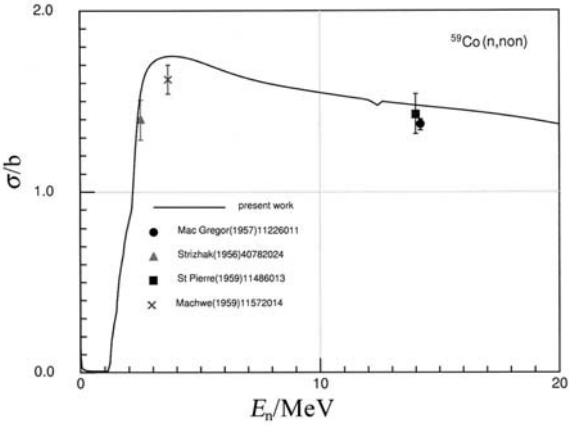

Fig.4 Calculated σ_{non} of n+ $^{59}_{27}$Co ($E_n \leqslant 20$ MeV) and compared with exp. data and ENDF/B-6, JENDL-3,CENDL2

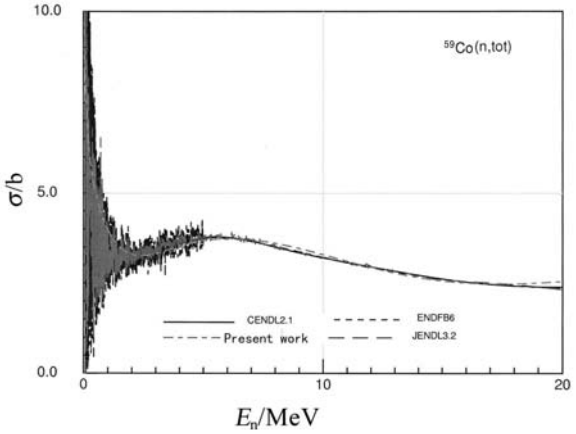

Fig.2 Calculated σ_t of n+ $^{59}_{27}$Co ($E_n \leqslant 20$ MeV) and compared with exp. data and ENDF/B-6, JENDL3, CENDL2

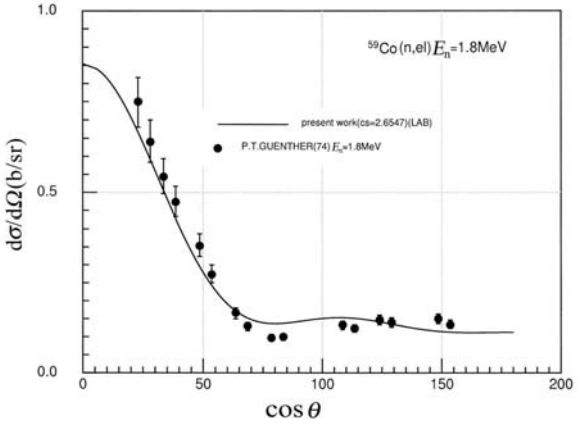

Fig.5 Calculated $\sigma_{el}(\theta)$ of n+ $^{59}_{27}$Co at E_n=1.8 MeV and compared with experimental data

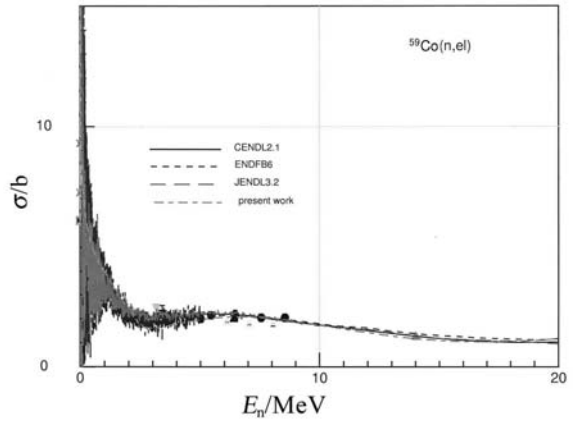

Fig.3 Calculated σ_{el} of n+ $^{59}_{27}$Co ($E_n \leqslant 20$ MeV) and compared with exp. data and ENDF/B-6, JENDL-3,CENDL2

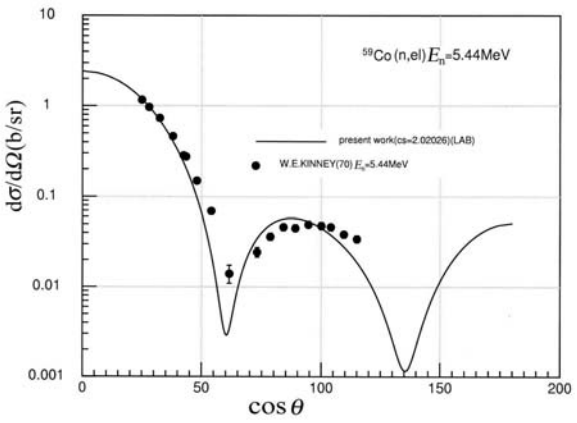

Fig.6 Calculated $\sigma_{el}(\theta)$ of n+ $^{59}_{27}$Co at E_n=5.44 MeV and compared with experimental data

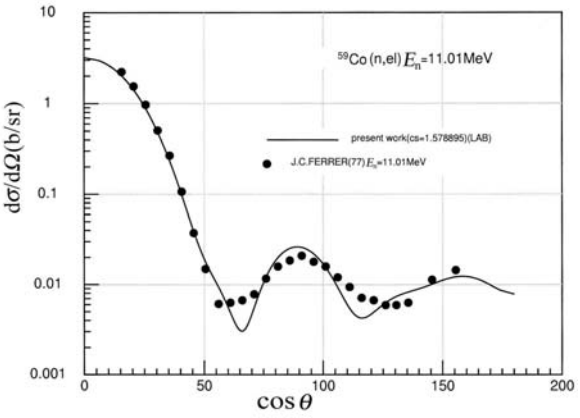

Fig.7 Calculated $\sigma_{el}(\theta)$ of n+ $^{59}_{27}$Co at E_n=8.97 MeV and compared with experimental data

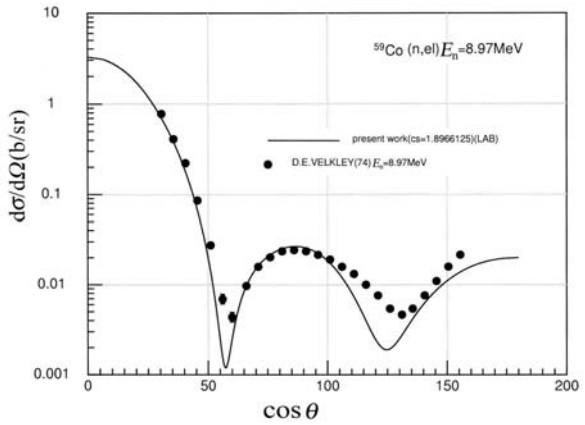

Fig.8 Calculated $\sigma_{el}(\theta)$ of n+ $^{59}_{27}$Co at E_n=11.01 MeV and compared with experimental data

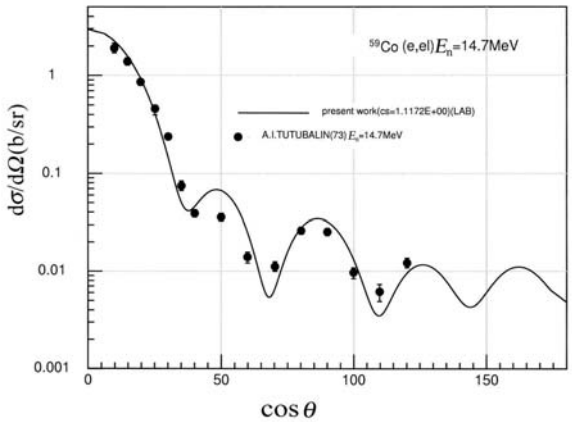

Fig.9 Calculated $\sigma_{el}(\theta)$ of n+ $^{59}_{27}$Co at E_n=14.7 MeV and compared with experimental data

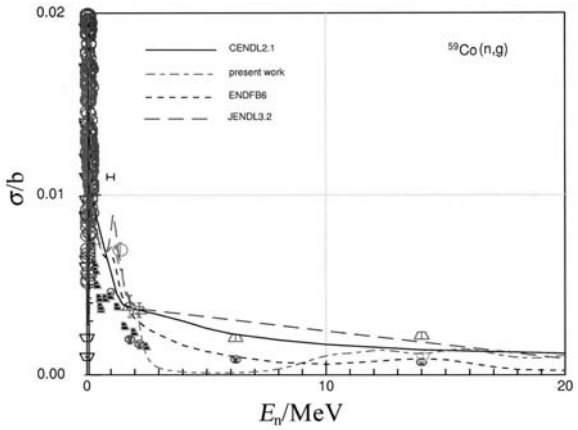

Fig.10 Calculated σ(n,γ) of n+ $^{59}_{27}$Co (E_n≤20 MeV) compared with exp. data and ENDF/B-6, JENDL3, CENDL2

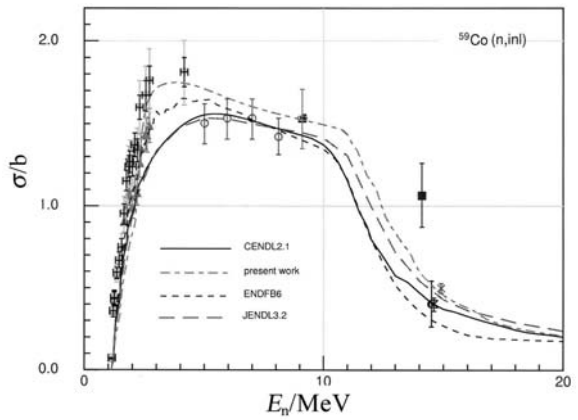

Fig.11 Calculated $\sigma(n,inl)$ of n+ $^{59}_{27}$Co (E_n≤20MeV)compared with exp. data and ENDF/B-6, JENDL3, CENDL2

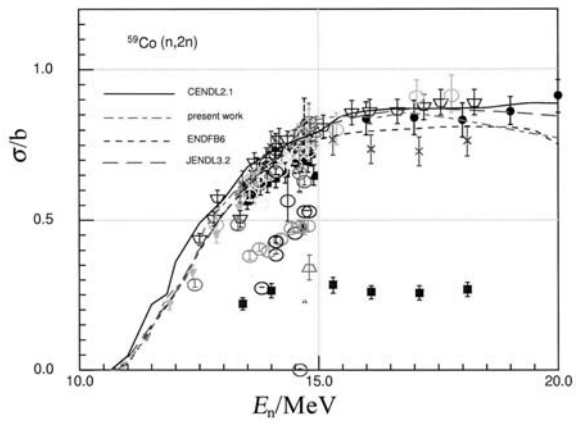

Fig.12 Calculated σ(n,2n)of n+ $^{59}_{27}$Co (E_n≤20 MeV) compared with exp. data and ENDF/B-6, JENDL3, CENDL2

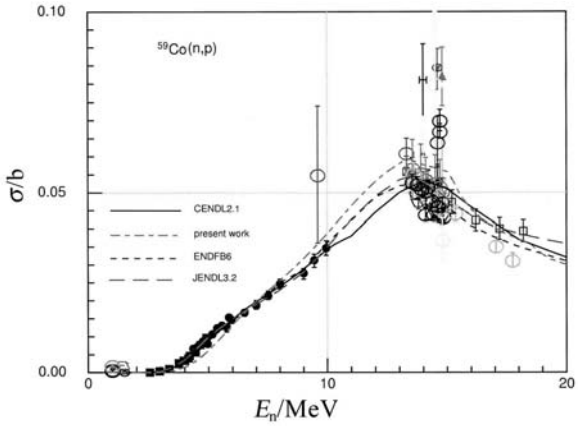

Fig.13 Calculated $\sigma(n,p)$ of n+ $^{59}_{27}$Co ($E_n \leqslant 20$ MeV) compared with ENDF/B-6, JENDL3, CENDL2

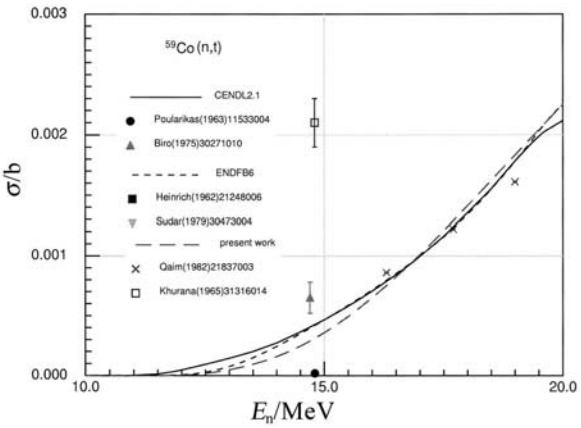

Fig.14 Calculated $\sigma(n,t)$ of n+ $^{59}_{27}$Co ($E_n \leqslant 20$ MeV) compared with ENDF/B-6, JENDL3, CENDL2

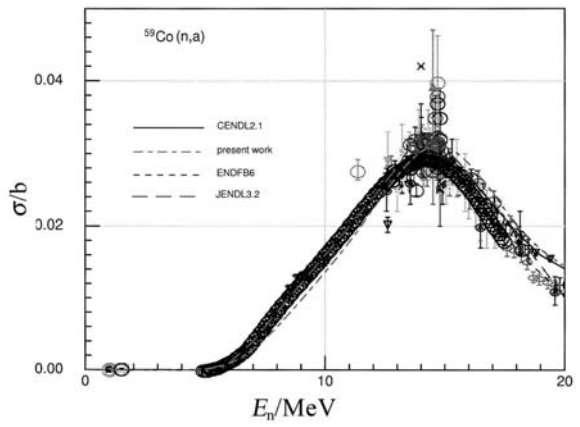

Fig.15 Calculated $\sigma(n,\alpha)$ of n+ $^{59}_{27}$Co ($E_n \leqslant 20$ MeV) compared with ENDF/B-6, JENDL3, CENDL2

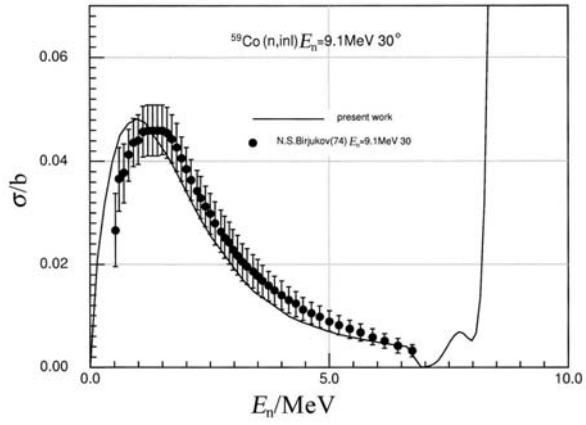

Fig.16 Calculated double differential cross sections compared with experimental data for n+ $^{59}_{27}$Co (n,inl) at 9.1 MeV, 30°

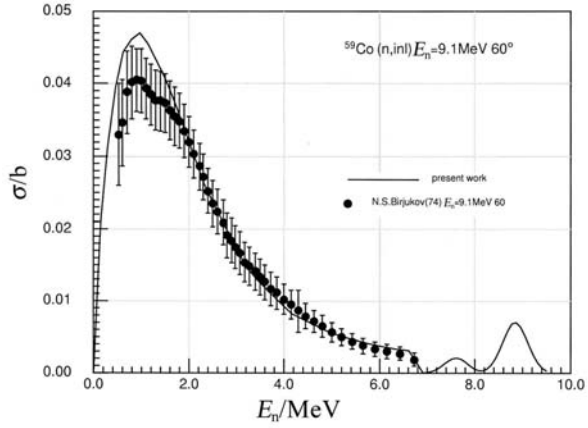

Fig.17 Calculated double differential cross sections compared with experimental data for n+ $^{59}_{27}$Co (n,inl) at 9.1 MeV, 60°

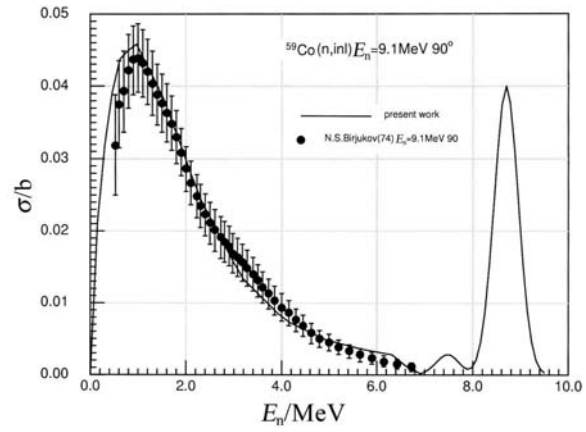

Fig.18 Calculated double differential cross sections compared with experimental data for n+ $^{59}_{27}$Co (n,inl) at 9.1 MeV, 90°

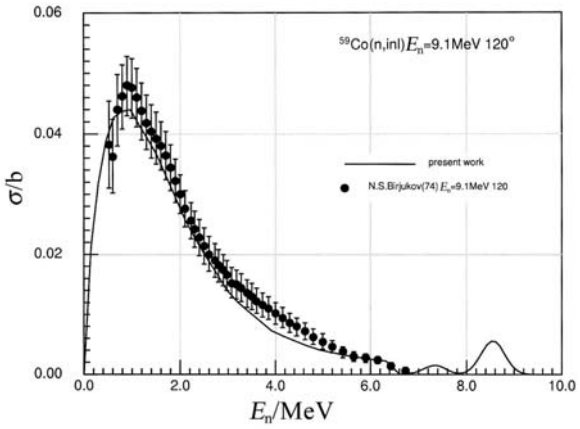

Fig.19 Calculated double differential cross sections compared with experimental data for n+ $^{59}_{27}$Co (n,inl) at 9.1 MeV, 120°

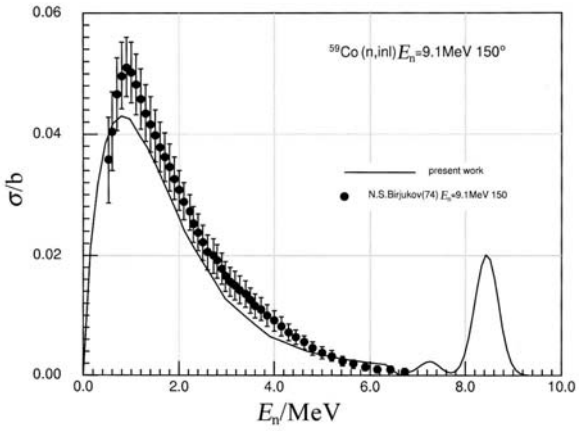

Fig.20 Calculated double differential cross sections compared with experimental data for n+ $^{59}_{27}$Co (n,inl) at 9.1 MeV, 150°

References

[1] SHEN Qingbiao, CNDP.7,43,1992.

[2] J. Raynal, Note on ECIS94, CEN-N2772,1994.

[3] ZHANG Jingshang, CHIC-01616, CNDC-0032, 2001.

[4] P.D. Kunz, A DWBA code DWUCK-4, University of Colorado USA (unpublished).

[5] WANG Shunuan et al, ^{55}Mn Neutron Data Calculation and Analysis (≤20MeV), Communication of Nuclear Data Progress, No.29, 37(2003.12).

[6] Carlson B V. The Optical Model and ECIS95. SMR/1220-4, Workshop on Nuclear Reaction Data and Nuclear Reactors: Physics, Design and Safety, 13 March-14 April 2000, Trieste, Italy

[7] C.Kalbach, Nucl.Phys.A210,590(19730.

[8] SUN Ziyang, WANG Shunuan, ZHANG Jingshang, ZHUO Yizhong,Z.Phys.A 305,61-68(1982).

[9] SUN Ziyang, WANG Shunuan, ZHANG Jingshang, ZHUO Yizhong, K.H. Bockhoff(ed.), Nuclear Data for Science and Technology, 603-605(1983).

[10] D. Hermsdorf et al., Zeentralinstitut fur Kernforschung, Rossendorf bei Dresden Report No.ZFK-277(1974).

[11] SHEN Qingbiao, TIAN Ye, WANG Shunuan et al., Chinese Jour.Nucl.Phys., Vol.6,245(1984).

Calculation and Recommendation of the Complete Sets of Nuclear Data for n+^{92,94,96}Mo below 20 MeV

CAI Chonghai LIANG Chuntian

Department of Physics, Nankai University, Tianjin 300071, P.R.China

【**abstract**】 *The complete sets of nuclear data were calculated and evaluated for n + ^{92,94,96}Mo below 20 MeV, which include all kinds of cross sections, especially for some reactions corresponding to the residual nuclei in isomeric states; angular distributions of elastic scattering, energy spectra and/or double–differential cross sections of all emitted particles, and gamma production data (production cross sections and multiplicity, energy spectra) for all kinds of reactions. The calculated results are generally in good accordance with the experimental values. In our final evaluation files, most data were directly taken from the calculated values, only a few of them are changed based on experimental data and referred to JENDL3.2.*

Introduction

For the element molybdenum, there are seven stable isotopes: ^{92}Mo(15.86%), ^{94}Mo(9.12%), ^{95}Mo(15.70%), ^{96}Mo(16.5%), ^{97}Mo(9.45%), ^{98}Mo(23.75%) and ^{100}Mo(9.62%), which are important fission products, also rather important structure material nuclei. Only four of them (^{95,97,98,100}Mo) were evaluated in CENDL-3. The existing evaluation files for ^{92,94,96}Mo are included in ENDF/B-6, JEF-2 and JENDL-3.2. However the evaluations of ^{92,94,96}Mo in ENDF/B-6 are incomplete and/or rough. For ^{92}Mo, there are only (n,γ) data (MT=102 in MF=3,8,9); for ^{94,96}Mo, there are only total, elastic, inelastic and (n,γ) cross sections; and all angular distributions are simply assumed as isotropic and the uniquely given neutron spectra of continuous inelastic were taken as evaporation spectra. So our calculation and evaluation values, JEF-2 and JENDL-3.2 were compared with each other and with experimental data shown in Figs.1 to 13. All the experimental data in these figures were taken from EXFOR master file. In this paper we will not give the references indicated in EXFOR for every set of data respectively. In some cases we perhaps indicate the first author or authors and the published year.

The evaluated neutron nuclear data of ^{92,94,96}Mo in JEF-2 files are incomplete and rough, for example, there are no $\sigma_{n,2n}$ and $\sigma_{n,xn}$ given in it, those in JENDL-3.2 are much better than in JEF-2. The evaluation of ^{92,94,96}Mo in JENDL-3.2 were finished in 1993, the experimental data after 1992 were not used in their evaluation. The angular distributions of elastic scattering above 6 MeV and some reaction cross sections of ^{92,94,96}Mo in JENDL-3.2 are not in good agreement with experimental data, and their data were given with files 1, 2, 3, 4 and 5. The new version 2001 of program UNF[1] have many excellent functions. For example, it can calculate the double–differential cross sections of total emission neutrons at five given angles for a given incident energy point to benefit user in comparison with experimental values, and the users can choose one of the two kinds of B6 format output: files 3, 4 and 5 or files 3, 4, 6, 12, 14 and 15. Especially it can calculate the reaction cross section leaving the residual nucleus in a metastable isomeric state, and the target can be in ground or an isomeric state.

Considering some newer reliable experimental data and those of isomeric state, we will in a consistent way calculate and give better and more reliable complete sets of neutron nuclear data for ^{92,94,96}Mo including double–differential cross sections and gamma production data in B-6 format output. In all figures, “this work” means our calculated result, “this evaluation” means our evaluated value if it is different from the calculated value.

1 Parameters Used in UNF and Direct Inelastic Contribution

Firstly, we used the program APMN[2] to automatically search for the optimal optical potential parameters of ^{92,94,96}Mo in neutron channel based on their experimental total cross sections, angular distributions of elastic scattering and one set of σ_{tot} of natural molybdenum in 2~20 MeV given by Larson et al. in 1980.

For five charged particle channels, we usually used the universal optical potential parameters[3]. Sometime we need adjust some optical potential parameters (usually the diffusion parameters a_r, a_s, a_v and a_{so} as well as the radius parameters r_r, r_s, r_v and r_{so}) in charged particle channels by hand in proper range to make the calculated reaction cross sections in better agreement with experimental data.

The optical potential parameters used in our final calculations are given in Table 1~3 for ^{92,94,96}Mo, respectively. The same set of optimal optical potential parameters in neutron channel were also used in calculations of the direct inelastic cross sections as well as the Legendre coefficient of their angular distributions with the code DWUCK4[4]. Levels and their deformation parameters β_2 used in direct inelastic calculation are given in Table 4.

The optical potential parameters in Table 1~3, the direct inelastic cross sections as well as the Legendre coefficients of their angular distributions obtained with DWUCK4 were used as a part of input data for the main code UNF.

The Code UNF consists of spherical optical model, the unified Hauser–Feshbach and exciton model. The emissions to discrete level in the multi–particle emissions for all opened channels are included. The gamma production data and the reaction cross sections leaving the residual nucleus in an isomeric state can also be calculated.

In UNF, Gilbert–Cammeron formula is employed for calculation of the level density. The level density parameter a, the pair energy correction Δ and the two peak giant resonance parameter for gamma emission were obtained from the Parameters Library in CNDC. The data of levels and their spin, parity and the branch ratio of gamma emission were taken from the Parameters Library in CNDC and/or the Web site of the National Nuclear Data Center at Brookhaven National Laboratory. In order to make the calculated cross sections in better accordance with experimental data, we often adjust some of the level density parameters a and the pair energy corrections Δ by hand in some range. The a and Δ values used in our final calculations are given in Table 5.

Table 1 Optical potential parameters of ^{92}Mo used in this work

channel	n	p	α	^{3}He	d	t
a_r	0.651 827 8	0.75	0.52	0.72	0.71	0.72
a_s	0.626 347 1	0.51	0.52	0.88	0.78	0.84
a_v	0.350 002 6	0.51	0.52	0.88	0.78	0.84
a_{so}	0.651 827 8	0.75	0.52	0.72	0.71	0.72
r_r	1.200 006 0	1.17	1.442	1.20	1.17	1.20
r_s	1.254 836 0	1.32	1.442	1.40	1.30	1.40
r_v	1.145 909 0	1.32	1.442	1.40	1.30	1.40
r_{so}	1.200 006 0	1.01	1.442	1.20	0.64	1.20
r_c	1.250 000 0	1.25	1.25	1.30	1.30	1.30
W_{v0}	–2.853 785	–2.70	22.4	0.0	0.0	0.0
W_{v1}	0.265 674 60	0.22	0.0	0.0	0.0	0.0
W_{v2}	–0.000 233 6	0.0	0.0	0.0	0.0	0.0
V_0	55.531 530	54.0	164.7	151.9	90.6	165.0
V_1	–0.517 263 9	–0.32	0.0	–0.17	0.0	–0.17
V_2	0.011 100 24	0.0	0.0	0.0	0.0	0.0
V_3	–24.000 00	24.0	0.0	50.0	0.0	–6.4
V_4	0.150 104 3	0.4	0.0	0.0	0.0	0.0
V_{so}	6.200 000	6.2	0.0	2.5	7.13	2.5
W_{s0}	8.787 496	11.8	0.0	41.7	12.0	46.0
W_{s1}	–0. 033 215 6	–0.25	0.0	–0.33	0.0	–0.33
W_{s2}	–12.000 00	12.0	0.0	44.0	0.0	–110.0

And a_{s1}=0.7, a_{v1}=0.7 for p channel.

Table 2 Optical potential parameters of ^{94}Mo used in this work

channel	n	p	α	^{3}He	d	t
a_r	0.615 630 6	0.75	0.52	0.72	0.71	0.72
a_s	0.584 858 2	0.51	0.52	0.88	0.78	0.84
a_v	0.717 997 6	0.51	0.52	0.88	0.78	0.84
a_{so}	0.615 630 6	0.75	0.52	0.72	0.71	0.72
r_r	1.259 108 0	1.17	1.442	1.20	1.17	1.20
r_s	1.257 917 0	1.32	1.442	1.40	1.30	1.40
r_v	1.254 055 0	1.32	1.442	1.40	1.30	1.40
r_{so}	1.259 108 0	1.01	1.442	1.20	0.64	1.20
r_c	1.250 000 0	1.25	1.25	1.30	1.30	1.30
W_{v0}	–2.781 708	–2.70	22.4	0.0	0.0	0.0
W_{v1}	0.272 699 0	0.22	0.0	0.0	0.0	0.0
W_{v2}	0.000 061 98	0.0	0.0	0.0	0.0	0.0
V_0	54.056 850 0	54.0	164.7	151.9	90.6	165.0
V_1	–0.690 542 60	–0.32	0.0	–0.17	0.0	–0.17
V_2	0.016 875 240	0.0	0.0	0.0	0.0	0.0
V_3	–24.000 00	24.0	0.0	50.0	0.0	–6.4
V_4	–0.284 375 1	0.4	0.0	0.0	0.0	0.0
V_{so}	6.200 000 0	6.2	0.0	2.5	7.13	2.5
W_{s0}	8.460 502 0	11.8	0.0	41.7	12.0	46.0
W_{s1}	0.028 951 8	–0.25	0.0	–0.33	0.0	–0.33
W_{s2}	–12.000 00	12.0	0.0	44.0	0.0	–110.0

And a_{s1}=0.7, a_{v1}=0.7 for p channel.

Table 3 Optical potential parameters of ^{96}Mo used in this work

channel	n	p	α	^{3}He	d	t
a_r	0.562 619 7	0.75	0.52	0.72	0.71	0.72
a_s	0.803 356 0	0.51	0.52	0.88	0.78	0.84
a_v	0.575 798 0	0.51	0.52	0.88	0.78	0.84
a_{so}	0.562 619 7	0.75	0.52	0.72	0.71	0.72
r_r	1.227 960 0	1.17	1.442	1.20	1.17	1.20
r_s	1.049 811 0	1.32	1.442	1.40	1.30	1.40
r_v	1.298 168 0	1.32	1.442	1.40	1.30	1.40
r_{so}	1.227 960 0	1.01	1.442	1.20	0.64	1.20
r_c	1.250 000 0	1.25	1.25	1.30	1.30	1.30
W_{v0}	–3.532 810	–2.70	22.4	0.0	0.0	0.0
W_{v1}	0.044 824 0	0.22	0.0	0.0	0.0	0.0
W_{v2}	–0.024 374 0	0.0	0.0	0.0	0.0	0.0
V_0	55.515 070 0	54.0	164.7	151.9	90.6	165.0
V_1	–0.820 072 4	–0.32	0.0	–0.17	0.0	–0.17
V_2	0.018 891 94	0.0	0.0	0.0	0.0	0.0
V_3	–24.000 00	24.0	0.0	50.0	0.0	–6.4
V_4	–0.036 956 0	0.4	0.0	0.0	0.0	0.0
V_{so}	6.200 000 0	6.2	0.0	2.5	7.13	2.5
W_{s0}	7.510 563 0	11.8	0.0	41.7	12.0	46.0
W_{s1}	0.117 767 1	–0.25	0.0	–0.33	0.0	–0.33
W_{s2}	–12.000 00	12.0	0.0	44.0	0.0	–110.0

And a_{s1}=0.7, a_{v1}=0.7 for p channel.

Table 4 Levels and deformation parameters β_2 used in direct inelastic calculation

^{92}Mo				^{94}Mo				^{96}Mo			
Level	J	π	β_2	Level	J	π	β_2	Level	J	π	β_2
1.509 51	2.0	+1	0.21	0.871 096	2.0	+1	0.17	0.778 245	2.0	+1	0.15
2.282 57	4.0	+1	0.21	1.573 72	4.0	+1	0.17	1.497 800	2.0	+1	0.11
2.612 31	2.0	+1	0.21	1.864 29	2.0	+1	0.08	1.625 925	2.0	+1	0.08
				2.067 62	2.0	+1	0.06	1.978 453	3.0	+1	0.08
(in MeV)				2.393 22	2.0	+1	0.04	2.095 529	2.0	+1	0.04

Table 5 The a and Δ values used in The calculations

reaction channel		n,γ	n,n'	n,p	n,α	n,^{3}He	n,d	n,t	n,2n	n,nα	n,2p	n,3n
^{92}Mo	a	10.833	12.259	14.260	12.663	9.7150	16.384	11.228	10.955	11.260	9.8790	11.513
	Δ	+0. 43	+0.00	–1.54	–1.98	+2.55	–2.70	+0.25	–7.60	–2.25	+1.45	+2.77
^{94}Mo	a	12.612	11.528	12.482	11.329	10.554	13.074	11.080	11.333	8.9150	11.610	10.659
	Δ	+0.25	+0.00	–1.60	–0.25	+2.50	–0.20	+0.10	+2.15	+1.75	+2.05	+2.37
^{96}Mo	a	13.808	12.683	15.446	12.810	12.066	11.223	12.852	12.212	11.554	12.771	11.528
	Δ	+0.37	+0.10	–0.60	–0.80	+2.47	–3.90	–0.30	+0.15	+0.50	+1.35	+1.22

The adjustable Kulbach parameter in exciton model was determined mainly based on the total neutron spectra, its value obtained is CK=1 500.0 for ^{92}Mo, 730.0 for ^{94}Mo and 900.0 for ^{96}Mo.

Besides above mentioned parameters, there are the adjustable factor in (n,γ) cross section calculation CE1=5.0 for ^{92}Mo and 5.5 for ^{94,96}Mo, the adjustable parameter in direct (n,γ) calculation DGM=0.56 for ^{92,94,96}Mo.

2 Results and Discussion

Our calculated σ_{tot} for ^{92,94,96}Mo are all in a little better agreement with the experimental data (Pasechnik 80, Smith 75, Lambropoulos 73, Divadeenam 68 and Larson 80) than JENDL-3.2, much better than JEF-2, see Fig.1.

Our calculated angular distributions of elastic scattering for ^{92}Mo below 7 MeV are in the same or a little better accordance with experimental data than JENDL3.2, and are much better than JEF-2, especially for large angles; at 9, 11, 20 and 26 MeV, our calculated values are in good agreement with experimental data, see Fig. 2(a)~2(d). Similar to ^{92}Mo, our elastic scattering angular distributions of ^{94,96}Mo are also good in accordance with experimental data.

The comparisons of calculated total neutron spectra of ^{92,94,96}Mo at 14 MeV with experimental data and JENDL-3.2 are given in Fig.3b, 2c; it can be seen that our results are in a little better accordance with experimental data than JENDL-3.2.

There are no experimental $\sigma_{n,n'}$ for ^{92}Mo. The comparisons of our calculated $\sigma_{n,n'}$ of ^{94,96}Mo with experimental data and JENDL-3.2, JEF-2 are shown in Fig.3, 4a and 4b, respectively.

From Fig.5a we can see that for the $\sigma_{n,2n}$ of ^{92}Mo, JENDL-3.2 did not consider the data of Bormann76 above 15 MeV and took lower evaluated values ($\sigma_{n,2n}$ of ^{92}Mo in JENDL-3.2 were really adopted from JENDL fusion file), we consider this set of data and obtain some larger calculated values. For ^{94}Mo, there is only one experimental $\sigma_{n,2n}$ data itself given by Greenwood(1989), but there are 8 set of experimental data (Molla 97, Kong 95, Garlea 92, Ikeda 88, Marcikovski 86, Amemiya 82, Srinivasa Rao 79, Fujino 77) corresponding to the residual nucleus in its metastable state; from Fig.5b we can see that our calculated values corresponding to metastable state passing through most of the experimental data, at the same time our calculated $\sigma_{n,2n}$ themselves are also passing through the upper limit of the unique data, but JENDL-3.2 gave much higher evaluated values. There are no experimental $\sigma_{n,2n}$ for ^{96}Mo, from Fig.5c we can see that both our calculated values and those in JENDL-3.2 are much higher than those of ^{94}Mo and lower than those of ^{100}Mo, which is reasonable in physics.

Our calculated $\sigma_{n,\gamma}$ and those in JENDL-3.2 and JEF-2 are almost in the same good accordance with experimental data for ^{92,94,96}Mo below 0.2 MeV, respectively, see Fig.6.

From Fig.7 we can see that for ^{92}Mo, our calculated $\sigma_{n,p}$ are in much better accordance with the only two sets of experimental data given by Qaim et al. (1989), Rahman and Qaim (1985) than JENDL-3.2, at the same time, our calculated $\sigma_{n,p}$ corresponding to the residual nucleus in its metastable state are also in good agreement with five sets of data given by Filatenkov et al. (1999), Molla et al. (1997), Kong et al. (1995), Ikeda et al. (1988) and Marcinkowski et al. (1986), respectively; the set given by Kanda (1972) with much smaller values and another three sets of data given by Doczi et al. (1998), Qaim et al. (1989) and Liskien et al. (1989), respectively, with much larger values, are not considered in our calculation. The $\sigma_{n,p}$ in JEF-2 is really an inclusive $\sigma_{n,p}$, which pass through the lower limit of the data set Qaim89. Similar to ^{92}Mo, both our calculated $\sigma_{n,p}$ and those in JENDL-3.2 of ^{94,96}Mo are in good accordance with the experimental data.

From Fig.8 we can see that for ^{92}Mo, our calculated $\sigma_{n,\alpha}$ are in good agreement with all experimental data except the set given by Kanda (1972) which are with much larger values than other sets, especially passing through three sets of data given by Filatenkov et al. (1999), Doczi et al. (1998) and Liskien et al. (1989), respectively; those in JENDL-3.2 are with a little lower values. At the same time, our calculated $\sigma_{n,\alpha}$ corresponding to the residual nucleus in its metastable state are also in good accordance with three sets of data given by Filatenkov et al. (1999), Garlea et al. (1992) and Ikeda et al. (1988), respectively, and the set of data given by Kanda (1972) with much smaller values are not considered in our calculation. For ^{94,96}Mo, our calculated $\sigma_{n,\alpha}$ are passing through the experimental data.

For ^{92}Mo, there is only one data given by Haight et al.(1981) for $\sigma_{n,d}$, but there are one new set of data given by Filatenkov et al. (1999) for reaction ^{92}Mo(n,x)^{91}Nb and three sets of data for reaction ^{92}Mo(n,x)^{91}Nb corresponding to the residual nucleus ^{91}Nb in its isomeric state. From Fig.9 we can see that our calculated $\sigma_{n,d}$ pass through the unique data, our calculated cross sections of reaction ^{92}Mo(n,x)^{91}Nb pass through the set of data given by Filatenkov et al.(1999), and those corresponding to the residual nucleus ^{91}Nb in its isomeric state are also in rather good agreement with the data given by Filatenkov et al. (1999) and Liskien et al. (1989), another data given by Wang et al. (1993) with much smaller value is not considered in our calculation. The $\sigma_{n,d}$ in JENDL-3.2 are with much smaller values in comparison with the unique data and our calculated values, those in JEF-2 pass through the unique data but with unreasonable shape.

From Fig.10 we can see that for ^{92}Mo, our calculated $\sigma_{n,n\alpha}$ pass through all the 4 sets of experimental data (Wang93, Katoh89, Qaim86, Kawade85), those in JENDL-3.2 are higher than the 4 sets of data. For ^{94,96}Mo, there are no any experimental data of $\sigma_{n,n\alpha}$, so we do not draw figures to compare. For ^{92,94,96}Mo, there are no any $\sigma_{n,n\alpha}$ data given in JEF-2.

The resonance parameters were simply taken from JENDL-3.2 files. In order to smoothly connect σ_{tot} and σ_{el} above 0.1 MeV and those in resonance region, in our evaluation we changed our calculated σ_{tot} and σ_{el} to the evaluated values in 0.1~0.5 MeV for ^{92}Mo, in 0.10~0.17 MeV for ^{94}Mo, in 0.1~0.32 MeV for ^{96}Mo. As for $\sigma_{n,\gamma}$, our calculated values at 0.1 MeV are already in ageement with those in JEND-3.2, so we do not need to change them in our evaluation. Some calculated results, such as in Fig.3a the total neutron spectra of ^{92}Mo at 14 MeV, are not in good accordance with experimental data, we changed our calculated $\sigma_{n,n'}$ near 14 MeV to some smaller values in our evaluation in a consistent way to automatically make the evaluated total neutron spectra at 14 MeV in better agreement with experimental data. The calculated $\sigma_{n,n'}$ in Fig.4a and 4b for ^{94,96}Mo are changed some in our evaluation to make them in better agreement with experimental data and/or for considering the consistency of evaluation data. In order to make the calculated σ_{el} in MeV region in better agreement with experimental data and with better shape and/or to keep data in consistency, we also changed our calculated σ_{tot} and σ_{el} some in the evaluation in MeV energy region.

With the version 2001 of the code UNF and based on some newer reliable experimental data, such as those given by Filatenkov et al. in 1999, Molla et al. in 1997 and Kong et al.in 1995, in a consistent way we calculate and evaluate the complete sets of nuclear data for n+^{92,94,96}Mo below 20 MeV, and have obtained better results than JENDL-3.2 (the best open released files), especially for the angular distribution of elastic scattering and some reaction cross sections, such as $\sigma_{n,p}$ of ^{92}Mo, $\sigma_{n,d}$ of ^{92,94,96}Mo and $\sigma_{n,n\alpha}$ of ^{92}Mo. And our evaluation files are given in both kinds of B-6 format: files 1,2, 3, 4 and 5 as well as files 1,2, 3, 4, 6, 12, 14 and 15.

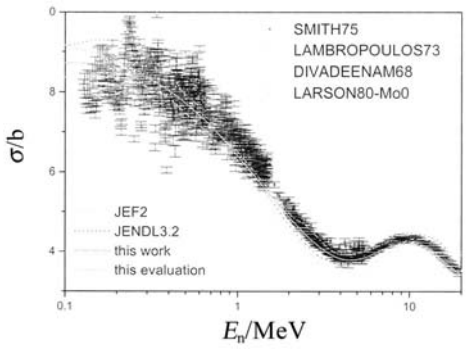

Fig.1 Total cross sections of ^{96}Mo

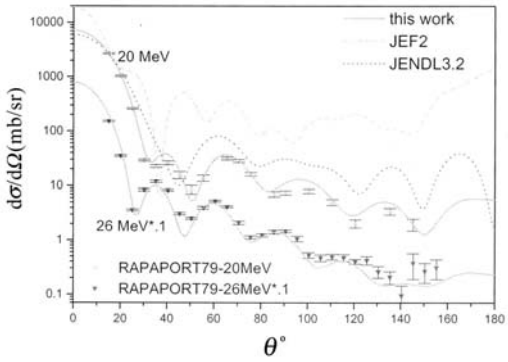

Fig.2d Elastic scattering angular distrubutions of ^{92}Mo (4)

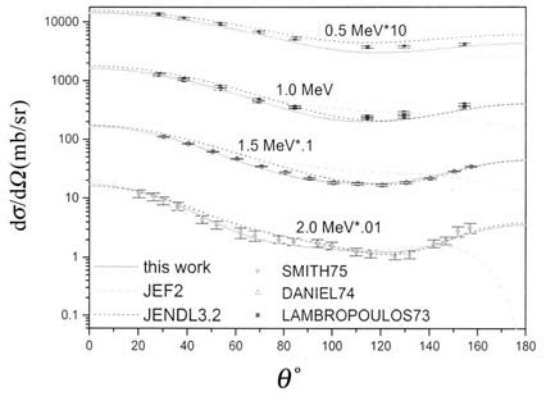

Fig.2a Elastic scattering angular distrubutions of ^{92}Mo

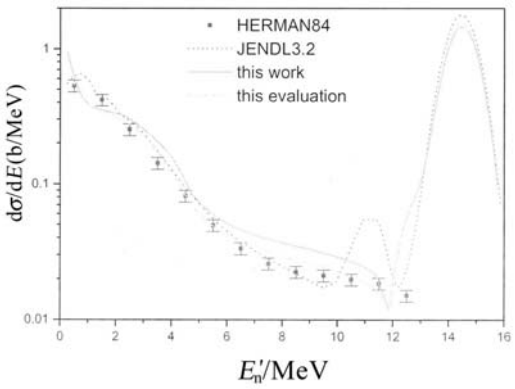

Fig.3a Total neutron spectra of ^{92}Mo at 14.0 MeV

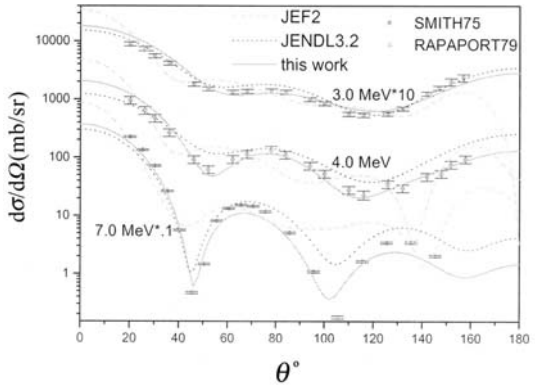

Fig.2b Elastic scattering angular distrubutions of ^{92}Mo

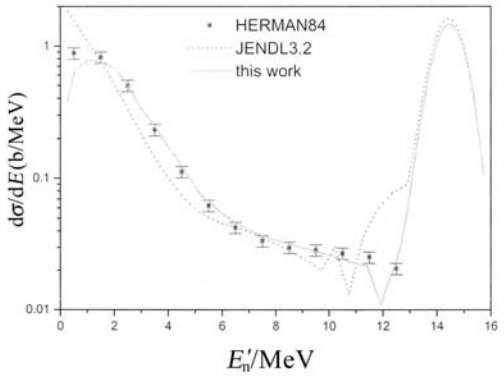

Fig.3b Total neutron spectra of ^{94}Mo at 14.0 MeV

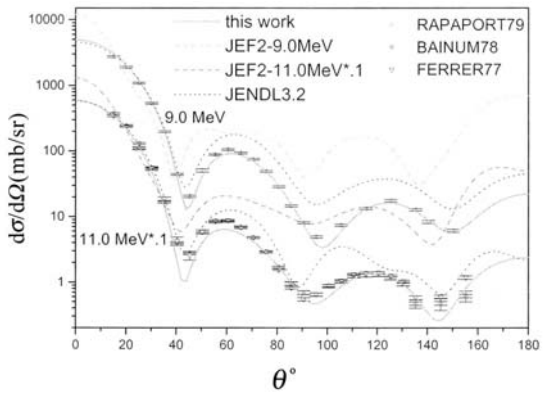

Fig.2c Elastic scattering angular distrubutions of ^{92}Mo

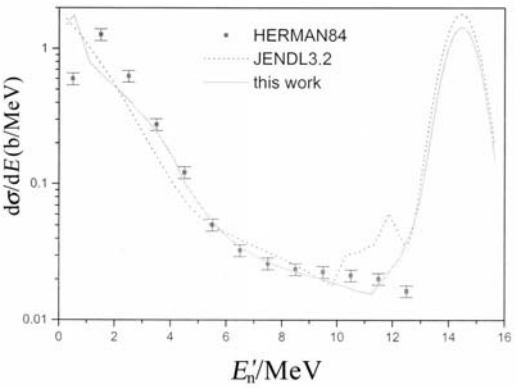

Fig.3c Total neutron spectra of ^{96}Mo at 14.0 MeV

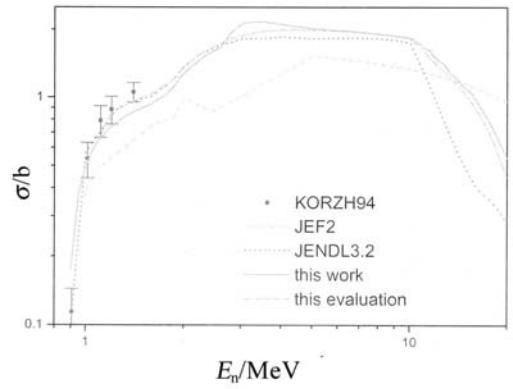

Fig.4a Inelastic scattering cross sections of ^{94}Mo

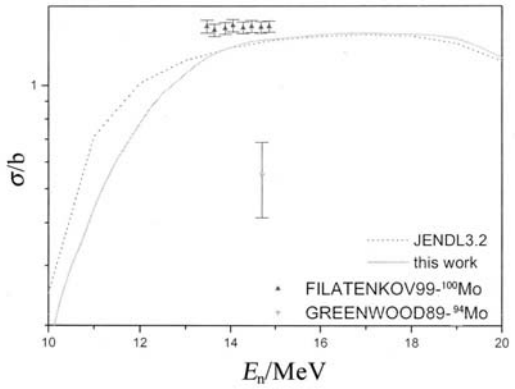

Fig.5c (n,2n) reaction cross sections of ^{96}Mo

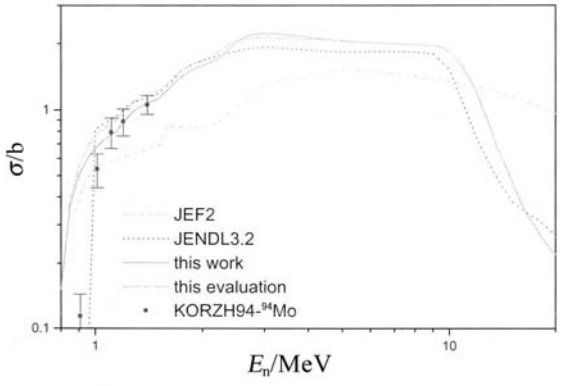

Fig.4b Inelastic scattering cross sections of ^{96}Mo

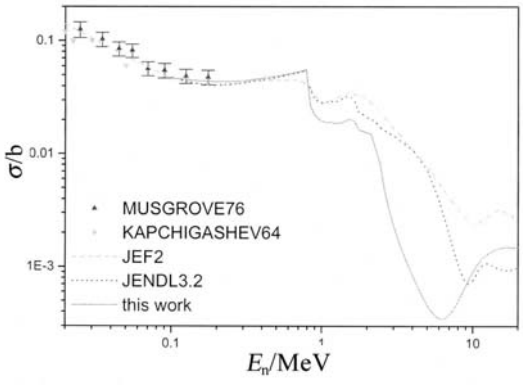

Fig.6 Capture cross sections of ^{96}Mo

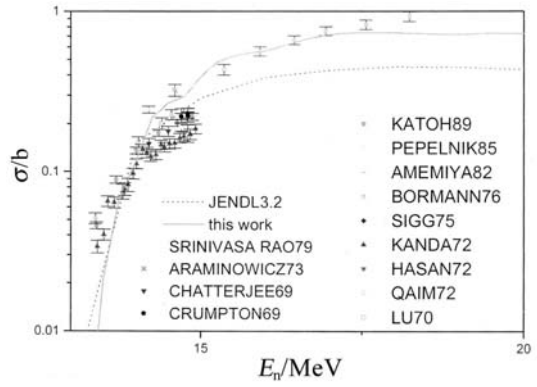

Fig.5a (n,2n) reaction cross sections of ^{92}Mo

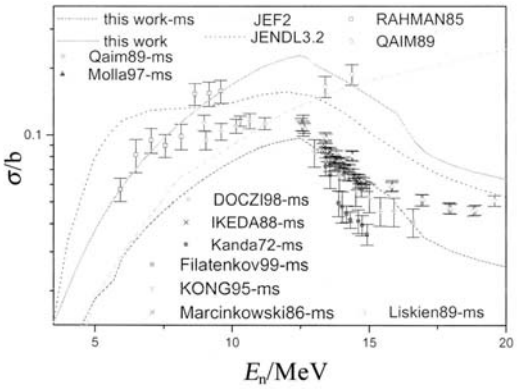

Fig.7 (n,p) reaction cross sections of ^{92}Mo

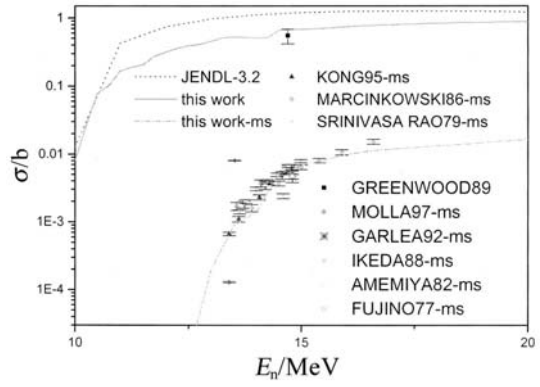

Fig.5b (n,2n) reaction cross sections of ^{94}Mo

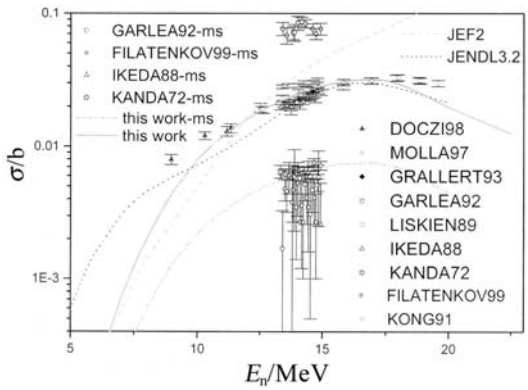

Fig.8 (n,α) reaction cross sections of ^{92}Mo

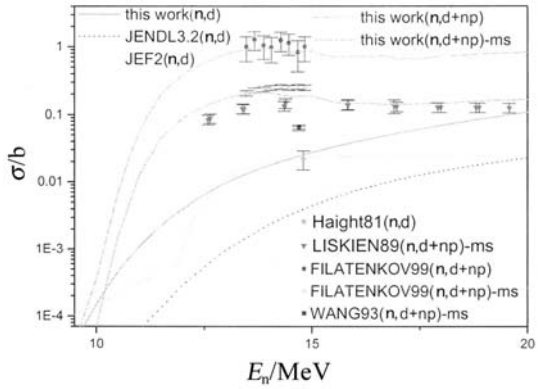

Fig.9 (n,d) and (n,d+np) reaction cross sections of ^{92}Mo

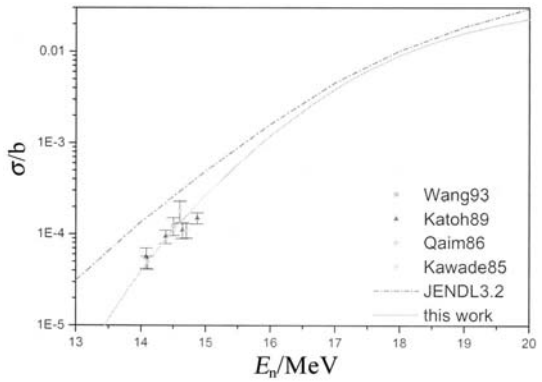

Fig.10 (n,nα) reaction cross sections of ^{92}Mo

References

[1] ZHANG Jingshang, User Manual of UNF Code, CNDC-0032, CNIC-01616, China Institute of Atomic Energy, P.O. Box 275(41), Dec. 2001; also New Functions in UNF Code and Illustration, Commu. Nucl. Data Progress (INDC(CRP)-053/L) No.25, p22, June 2001;

[2] SHEN Qingbiao, A Code APMN for Automatically Searching Optimal Optical Potential Parameters below 300 MeV, Commu. Nucl. Data Progress (INDC(CRP) -053/L) No.25, p19, June 2001;

[3] C.M.PEREY, F.G.PEREY, Compilation of Phenomenological Optical-Model Parameters, Atomic Data & Nucl. Data Tables, 17, p1-101, 1976;

[4] P.D.Kunz, a DWBA Code DWUCK4, University of Colorado, USA (unpublished);

The Cross Section Calculation of ^{102,104,106}Mo below 20 MeV

LIANG Chuntian CAI Chonghai

Department of Physics, Nankai University, Tianjin 300071, P.R.China

【**abstract**】*The cross section calculation of ^{102,104,106}Mo below 20 MeV was carried out. Because there are no any experimental data for three unstable isotopes of element molybdenum, our results of ^{102,104,106}Mo are compared each other and with evaluated data of ^{92,94,96,98,100}Mo which are generally in good accordance with experimental data. In our final evaluation files, the most of the data are directly taken from our calculated values, which are reasonable in physics.*

1 Parameters Used in UNF and Direct Inelastic Contribution

For unstable isotopes of element molybdenum without any experimental data, we used the program APMN[1] to automatically search for a common optimal set of optical potential parameters in neutron channel based on the experimental data of total cross sections (with weight 8.0) and elastic scattering angular distributions (with weight 1.0) of 6 stable isotopes $^{92,94\sim96,98,100}$Mo, and natural element molybdenum. All these experimental data were taken from EXFOR. The code DWUCK4[2] was used to calculate the direct inelastic cross sections and the Legendre coefficients of their angular distributions. And our main tool for the calculation of complete cross section data below 20 MeV is the version 2001 of program UNF[3]. For five charged particle channels, we used the universal optical potential parameters[4].

The optical potential parameters given in Table 1 were used in our final calculations for all these unstable isotopes. The same set of optimal optical potential parameters in neutron channel were also used in calculations of the direct inelastic cross sections as well as the angular distributions with DWUCK4. Levels and their deformation parameters β_2 used are given in Table 2. We take β_2=0.11 for all levels.

In UNF, Gilbert-Cammeron formula was employed for calculation of the level density. The level density parameter *a*, the pair energy correction Δ and the two peak giant dipole resonance parameter for gamma emission were obtained from the Parameters Library in CNDC. The data of levels and their spin, parity were taken from the Parameters Library in CNDC and/or the Web site of the National Nuclear Data Center at Brookhaven National Laboratory. In order to make the calculated cross sections reasonable in physics, the level density parameters *a* and the pair energy corrections Δ were adjusted by hand in suitable range. The values of *a* and Δ used in our final calculations are given in Table 3.

For 3 unstable isotopes concerned, we took the adjustable Kulbach parameter in exciton model as CK=822.0, which is the average value of that of ^{92,94,96,98,100}Mo. The adjustable factor in (n,γ) cross section calculation CE1=8.3, which is the same value as ^{100}Mo .The adjustable parameter in direct (n,γ) calculation DGM=0.65.

2 Results and Discussion

With above mentioned parameters and the calculated direct inelastic data by DWUCK4 as the input data, we calculated the neutron nuclear data of ^{102,104,106}Mo with the code UNF. The calculated results were compared with each other and with evaluated data of ^{92,94,96,98,100}Mo which are presented in Fig. 1~9.

Our calculated values of σ_{tot} above resonance region are given in Fig.1, from which we can see that our σ_{tot} of ^{102,104,106}Mo are with in small differences in comparison with each other, within larger differences in comparison with σ_{tot} of ^{92,94,96,98,100}Mo. The reason is that a common optical potential parameters for ^{102,104,106}Mo were obtained on the basis of experimental σ_{tot} and angular distributions of elastic scattering of 6 stable isotopes (there are no any experimental data for ^{97}Mo) and natural element molybdenum, which are different from those for ^{92,94,96,98,100}Mo based on their own experimental σ_{tot} respectively.

Table 1 Optical potential parameters used in this work

channel	n	p	α	^{3}He	d	t
a_r	0.583 222 03	0.75	0.52	0.72	0.71	0.72
a_s	0.678 118 82	0.51	0.52	0.88	0.78	0.84
a_v	0.716 305 85	0.51	0.52	0.88	0.78	0.84
a_{so}	0.225 942 94	0.75	0.52	0.72	0.71	0.72
r_r	1.209 779 26	1.17	1.442	1.20	1.17	1.20
r_s	1.211 337 09	1.32	1.442	1.40	1.30	1.40
r_v	1.508 646 37	1.32	1.442	1.40	1.30	1.40
r_{so}	0.924 287 32	1.01	1.442	1.20	0.64	1.20
r_c	1.300 000 00	1.25	1.25	1.30	1.30	1.30
W_{v0}	−0.942 049 56	−2.70	22.4	0.0	0.0	0.0
W_{v1}	0.449 992 60	0.22	0.0	0.0	0.0	0.0
W_{v2}	−0.012 814 66	0.0	0.0	0.0	0.0	0.0
V_0	55.643 169 40	54.000 00	164.700 00	151.900 00	90.600 000	165.000 00
V_1	−0.507 165 31	−0.32	0.0	−0.17	0.0	−0.17
V_2	0.006 078 12	0.0	0.0	0.0	0.0	0.0
V_3	−22.314 836 5	24.0	0.0	50.0	0.0	−6.4
V_4	−0.139 821 89	0.4	0.0	0.0	0.0	0.0
V_{so}	4.858 808 04	6.2	0.0	2.5	7.13	2.5
W_{so}	0.249 576 23	11.8	0.0	41.7	12.0	46.0
W_{s1}	0.087 566 1	−0.25	0.0	−0.33	0.0	−0.33
W_{s2}	20.387 477 87	12.0	0.0	44.0	0.0	−110.0

And a_{s1}=0.7, a_{v1}=0.7 for p channel.

Table 2 levels and deformation parameters β_2 used in direct inelastic calculation

^{102}Mo				^{104}Mo				^{106}Mo			
Level/MeV	***J***	π	β_2	Level/MeV	***J***	π	β_2	Level/MeV	***J***	π	β_2
0.296 597	2.0	+1	0.11	0.192 19	2.0	+1	0.11	0.171 548	2.0	+1	0.11
0.743 74	4.0	+1	0.11	0.560 68	4.0	+1	0.11	0.522 29	4.0	+1	0.11
0.848 06	2.0	+1	0.11	0.812 36	2.0	+1	0.11	0.710 71	2.0	+1	0.11
1.245 58	3.0	+1	0.11	1.028 35	3.0	+1	0.11	0.885 60	3.0	+1	0.11
1.249 75	2.0	+1	0.11	1.079 98	6.0	+1	0.11	1.033 7	6.0	+1	0.11
1.327 92	6.0	+1	0.11	1.214 82	4.0	+1	0.11	1.068 2	6.0	+1	0.11
1.398 43	4.0	+1	0.11	1.275 19	4.0	+1	0.11	1.279 9	6.0	+1	0.11
				1.468 61	4.0	+1	0.11	1.435 77	6.0	+1	0.11
				1.475 67	5.0	+1	0.11				

Table 3 the *a* and Δ values used in the calculations

channel		(n,γ)	(n,n′)	(n,p)	(n,α)	(n,^{3}He)	(n,d)
^{102}Mo	*a*	17.889 04	17.131 92	18.119 28	16.671 60	16.004 00	17.363 92
	Δ	1.05	0.62	–0.32	–0.90	2.70	0.25
^{104}Mo	*a*	18.901 68	18.117 63	19.133 50	16.741 76	16.961 38	18.351 31
	Δ	1.13	0.67	–0.44	0.03	2.60	0.55
^{106}Mo	*a*	19.082 81	18.783 20	19.324 22	17.725 89	17.605 12	19.021 80
	Δ	0.88	0.31	0.08	0.91	2.49	0.84
channel		(n,t)	(n,2n)	(n,nα)	(n,2p)	(n,3n)	
^{102}Mo	*a*	18.028 00	16.808 32	14.761 15	16.741 76	15.854 40	
	Δ	–0.25	–0.70	2.45	1.03	–0.07	
^{104}Mo	*a*	18.119 28	16.889 04	16.004 00	17.725 89	17.131 92	
	Δ	–0.32	–1.00	2.70	0.91	1.02	
^{106}Mo	*a*	19.133 50	18.901 68	16.961 38	17.894 52	18.117 63	
	Δ	–0.44	0.73	2.60	1.43	2.42	

The calculated values of σ_{el} above resonance region are given in Fig.2, from which we can see that the values below 3 MeV are very divergent for different isotopes, and above 3 MeV the values of σ_{el} are almost the same for ^{102,104,106}Mo, however with small differences in comparison with ^{92,94,96,98,100}Mo respectively. The reason is that in lower energy region, the compound nucleus elastic scattering cross sections are obviously larger than zero, then the values of σ_{el} depend on both the set of optical potential parameters and the different level structure of each isotope. In higher energy region, the compound nucleus elastic scattering cross sections are almost zero, the values of σ_{el} only depend on the set of optical potential parameters.

All calculated $\sigma_{n,n'}$ are given in Fig.3, from which we can see that near threshold energy, the larger the mass number of certain isotope, the larger the values of $\sigma_{n,n'}$ of the corresponding isotope.

Our radiative capture cross sections of ^{92,94,96,98,100,102,104,106}Mo are given in Fig.4, from which we can see that the $\sigma_{n,\gamma}$ values for ^{100,102,104,106}Mo are with small differences below 0.15 MeV, and the $\sigma_{n,\gamma}$ values for all isotopes are very divergent in higher energy region.

Our calculated (n,p) reaction cross sections of all these isotopes are given in Fig.5, from which we can see that the $\sigma_{n,p}$ values are lower and lower, and the threshold energies of them are higher and higher when the mass number of corresponding isotope is larger and larger.

Our calculated (n,α),(n,d) reaction cross sections of all these isotopes are given in Fig.6,7 from which we can see that the (n,α) reaction cross sections become smaller, and the threshold energies of them become higher when the mass number of corresponding isotope becomes larger.

Our calculated (n,2n), (n,3n) reaction cross sections of all these isotopes are given in Fig.8,9 from which we can see that the threshold energy of (n,2n) and (n,3n) reactions becomes lower and lower when the mass number of corresponding isotope becomes larger and larger. In E_n>13 MeV energy region we find that $\sigma_{n,2n}$ values drop at lower energy for heavier isotope because (n,3n) reaction of heavier isotope has lower threshold energy and $\sigma_{n,2n}+\sigma_{n,3n}$ should keep about constant in this energy region.

In summary, in this work we give complete cross sections in the energy region from 1 keV to 20 MeV for all even unstable isotopes (102~106) of element molybdenum. In our calculation and evaluation, the common optimal set of optical potential parameters are automatically searched with the code APMN to suit all isotopes of element molybdenum, with which the calculated total cross sections and angular distributions of elastic scattering are in optimal accordance with experimental data for $^{92,94\sim96,98,100}$Mo. For calculations of the cross sections in different reaction channels, the total changing trend are considered being kept reasonable in physics.

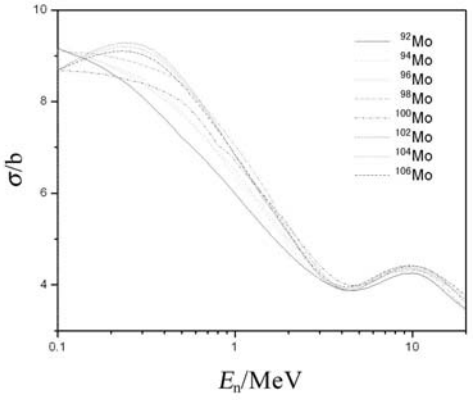

Fig.1 Total cross sections

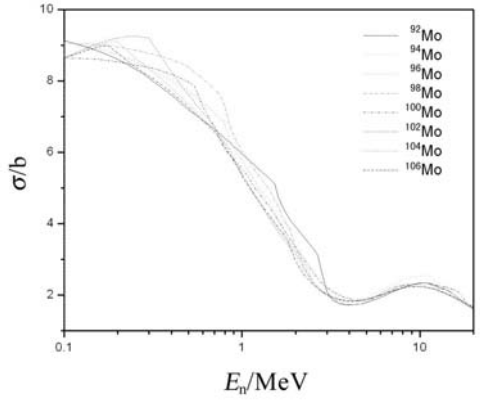

Fig.2 Elastic scattering cross sections

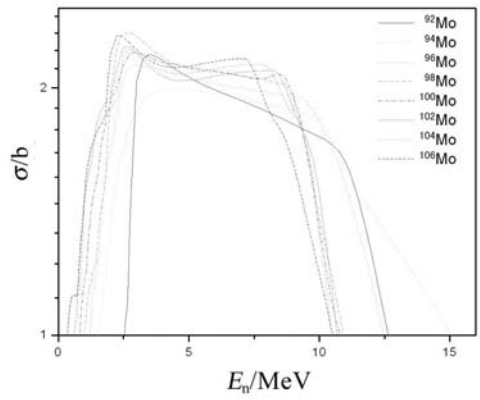

Fig.3 (n,n′) cross sections

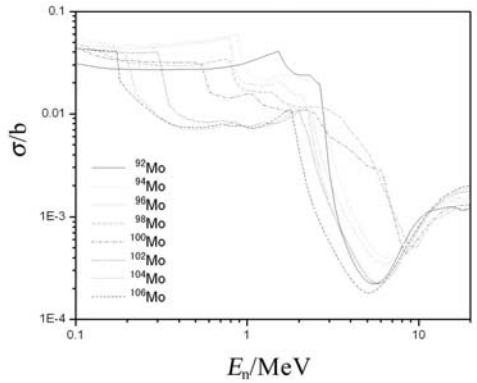

Fig.4 (n,γ) cross sections

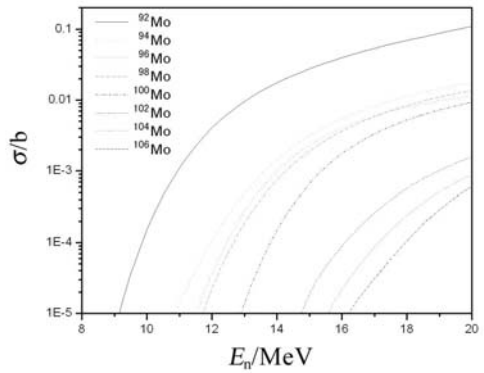

Fig.7 (n,d) cross sections

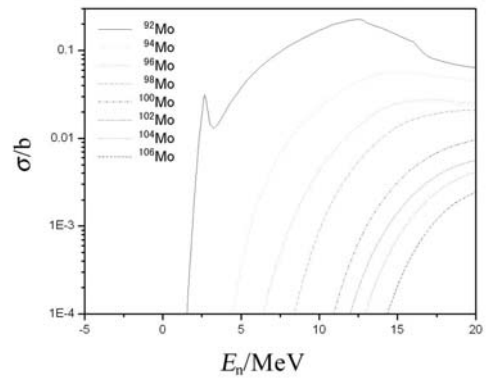

Fig.5 (n,p) cross sections

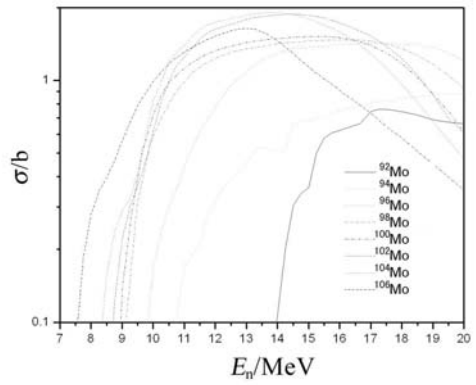

Fig.8 (n,2n) cross sections

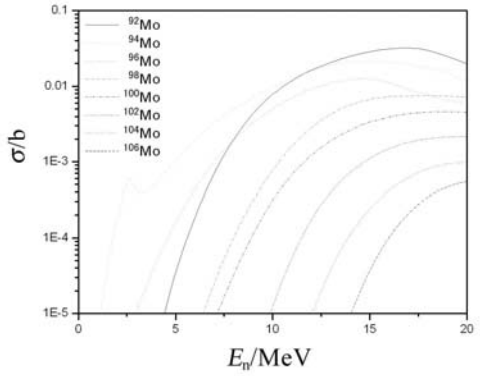

Fig.6 (n,α) cross sections

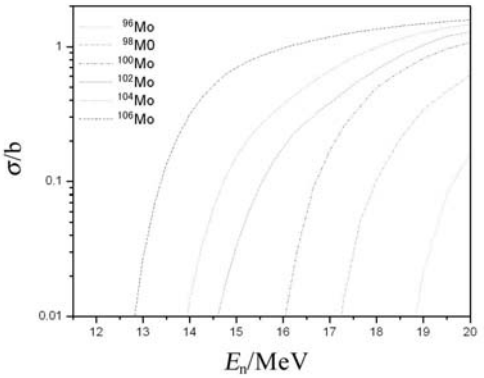

Fig.9 (n,3n) cross sections

References

[1] SHEN Qingbiao, "APMN-A Program for Automatically Searching Optimal Optical Potential Parameters in E≤300 MeV Energy Region", Nucl. Sci. Eng., 141(1), 78, (2002);

[2] P.D.KUNZ, "a DWBA Code DWUCK4", University of Colorado, USA (unpublished);

[3] ZHANG Jingshang, "User Manual of UNF Code", CNDC-0032, CNIC-01616, China Institute of Atomic Energy, P.O. Box 275(41), Dec. 2001; also New Functions in UNF Code and Illustration, Commu. Nucl. Data Progress (INDC(CRP)-053/L) No.25, p22, June 2001;

[4] C.M.PEREY, F.G.PEREY, "Compilation of Phenomenological Optical-Model Parameters", Atomic Data & Nucl. Data Tables, 17, pp1-101, 1976;

n+$^{106,108,110\sim114,116,Nat}$Cd($E_n \leqslant 20$ MeV) Nuclear Data Calculation and Analysis

WANG Shunuan

China Nuclear Data Center, CIAE, P.O.Box 275(41), Beijing 102413, P.R.China

Introduction

The nuclear data calculations for n+$^{106,108,110\sim114,116,Nat}$Cd ($E_n \leqslant 20$ MeV) has been carried out by using spherical optical model, coupled channel optical model, pre-equilibrium exciton model and equilibrium statistical model. The calculated cross sections, angular distributions, spectrum and double differential cross sections by using codes of APOM[1], ECIS95[2] and UNF[3] are compared with all existing experiment data, which were taken from EXFOR. The calculated results are analyzed from theoretical model and model parameters. The work is for CENDL-3.

1 A Brief Review of Exist Evaluated Data from ENDF/B-6, JENDL-3 and CENDL-2

There are total 8 elements of Cd. The percent abundances for $^{106,108,110\sim114,116}$Cd are 1.25, 0.89, 12.49, 12.80, 24.13, 28.73, 7.49 respectively. The total percent abundances for even-even and odd nuclides of Cd are 74.98 and 25.02 respectively. In ENDF/B-6 and JENDL-3 libraries there are all together 9 elements including natural element, i.e. $^{106,108,110\sim114,116,Nat}$Cd, evaluated, while in CENDL-2 library there is only the natural element evaluated. In the present work the 9 nuclides are calculated. In ENDF/B-6 and CENDL-2, the direct reaction contribution was not taking into account, in JENDL-3 the direct reaction contribution was taking into account properly only for one or two levels by using DWUCK-4 code[4] and only for even-even nuclides. In JENDL-3 the spherical optical model parameters were obtained only by using experimental data σ_t of $^{111}_{48}$Cd, and the results were generalized for all other elements of Cd, as well as the natural one; the (n,2n), (n,p), (n,α) cross sections were normalized at 14.5 MeV for $^{108}_{48}$Cd, $^{110}_{48}$Cd; the (n,p),(n,α) cross sections were normalized at 14.5 MeV for $^{112}_{48}$Cd, $^{114}_{48}$Cd; the (n,γ) cross section at 14 MeV and the (n,p), (n,α) cross sections at 14.5 MeV for $^{112}_{48}$Cd were normalized; the (n,p) cross section were normalized at 14.5 MeV for $^{116}_{48}$Cd.

2 Spherical Optical Model Calculation

The situation of n+$^{106,108,110\sim114,116}$Cd($E_n \leqslant 20$ MeV) of all experimental data for total cross section and non-elastic cross section as well as angular distributions of elastic cross sections taking from EXFOR are briefly shown in Table 1.

According to the situation of existing all experimental data mentioned above and the review and comparison between ENDF/B-6 and JENDL-3 with experimental data, with running code APOM by using σ_t, σ_{non} of the newest ENDF/B-6 evaluated data and all exist experimental data $\sigma_{el}(\theta)$ for each Cd element as well as taking parameters obtained by CENDL-2 for natural Cd as the initial input ones, the whole set of optimum spherical optical model 21 parameters for n+$^{106,108,110\sim114,116}$Cd ($E_n \leqslant 20$ MeV) were obtained respectively by automatically searching for main 14 parameters among 21 parameters based on the formula described in Ref.[3]. The results are shown in Table 2.

The calculated total cross section, elastic cross section and its angular distributions, non-elastic cross section are compared with all exist measured data taking from EXFOR and also with ENDF/B-6 and JENDL-3. The satisfied agreement is obtained in general view. It will be shown in Sec.7.

Table 1 The situation of n+$^{106,108,110\sim114,116,Nat}$Cd(≤20 MeV) existing all experimental data for σ_t, σ_{non}, $\sigma_{el}(\theta)$

	σ_t	σ_{non}	$\sigma_{el}(\theta)$
^{Nat}Cd	yes(more)	no	yes(0.87,4.5,5,5.5,5.9,6.5,7.14,8.08,8.41,9.06,9.5,9.99,8.05,14.2 MeV)
^{106}Cd	no	no	yes(0.4,0.6,0.8,1,1.06 MeV)
^{108}Cd	yes(a few)	no	no
^{110}Cd	yes(more)	no	yes(0.4,0.6,0.8,1,1.06,1.24 MeV)
^{111}Cd	yes(a few)	no	yes(0.4,0.6 MeV)
^{112}Cd	yes(a few)	no	no
^{113}Cd	yes (a few)	no	no
^{114}Cd	yes	no	yes(4 MeV)
^{116}Cd	yes(more)	no	yes(0.6,0.8,1,1.06,1.24 MeV)

Table 2 Obtained optimum model parameters

	^{106}Cd	^{108}Cd	^{110}Cd	^{111}Cd	^{112}Cd	^{113}Cd	^{114}Cd	^{116}Cd
AR	0.656 933 61	0.657 005 13	0.657 419 38	0.656 707 11	0.657 890 26	0.656 871 02	0.657 422 36	0.657 711 21
AS	0.480 209 77	0.480 200 83	0.480 099 5	0.480 194 87	0.480 002 64	0.480 184 44	0.480 103 97	0.480 110 11
AVV	0.659 259 44	0.659 223 68	0.659 202 81	0.658 988 24	0.658 997 18	0.659 214 74	0.659 274 34	0.850 000 02
ASO	0.656 933 61	0.657 005 13	0.657 419 38	0.656 707 11	0.657 890 26	0.656 871 02	0.657 422 36	0.657 711 21
XR	1.258 497 6	1.258 509 52	1.258 563 16	1.258 479 71	1.258 610 84	1.258 503 56	1.258 569 12	1.258 636 24
XS	1.267 350 2	1.267 338 28	1.267 219 07	1.267 391 92	1.267 076 02	1.267 368 08	1.267 219 07	1.267 167 93
XV	1.250 817 4	1.249 732 61	1.244 213 22	1.241 715 79	1.233 651 28	1.249 494 19	1.247 866 99	1.236 668 23
XSO	1.258 497 6	1.258 509 52	1.258 563 16	1.258 479 71	1.258 610 84	1.258 503 56	1.258 569 12	1.258 636 24
XC	1.25	1.25	1.25	1.25	1.25	1.25	1.25	1.25
								(in fm)
U_0	0.033 531 58	0.033 214 74	0.019 948 98	0.030 608 15	0.008 549 68	0.029 192 82	0.020 536 74	0.020 608 83
U_1	0.226 758 60	0.241 469 76	0.050 722 84	0.050 722 84	0.0	0.223 950 49	0.199 520 05	0.058 829 15
U_2	0.005 592 74	0.005 413 53	0.006 082 62	0.001 702 14	0.004 887 78	0.005 713 61	0.006 980 90	0.002 600 24
V_0	47.301 757 8	47.307 289 12	47.297 561 65	47.341 430 66	47.252 929 69	47.339 141 85	47.320 259 09	47.299 526 21
V_1	0.129 573 9	0.117 635 47	0.101 553 76	0.078 146 27	0.030 801 85	0.105 124 45	0.228 792 47	0.137 201 38
V_2	–0.000 416 7	–0.000 973 63	0.000 010 86	–0.001 782 9	0.001 586 28	–0.000 911 5	0.002 271 27	–0.009 755 04
V_3	–24	–24	–24	–24	–24	–24	–24	–24
V_4	0.0	0.0	0.0	0.0	0.0	0.0	0.0	0.0
V_{SO}	6.2	6.2	6.2	6.2	6.2	6.2	6.2	6.2
W_0	9.524 559 02	9.524 463 65	9.522 794 72	9.524 606 7	9.521 030 43	9.524 368 29	9.522 842 41	9.523 064 61
W_1	–0.051 281 9	–0.051 577 12	–0.054 027 62	–0.053 243 699	–0.057 461 78	–0.051 609 35	–0.05 240 76	–0.052 368 07
W_2	–12	–12	–12	–12	–12	–12	–12	–12
								(in MeV)

3 Coupled Channel Optical Model ECIS95 Calculations

The direct inelastic scattering cross section and angular distributions for two discrete levels of $^{106,108,110\sim114,116}$Cd and for four discrete levels of $^{113}_{48}$Cd have been calculated by using coupled channel optical model codes of ECIS95[2] and PRECIS[5], the spherical optical model parameters obtained in the present work as mentioned above with β_2=0.2 and β_4=0.02.

4 Cross Sections, Spectrum, Double Differential Cross Sections of Pre-equilibrium and Equilibrium Statistical Model UNF Calculation

In spectrum, double differential cross sections of pre-equilibrium exciton model calculations, the free parameter *K*-value of the square of the average two-body residual interaction matrix element formulated by C. Kalbach et al.[6] was taken as K=600 MeV^3. This consideration is referenced to our previous papers[7~10]. The calculated results and comparison with experimental data will be presented in Sec.6.

5 Natural Element Cd Calculation

According to the detailed calculation of n+$^{106,108,110\sim114,116}$Cd ($E_n\leqslant$20 MeV) and the percent abundances of each Cd elements, a consistent synthesis method is used to get the whole set of evaluated data for natural element Cd without any models and any parameters as well as parameters adjustment.

In the consistent synthesis method calculations, the selected levels of ^{Nat}Cd are 3 from ^{106,108}Cd respectively, 4 from ^{116}Cd, 5 from $^{110,112\sim114}$Cd respectively, 6 from ^{111}Cd. Total levels number of ^{Nat}Cd is 36 . There are many experimental data of ^{Nat}Cd (n,tot) ($E_n\leqslant$20 MeV) cross sections, ^{Nat}Cd (n,el) ($E_n\leqslant$ 20 MeV) cross sections and its angular distributions (at different energies), ^{Nat}Cd (n,non) cross sections, as well as ^{Nat}Cd (n,inl) double differential cross sections at 14 MeV with different angles. The consistent synthesis results of ^{Nat}Cd are compared with those data shown in Sec.6. The agreement is perfect as expected. The consistent synthesis method used in UNF code works effectively.

6 Calculated Results and Comparison with Experimental Data

Figs.1~3 show, respectively, the results of total cross section, elastic cross section, non-elastic cross section for natural element ^{Nat}Cd compared with experimental data and CENDL-2, ENDF/B-6, JENDL-3.

The agreements are satisfied in general words. It seems that the difference between ENDF/B-6, JENDL-3 for total cross section and elastic cross section at energy range of above 15 MeV is rather big. The results of CENDL-2 and the present work are in between ENDF/B-6 and JENDL-3.

The calculated results of angular distributions of elastic scattering at different energies from 0.87 to 14.2 MeV for natural element ^{Nat}Cd and compared with all existing valuable experimental data taking from up-data EXFOR contributed by different Labs. The agreement is perfectly well. Some of the results of the comparison are shown in Figs.4~7, respectively.

Figs.8~14 show respectively the calculated results of σ(n,inl), σ(n,2n), σ(n,p), σ(n,t), σ(n,d), σ(n,α), σ(n,3n) for natural element ^{Nat}Cd, compared with experimental data and CENDL-2, ENDF/B-6, JENDL-3. There are some data at low energy range for σ(n,inl). There is only one experimental value at 14 MeV for σ(n,2n). There are no any data for other reaction channels, but the present results are in the middle among CENDL-2, ENDF/B-6, and JENDL-3, generally speaking. The shapes of σ(n,p), σ(n,α), σ(n,2n) of ENDF/B-6 at above 15 MeV seem not reasonable.

The calculated double differential cross sections for n+^{Nat}Cd (n,inl) at 14 MeV with 61°, 91°, 121°, 151° of mass center system are compared with existing experimental data respectively. The experimental data were taken from Ref. [11]. From the comparison between calculated results and the experimental data, it is clear that the theoretical calculation of equilibrium contribution is not taken into account enough properly in the forward angular range, but in the backward angular range, it looks properly suitable.

In summary, the whole set of nuclear data calculation in ENDF/B-6 format for n+$^{106,108,110\sim114,116,Nat}$Cd ($E_n \leqslant 20$ MeV) has been carried out. From the agreement of the comparison between theoretical results and existing experimental data, it can be concluded that the model and its parameters used in the present work are properly suitable. Based on the detailed calculation of n+$^{106,108,110\sim114,116}$Cd ($E_n \leqslant 20$ MeV) and the percent abundances of each Cd isotopes, the consistent synthesis method used to get the whole set of evaluated data for Cd-Nat natural element without any models and any parameters adjustment works quite reasonably, effectively, reliably and consistentntly from physical point of view.

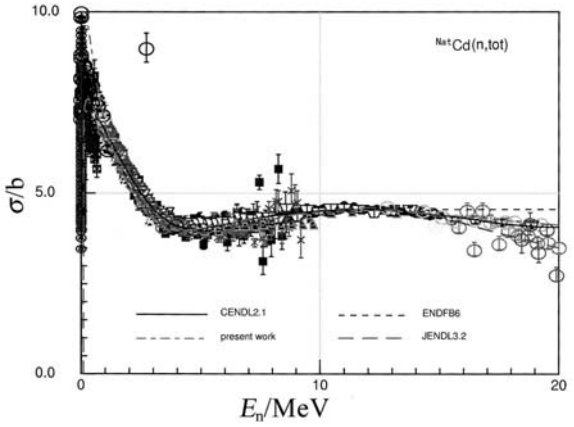

Fig.1 Calculated total cross section and compared with exp. data and ENDF/B-6, JENDL3, CENDL2

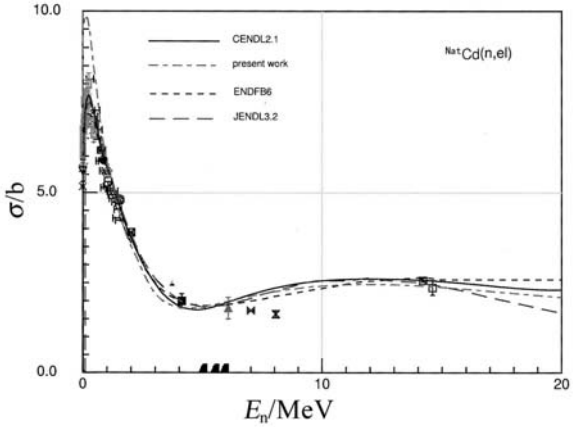

Fig.2 Calculated elastic cross section and compared with exp. data and ENDF/B-6, JENDL-3, CENDL2

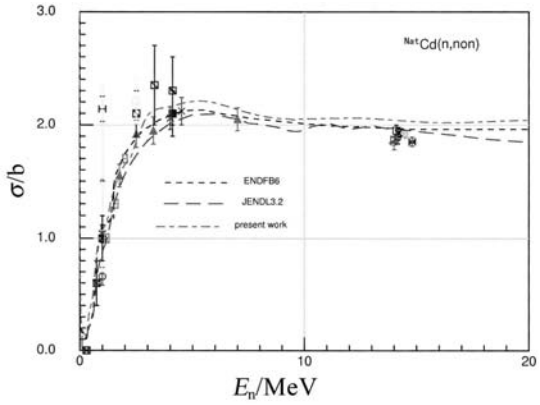

Fig.3 Calculated non-elastic cross section and compared with exp. data and ENDF/B-6, JENDL-3, CENDL2

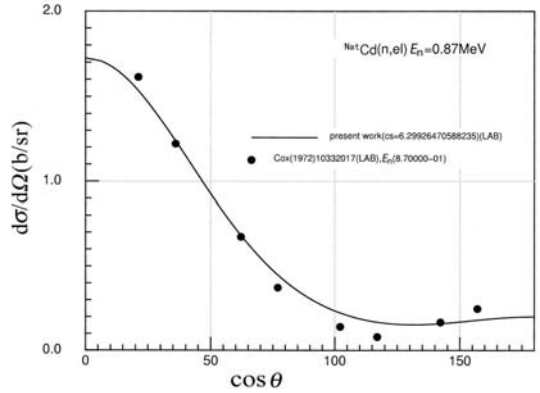

Fig.4 Calculated angular distribution of ^{Nat}Cd (n,el) at E_n=0.87 MeV and compared with experimental data

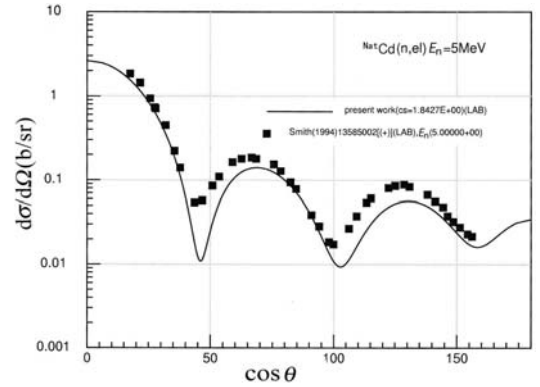

Fig.5 Calculated angular distribution of ^{Nat}Cd(n,el) at E_n=5 MeV and compared with experimental data

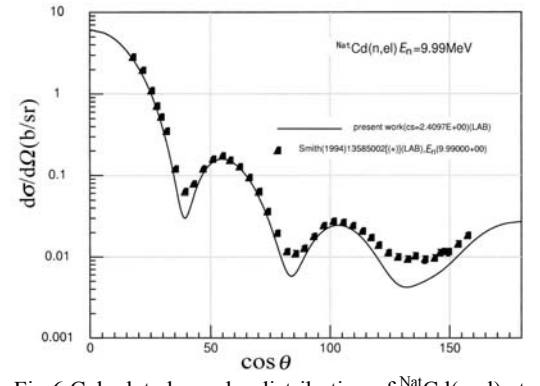

Fig.6 Calculated angular distribution of ^{Nat}Cd(n,el) at E_n=9.99 MeV and compared with experimental data

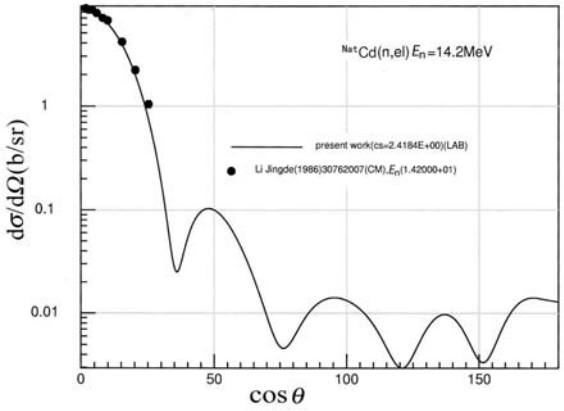

Fig.7 Calculated angular distribution of ^{Nat}Cd(n,el) at E_n=14.2 MeV and compared with experimental data

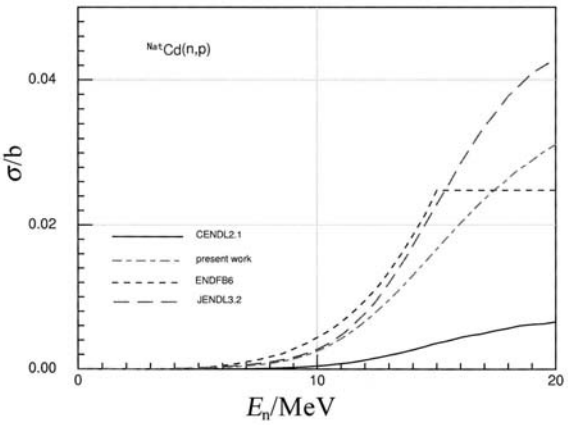

Fig.10 Calculated σ(n,p) compared with ENDF/B-6, JENDL3 and CENDL2

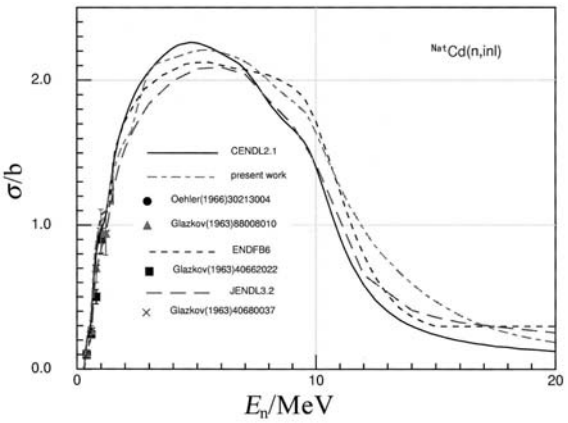

Fig.8 Calculated σ(n,inl) compared with exp. data and ENDF/B-6, JENDL3, CENDL2

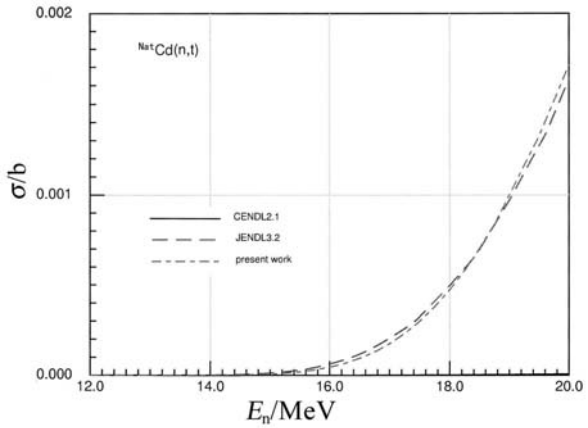

Fig.11 Calculated σ(n,t) compared with ENDF/B-6, JENDL3 and CENDL2

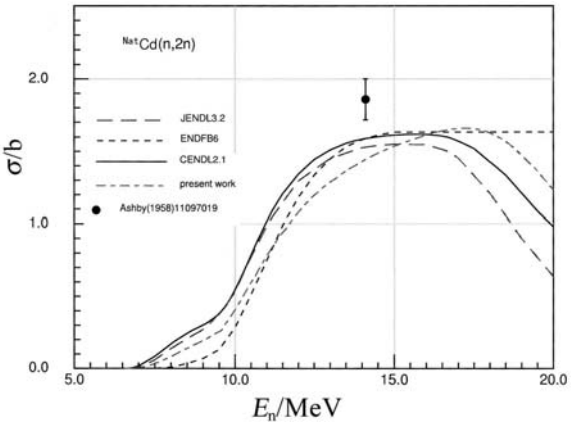

Fig.9 Calculated σ(n,2n) compared with exp. data and ENDF/B-6, JENDL3, CENDL2

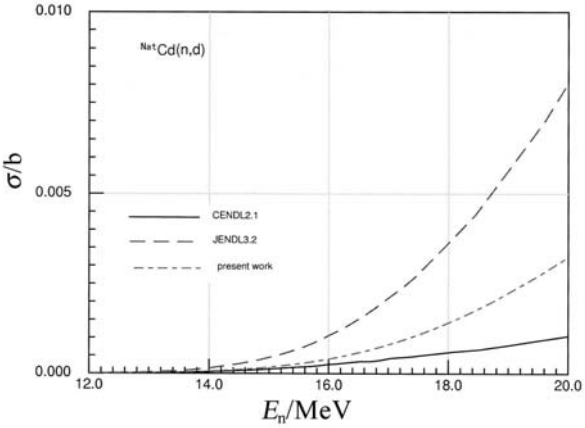

Fig.12 Calculated σ(n,d) compared with ENDF/B-6, JENDL3 and CENDL2

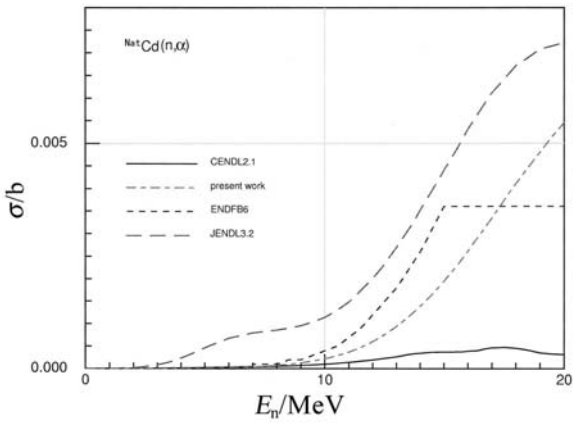

Fig.13 Calculated σ(n,α) compared with ENDF/B-6, JENDL3 and CENDL2

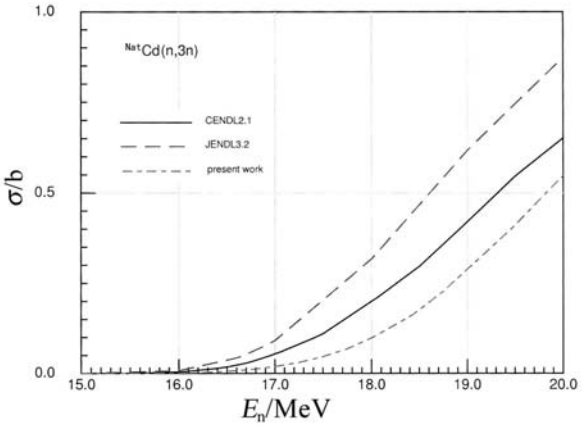

Fig.14 Calculated σ(n,3n) compared with ENDF/B-6, JENDL3 and CENDL2

References

[1] SHEN Qingbiao, CNDP.7,43,1992.
[2] J. Raynal, Note on ECIS94, CEN-N2772,1994.
[3] ZHANG Jingshang, CHIC-01616,CNDC-0032,2001.
[4] P.D. Kunz, A DWBA code DWUCK-4, University of Colorado USA (unpublished).
[5] Carlson B.V. The Optical Model and ECIS95. SMR/ 1220-4, Workshop on Nuclear Reaction Data and Nuclear Reactors: Physics, Design and Safety, 13 March-14 April 2000, Trieste, Italy
[6] C.Kalbach, Nucl.Phys.A210,590(1973).
[7] SUN Ziyang, WANG Shunuan, ZHANG Jingshang, ZHUO Yizhong, Z.Phys.A 305,61-68(1982).
[8] SUN Ziyang, WANG Shunuan, ZHANG Jingshang, ZHUO Yizhong, K.H. Bockhoff (ed.), Nuclear Data for Science and Technology, 603-605(1983).
[9] D. Hermsdorf et al., Zeentralinstitut fur Kernforschung, Rossendorf bei Dresden Report No.ZFK-277 (1974).
[10] SHEN Qingbiao, Tian Ye, Wang Shunuan et al., Chinese Jour.Nucl.Phys., Vol.6, 245(1984).
[11] Sal Nikov, V.B. Anufrienko, G.N. Lovchikova, EXFOR-40238017-20, R, YK-15, 129,1974.

Re-Evaluation of Complete Neutron Data for ^{233}U

YU Baosheng

China Nuclear Data Center, CIAE, P.O.Box 275(41), Beijing 102413, P.R.China

【**abstract**】 *The revision of a complete set of n +^{233}U nuclear data from 10^{-5} eV~20 MeV were carried out and recommended based on evaluated experimental data and feedback information of various benchmark tests for previous evaluated data. The theoretical calculations were made using FUNF code 2003 version. The main revised quantities are the resonance parameters, fission cross sections, inelastic and elastic scattering cross sections as well al angular distributions etc. The preliminary benchmark tests indicate that the new evaluated data predicts various reactor characteristics more successfully than the previous version.*

Introduction

The accurate neutron nuclear data of ^{233}U play an important role for the improvements of the U-Th fuel cycles of all thermal and fast reactor systems. Based on various feedback information and new experimental data, a complete set of neutron nuclear data of ^{233}U was re-calculated and re-evaluated from 10^{-5} eV~20 MeV for CENDL-3 revision-1. The recommended data were based on evaluated experimental data and adjusted theoretical calculated results, except the resonance parameters that were taken from JENDL-3.3. The comparison of our evaluated data with other recommendations from ENDF/B-6 and JENDL-3 was performed.

1 Thermal Cross Sections and Resonance Parameters

The resonance parameters were taken from JENDL-3.3. The resolved resonance region is from 1 eV to 150 eV, which is the same as JENDL-3.2, based on the SAMMY analysis by H. Derrien[1]. The unresolved resonance parameters were modified for JENDL-3.3 so as to reproduce the evaluated cross sections very well in the energy region from 0.15 keV to 30 keV.

The total neutron number per fission is a sum of prompt and delayed neutron number per fission. The number of prompt (ν_p) and delayed (ν_d) neutrons emitted per fission event was evaluated for ^{233}U by YU Baosheng[2], based on absolute measurements and ones relative to the spontaneous fission ν of ^{252}Cf. Existent experimental data and some systematic were used. The dependence of prompt neutron number on incident neutron energy for ^{233}U was given by approximated linear function from 10^{-5} eV to 20 MeV. The delayed neutron spectra evaluated by T.R. England[3] were adopted in this work.

2 Reaction Cross Section Above 30 keV

2.1 Total Cross Section

Lots of experimental data of σ_{tot} cover all energy region. The data were measured by W.P. Poenitz[4,5] from 0.1 MeV to 4.43 MeV in 1978 and from 0.11 MeV to 4.8 MeV in 1981 by using time of flight technology with enriched 99.97% of ^{233}U sample at ANL. But the data measured by W.P. Poenitz[4,5] are higher by 8% around 1.6 MeV and 4.8% around 14 MeV than previous evaluated data, respectively. The data by W.P. Poenitz[6] are from 1.8 MeV to 20 MeV, which extends the energy region from 15 MeV to 20 MeV. Therefore, The measured data for σ_{tot} cover from 40 keV to 20 MeV. No experimental data exist from 30 keV to 40 keV, an extrapolation was made from the experimental data above 40 keV.

For elastic scattering angular distributions there are two sets of data at 0.7 MeV and 1.5 MeV, which were carried out by G. Haouat[7] in 1982. As the nonrealistic cross sections, these data were measured by R.F. Taschch[8] at 1.24 MeV and 1.6 MeV. In order to get the optimal optical potential parameter, below the threshold energy of (n,2n) reaction, the experimental data $\sigma_{n,\gamma}+\sigma_{n,n'}+\sigma_{n,f}$ were used as experimental σ_{non} for searching the potential parameters.

2.2 Fission Cross Section

Lots of fission cross section of ^{233}U were measured by using ratio measurement and absolute measurement in energy region from 30 keV to 20 MeV. For early measurements, the disagreement among different laboratories is 24%~28% around 6 MeV and lack of experimental data in some energy region. In order to resolve discrepancies of measured data and fill the gaps, some accurate measurements were performed and shown in Table 1.

The improvements of measurement technology were conducted by J.W. Behrens[9] using ionization fission chamber at the time-of-flight spectrometer at 100 MeV Linac in 1978. The new procedure is called "threshold cross section method" using three detectors: A, containing a high-purity threshold isotope (i.e. ^{234,236}U or ^{238}U); B, another to be measured fissile isotope ^{233}U (or ^{235}U) and a mixture of the threshold and to be measured fissile isotopes. The three fission chambers are exposed simultaneously to the same beam.

The $R(E)$ is the ratio of the counting rates γ_m of mixture fission chamber to the counting rates γ_p of the fissile chamber. Below the fission threshold of threshold fission isotope, Q represents a constant. η is atom ratio of fissile isotope to the threshold isotope. Mass spectrometer was used to measure the isotopic compositions.

Table 1 Collected data and relevant information for ^{233}U(n,f) reaction

Year	Author	E_n/MeV	Measured Values at 14.7 or 19.4 MeV	Mothod	Monitor	Comments
1976	J.W.Behrns	1.0~29.0	14.7 MeV 2.238±0.07, 19.4 MeV 2.033±0.07	T-O-F	^{235}U(n,f)	at Linac
1978	G.W.Carlson	0.000 85~29	14.7 MeV 2..274±0.06, 19.4 MeV 2.049±0.07	T-O-F	^{238}U(n,f)	at Linac
1978	W.P.Poenitz	0.137~8.1		T-O-F	Absolute	
1979	J.W.Meadows	14.74	2.37±0.02	Chamber	^{235}U(n,f)	
1980	E.A.Zhagrov	0.12				
1981	R.Arlt	14.7	2.244±0.039	ASSOP	Absolute	Enriched Samples 99.99%
1983	I.D.Alkhaziv	14.7	2.244±0.042	ASSOP	Absolute	FISCH Metallic Sample
1984	K.R.Zasadny	14.62	2.430±0.080	Activation	^{56}Fe(n,p)	Corrected Value
1986	I.D.Alkhazov	19.4	1.930±0.070	ASSOP	Absolute	FISCH Metallic Sample
1987	V.A.Kalinin	19.4	1.930±0.070	ASSOP	Absolute	FISCH Metallic Sample

ASSOP : Associated Particle Method; FISCH : Multilayer Ionization Chambers for Fission Fragments

$$\gamma_m(E)=\varphi(E)\beta_m N_A[\sigma_A(E)+\eta\sigma_B(E)] \quad (1)$$

$\varphi(E)$: Neutron Flux;

N_A: Neutron of atomic of isotope A;

β_m: efficiency for detecting fission fragments in the mixed chamber.

$$\gamma_p(E)=\varphi(E)\beta_p N_B\sigma_B(E) \quad (2)$$

$$R(E)=\frac{\gamma_m(E)}{\gamma_p(E)}=\frac{\beta_m N_A}{\beta_p N_B}\left[\frac{\sigma_A(E)}{\sigma_B(E)}+\eta\right] \quad (3)$$

Below the fission threshold of isotope A, $R(E)$ is a constant Q

$$\frac{\beta_m N_A}{\beta_p N_B}=\frac{Q}{\eta} \quad (4)$$

The cross section ratio is shown:

$$\sigma_{threshold}(E)/\sigma_{fissile}(E)=\eta[R(E)/Q-1] \quad (5)$$

Using the "threshold cross section method", the advantage is that it does not require knowledge of the relative masses within the high-purity fission chambers and the detector efficiency. Furthermore, the procedure is suitable to the white neutron source.

The accurate fission cross sections could be obtained in widely energy region using white neutron source. During 1976~1978, the fission cross sections of ^{233}U to ^{235}U were measured by J.W. Behrens[9] in energy region 1.0 MeV to 29 MeV and the ratio of ^{233}U to ^{238}U by G.W. Carlson[10] in energy region 0.85 keV to 29 MeV using the "threshold cross section method". Their data are consistent with each other within the errorbar. There is a significant improvement for either the experiment uncertainties or the discrepancy, which was eliminated or significantly reduced.

The data measured by J. Wbehrns[9] and G.W. Carlson[10] were re-normalized to standards cross sections. The standards cross sections for ^{235}U(n,F) and ^{238}U(n,F) reactions were taken from ENDF/B-6.

After the 1978s some measurements were made by W.P. Poenitz[11], J.W. Meadiws[12], E.A.Zhagrov[13] R. Arlt[14], I.D. Alkhaziv[15,16], K.R. Zasadny[17] and V.A. Kalinin[18]. The data around 14.7 MeV were measured by J.W. Meadiws[12] and K.R. Zasadny[17] with activation method, and by R. Arlt[14] and I.D. Alkhaziv[15] with enriched sample 99.99% of ^{233}U using associated particle method. The cross sections at 19.4 MeV were measured by I.D. Alkhaziv[15] and V.A. Kalinin[16] using associated particle method. These measured data are in better agreement with the

measured data by J. Wbehrns[9] and G.W. Carlson[10]. Therefore the measured data by J. Wbehrns[9] and G.W. Carlson[10] were examined. So those measured data mentioned above are reliable.

The modified unresolved resonance parameters of JENDL-3.3 were adopted in this work. In order to make the conjunction of cross sections at boundary, carefully adjustments were made for the cross sections concerned in smooth region. After adjusting, the cross section at boundary are of good conjunction within fixed errors.

2.3 Radiation Capture Cross Section

For the ^{233}U(n,γ)^{234}U reaction, there are experimental data available in energy region from 30 keV to 1 MeV. The alpha values measured by J.C. Hopkins[19] were multiplied by the fission cross section. Based on the theoretical calculated and experimental data, the evaluated data were obtained, which could reproduce the experimental data very well. The data for ^{233}U(n,γ)^{234}U reaction were reasonably adjusted at the connection boundary between the smooth cross section and unresolved resonance parameters. Because the both value are very close to each other, they only made a little change.

3 Theoretical Calculation and Parameter Adjusting

In order to recommend a complete set of neutron nuclear data of ^{233}U, the theoretical calculation were performed with FUNF code[20] 2003 version, based on the available total cross sections of ^{233}U, nonelastic scattering cross sections evaluated by us from (n,γ), (n,2n) etc. in energy region 0.001~14 MeV as well as a few experimental data of elastic angular distributions. A set of neutron optical potential parameters for ^{233}U was obtained in the energy region 0.001~20 MeV by using automatically searching code APFO96[21].

Legendare polynomial representations were used for scattering angular distributions. For previous calculation there appeared negative values in some angles for elastic scattering angular distribution. Now, the problems were revised and the Legendare coefficient arrive 24 order. In this work, the recommended Legendare coefficient for elastic scattering angular distribution is 22 order starting at 10.25 MeV and 24 order staring at 13.25 MeV, respectively. For elastic scattering angular distributions there are two sets of experimental data at 0.7 MeV and 1.5 MeV, measured by G.Haouat[7] in 1982. The calculated elastic scattering angular distribution could reproduce the experimental data well. The calculated results were compared with ENDF/B-6, JENDL-3.2, JENDL-3.3 and BROND-2.

For direct discrete levels, it was found that the previous evaluated direct inelastic scattering angles distribution appears negative values in some angules. Therefore, the inelastic scattering cross sections and its angular distribution data were re-calculated by using ECIS[22] and FUNF code[20] 2003 version.

In the few-MeV region inelastic scattering cross sections in fissile cases are much lesser accurate. Therefore the determination of the nonelastic cross sections were made by A.B.Smith[23] with the metallic samples of >95% isotopic purity in the time–of–flight apparatus of Argon National Laboratory. Because the total cross sections of ^{233}U measured by W.P. Poenitz[6] are known to be ⩽1.5%. Though the radiate-capture cross sections are not as well known but very small. Fission cross sections are known to be 2%~3% and nubar to be 1%~2%. Elastic scattering cross sections can measured with an accuracy of ⩽3%. The experimentally deduced the total inealstic scattering cross sections of ^{233}U were deduced by subtracting the elastic scattering, fission and capture cross sections from total cross section at 0.93, 1.27, 1.49, 1.85, 2.55, 3.55 MeV, respectively. But the data measured by A.B. Smith[23] do not contain contributions of the partial inelastic scattering to some low-lying excited states, and therefore the missing components were supplemented by the calculated. Now evaluated was made so as to reproduce the corrected data of A.B. Smith[23] in this calculation.

Using this set of neutron optical potential parameters and adjusted level density and giant dipole resonance parameters as well as fission parameters, the reaction cross sections, secondary neutron spectra and angular distributions of n + ^{233}U were calculated in this work.

4 Comprehensive Recommendation

The evaluated total cross section and calculated elastic scattering angular distribution with other evaluated data from ENDF/B-6, JENDL-3 and BROND-2 are shown in Fig.1,2.

The recommended fission cross sections were based on the evaluated data and feedback benchmark testing information. The benchmark testing for some experiments was made by RONG Jian[24]. It was found that the $k_{\rm eff}$ factor is strictly effected. After adjusting the magnitude of fission cross section within errors from 0.05 MeV to 8 MeV, the calculated results are in agreement with the $k_{\rm eff}$ experimental data very well, but the evaluated cross section are lower than JENDL-3.2 and ENDF/B-6.

It is found that the evaluated ^{233}U(n,f) cross section from JENDL-3.3 are lower than those of

JENDL-3.2 above 300 keV. But the revised data of JENDL-3.3 are in agreement with our evaluated ones better, especially in energy region blew 10 MeV, shown in Fig. 3.

The recommended cross sections for (n,γ) were given based on the measured and theoretically calculated data. The recommended cross sections for ^{233}U(n,γ) reactions could reproduce the experimental data very well.

In order to calculate the inelastic scattering cross sections, these direct inelastic scattering data and the optimum set of optical potential parameters are used as the input data of FUNF. The discrete levels were taken from China Nuclear Parameter Library[25]. The level scheme of China Nuclear Parameter Library was revised in 2003.

Above 0.6 MeV, the levels are assumed to be overlapped. The first three levels were calculated with coupled levels calculation code and adjusted the shape and magnitude for the three levels to reproduce the experimental data by A.B.Smith[23]. The adjusted first three levels and total inelastic scattering cross sections with other calculated data from ENDF/B-6 and JENDL-3 are shown in Fig.4.

The theoretical calculation were performed with FUNF code[20]. A complete set of neutron data were obtained based on evaluated and calculated data. Example of neutron energy spectra calculated with FUNF code[20] for some incident neutron points are presented in Figs. 5~7.

5 Remark Summary

The advantage of "threshold cross section method" are that it does not require knowledge of the relative masses within the high-purity fission chambers and the detector efficiency. Furthermore, the procedure is suitable to the white neutron source. Therefore, the accurate fission cross sections could be obtained in wide energy region. The data measured by J. Wbehrns[7] and G.W. Carlson[8] were re-nomolazed to standards cross sections from ENDF/B-6. Also, the evaluated data were made benchmark testing and the existed problems were found, ~2% reduction for the fission cross section from 0.05 MeV to 8 MeV made the calculation a significantly better agreement with the experiment. Therefore, the recommended data are improved. The preliminary benchmark tests indicate that the present evaluated data could predict various concerned U-Th fuel cycle characteristics

The inelastic scattering cross sections are of too much less accuracy for fissile nuclides. In present work, The calculation was performed based on the measured data by A.B. Smith[23] and the new evaluated discrete levels. The parameters were adjusted carefully for the shape and magnitude of first three coupled levels to make the calculated results reproduce the experimental data by A.B. Smith[23]. Therefore, the evaluated inelastic scattering cross sections are sought for requirement of fast-breeder -reactor accuracy goals.

Acknowledgments

The authors are indebted to Dr. LI Jingwen for the interesting and useful discussions and particularly to Dr. RONG Jing for providing the results of benchmark tests and making a good collaboration.

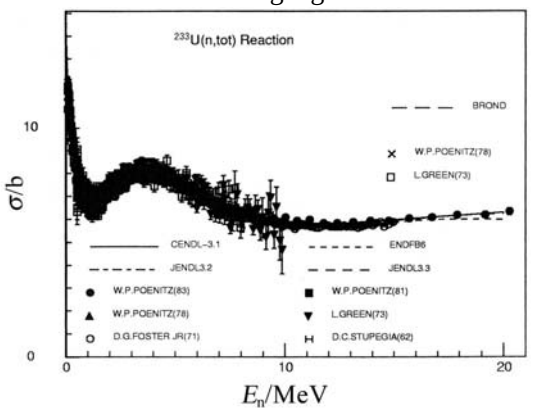

Fig. 1 Evaluated total cross section

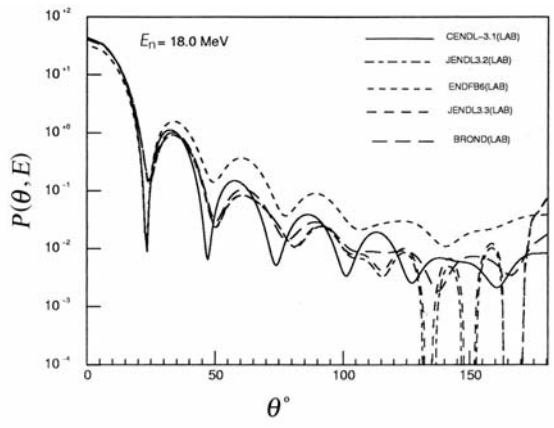

Fig. 2 ^{233}U Elastic scattering angular distribution at 18 MeV

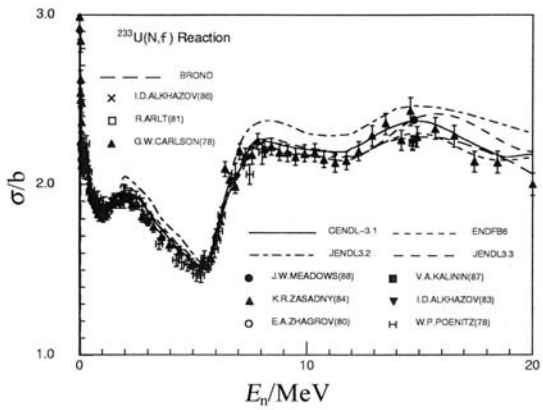

Fig. 3 Evaluated fission cross section

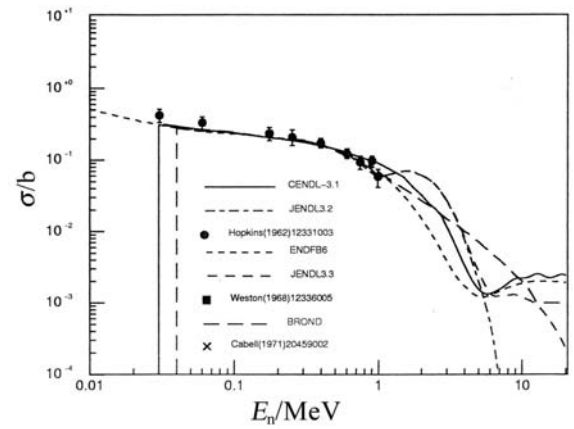

Fig. 4 Comparison of evaluated and measured ^{233}U(n,γ) cross section

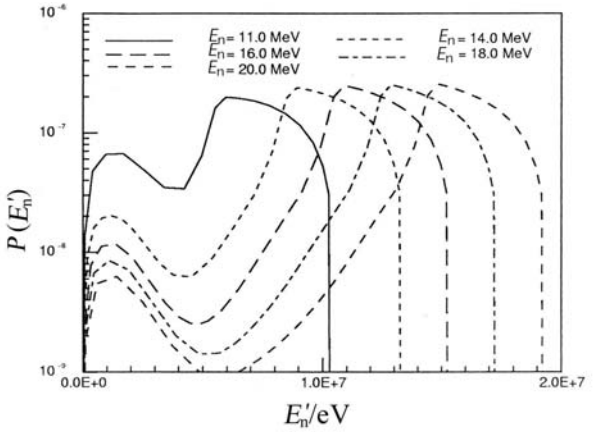

Fig. 6 Normalized secondary neutron spectra for ^{233}U(n,n') reaction MT=91

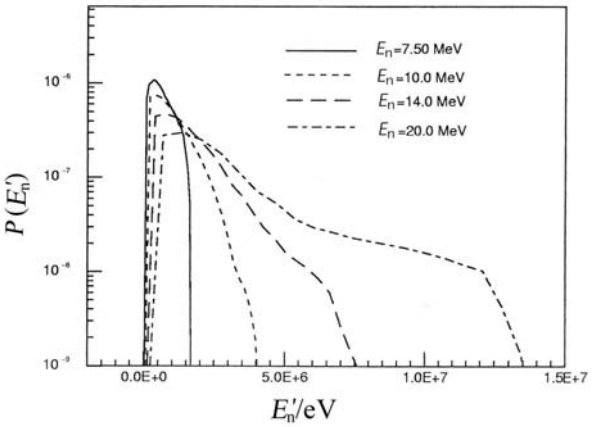

Fig. 5 Normalized secondary neutron spectra for ^{233}U(n,2n) reaction

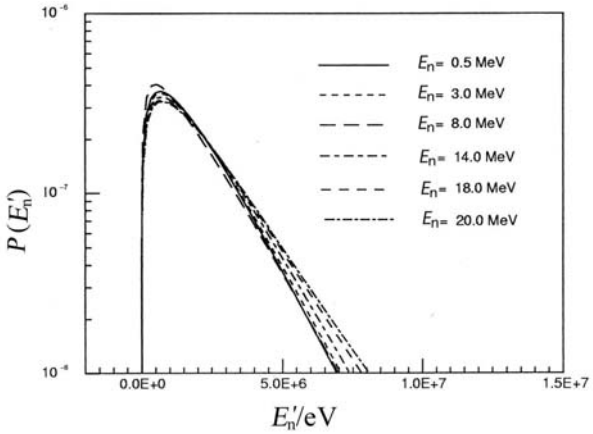

Fig. 7 Normalized secondary neutron spectra for ^{233}U(n,f) reaction

References

[1] H. Drrien et al., Nucl.Sci.Technol., 31,379(1994)
[2] YU Baosheng et al to be published (2003)
[3] T.R.Englang et al., Neucl. Sci. And Eng., 103,129(1989)
[4] W.P.Poenitz et al., Nucl. Sci. Eng., 68,358(1978)
[5] W.P.Poenitz et al., Nucl. Sci. Eng., 78,333(1981)
[6] W.P.Poenitz et al., ANL/NDM-80(1983)
[7] G.Haouat et al., Nucl. Sci. Eng., 81,491(1982)
[8] R.F.Tascheket al., EXFOR Data 12364002(1965)
[9] J.W.Behrns et al., Conf. on Nuclear Cross Sections and Technology, Washington Vol.2 ,591 (1975)
[10] G.W.Carlson et al., Nucl. Sci . and Eng.,66,205(1978)
[11] W.P.Poenitz et al., ANL-NDM-36(1978)
[12] J.W.Meadows et al., Annual of Nuclear Energy, 15,421 (1988)
[13] E.A.Zhagrov et al., Conf. on Nuclear Physics, Kiev, USSR, 15-19 Spe.,P-45(1980)
[14] R.Arlt et al., KE,24,98(1981)
[15] I.D.Alkhaziv et al., Conf. on Nuclear Spectroscopy and Nuclear Structure, Moskva,USSR, 19-21 Apr., Vol2, 201 (1983)
[16] K.R.Zasadny et al., ANS,47,425(1984)
[17] I.D.Alkhazov et al., YK,4,19(1986)
[18] V.A.Kalinin et al., YK,4,3(1986)
[19] J.C.Hopkins et al., Nucl. Sci. And Eng.,12,169(1962)
[20] ZHANG Jingshang, inter report(2003)
[21] SHENG Qingbiao, inter report(1998)
[22] J.Raynal et al., ECIS(1995) a code for coupled channel calculation notes on ECIS-94- note CEA-N-2772(1994)
[23] A.B.Smith et al., Conf. on Nuclear Data for Science and Technology, Antwerp ,P.39(1982)
[24] RONG Jing, private communication (1999)
[25] GE Zigong et al., inter report (2003)

Neutron Cross Section and Covariance Data Evaluation of Experimental Data for ^{27}Al

LI Chunjuan[1] LIU Tingjin[2] LIU Jianfeng[1]

[1]*Physics Department, Zhengzhou University, Zhengzhou 450052, P.R.China*

[2]*China Nuclear Data Center, CIAE, P.O.Box 275(41), Beijing 102413, P.R.China*

【**abstract**】 *The evaluation of neutron cross section and covariance data for ^{27}Al in the energy range from 210 keV to 20 MeV was carried out on the basis of the experimental data mainly taken from EXFOR library. After the experimental data and their errors were analyzed, selected and corrected, SPCC code was used to fit the data and merge the covariance matrix. The evaluated neutron cross section data and covariance matrix for ^{27}Al given can be collected for the evaluated library and also can be used as the basis of theoretical calculation concerned.*

Introduction

For one reaction channel, there are often many sets of data which sometimes disaccord with each other on numerical statement, this makes the users feel at loose ends, then the evaluation work becomes more and more important. With the development of the reactor physics and the improvement of experiment technology and laboratory apparatus, the experimental neutron data library is being improved constantly, then the evaluated library needs to be improved accordingly. Covariance data evaluation is now a front field task of the international nuclear data evaluation, complete error information is given out by the covariance matrix, which describes not only the accuracy of the data but also the correlation of them. Increasing covariance data file in evaluated library has also been an important task of nuclear data evaluation.

Aluminum is a very important structure material in nuclear engineering, its data are very important parameters for nuclear engineering design. And the neutron cross section data evaluation for aluminum is very important not only for nuclear engineering but also for the study of basic nuclear science. At present, there are still no covariance data file in all main evaluated libraries, so it is very necessary to evaluate the neutron cross section and covariance data of experimental data for aluminum.

1 Evaluation of Experimental Data and Their Errors

Evaluation includes two aspects, one is to evaluate physically, on the basis of experimental data being collected in every probable way and the experiment details being analyzed at large, necessary choice, adjustment and correction were done to make them accord with each other statistically. The other is to process to give the optimum data in mathematics and the reasonable error of them by merging or curve fitting the data sets.

One main way to get the experimental data is data retrieval, through the data management system retrieval code, the experimental data and their information were got from EXFOR[1] (experimental nuclear data) library by inputting corresponding nuclide sort, reaction channel, data type or databank coding. Then TT[2] code was used to draw and compare. The experimental data can also be got in other way, such as the publications about the neutron data, the proceedings of the international conference about nuclear data which is staged every four years, and so forth.

The data were first selected according to the energy range (the wider, the better), the date (the later, the better) and the number of data points (the more, the better). Then they were drawn with TT and the data sets whose statistic fluctuation is too big were

abandoned. If the trend is not right, the experimental information should be analyzed to find the reason. To concretely evaluate the left data sets, theirs labs, methods, detectors, monitors and measured objects were mainly considered.

To construct the covariance matrix, error analysis for the adopted data is very important, the statistical and systematical errors, or the short, middle and long range errors should be distinguished. Generally, the errors of the sample quantification, standard cross section etc. are long range error, the errors of detector efficiency calibration, correction of multiple scattering etc. are middle range error and the count statistical error is short one. But it should be pointed out that the statistical error could act as systematical one in some cases of the covariance analysis and evaluation, and the short range error could also act as long range one. For instance, the statistical error in one cross section measurement becomes systematical one when the cross section is used as standard for the relative measurement of another cross section. In EXFOR library, error of data is often given in two places: error analysis and the numerical value of data. Error analysis can be found in the information (BIB) part, often information of the value of error, kinds of factors that cause error and their percentage are contained. The numerical value of error is often given along with their data, the error should be total one, but sometimes it is only statistical or other partial one, we should analyze carefully. The key point to covariance data evaluation is the confirmation of the total and systematical errors. One thing is that not overall or even no information of errors is given in some EXFOR entry, in this case, the reference paper concerned should be read and a reasonable estimation of the systematical and total errors should be given according to the experimental set up such as the measurement methods, the detector efficiency calibration, the monitor used etc. Table 1[3] can be used as reference. Another thing is that the value of error given along with data is not agree with the percentage given in error analysis, then the reference paper concerned should be read and the experimental condition should be analyzed to check which one is reliable. In general, error analysis is the most important and also difficult step for the evaluation of covariance data, the evaluator should master the knowledge of the measurement and analyze carefully.

From the evaluated library CENDL-2.1 and JENDL-3.3, the upper limit of resonance region of ^{27}Al can be got and it is 210 keV, so the neutron cross section and covariance data for ^{27}Al in the energy range from 210 keV to 20 MeV were evaluated. The reaction channels for which the experimental data are available are (n,tot), (n,p), (n,α), (n,γ), (n,el) and (n,2n), the specific evaluation for these channels is given separately as follows.

1.1 ^{27}Al（n,tot）

The main measurement method of (n,tot) cross sections is TOF (the time of flight), and the smaller the ratio of Δt over L is, the better the energy resolution is, so the better the data are[4].

There are as many as one hundred and forty two sets of data for ^{27}Al(n,tot), and six sets of them were first selected according to the energy range, the date and the number of the data points, they are the data of R. B. Schwartz[5], F. G. Perey[6], S. Cierjacks[7], G. Rohr[8], J. Cabe[9] and M.Ohkubo[10]. Being plotted with TT and compared with the evaluated libraries ENDF/B-6, CENDL-2.1 and JENDL-3.3, R.B.Schwartz's data were abandoned because they are discrepant with other sets of data and around the energy point of 15 MeV. The remained 5 sets of data are in agreement in trend ultimately. But only the statistical error is given in F. G. Perey's data whose energy resolution is also lower than S. Cierjacks's while using the same measurement, so F. G. Perey's data were given up. Besides, for the low energy range, J. Cabe' data are in good accordance with M. Ohkubo's, but Ohkubo measured data in lower energy range, so J. Cabe' data were also abandoned and the left three sets of data were adopted. It is needed to be pointed out that though the time resolution factor of M. Ohkubo's data is not so good, the energy resolution factor is ok because the data are in low energy range. The data points of these three data sets are all much more, even accounting to 49 709 points for G. Rohr's data. These three sets were all measured with white light neutron source, then the data points can be merged. According to their energy range, we chose M. Ohkubo' data from 0.21 MeV to 0.3 MeV, G. Rohr's data from 0.3 MeV to 20 MeV and S. Cierjacks's data from 12.5 MeV to 20 MeV.

The relative error for M.Ohkubo's data is given from 0.9 percent to 3.2 percent, but there is no any information in BIB part for it. G.Rohr's data similarly only give the relative error which is from 1 percent to 10 percent. According to the measurement of the total cross section[11], the fluctuation error caused by the monitor is from 1 percent to 3 percent, then the systematical error for this reason is about from 0.5 percent to 1 percent. There are other factors to cause the systematical error, such as the quantification of sample (about 0.1 percent), the correction for dead time (about 0.1 percent) and the geometry factor (about 0.1 percent). The date of M.Ohkubo's data is late and the data points are many, the systematical error was estimated to be 0.5 percent and the given relative error was considered as statistical error. So G.Rohr's data are. Then their total error can be got

correspondingly. For S.Cierjacks' data, the upper limit of the total error is given as 3 percent in the error information, so the total error can be determined to be 2.5 percent, and because the date of this data set is old, systematical error was estimated as 1 percent.

1.2 ^{27}Al (n,α)

For the cross section such as (n,α), (n,p), (n,2n), (n,γ), the main measurement method is ACTIV (activation)[11]. And for this method, the more nucleus close to the threshold energy of the reaction used as standard the threshold energy of the reaction to be measured is, the more the measured data are reliable. Besides, for the cross section is measured by ACTIV, we should also distinguish the residual nucleus is in ground state or isometric state.

There are one hundred and ninety three sets of data for ^{27}Al(n,α). Firstly for the data sets measured before 1960, the one-point and the evaluated data sets were abandoned; for the second the data sets whose statistic fluctuation is too large were given up with the aid of TT. The eight data sets were firstly selected according to the energy range and the number of the data points, they are the data sets of Raics[12], Bulter[13], Enz[14], Swinhoe (20986003)[15], LU Hanlin[16], Paulsen[17], Kudo[18] and Filatcov[19]. It was found that Filatcov and Enz's data also can be given up because their energy ranges are narrow and the data points are nearly covered by other data sets. Then the left six sets of data were adopted. In fact, Bulter's data are not so good, because the date is early, the measurement is relatively measured and the cross section used as standard is ^{32}S(n,p), which is not recommended as a standard cross section in the world, while Al(n,α) itself is. But in the energy range from 10 MeV to 13 MeV, there is no other data set, so this set was chosen. The values of this standard cross section were given and the data of the evaluated library ENDF/B-6 were chosen as new standard to correct it. The ratio data of Raics are also relative to the cross section ^{238}U(n,f) as standard, the cross section ^{238}U(n,f) is recommended as a standard one in the world and the value[20] can be looked up to correct this data set. LU Hanlin's data were normalized to 115.8 mb at the energy point of 14.58 MeV, but the latest standard is 114.11 mb[20], the value of error is 0.55 mb, and the relative systematical error is 0.5 percent, correction was done with this new standard.

The value of the total error and the detailed error analysis were given for Kudo's data, then the systematical error was analyzed and estimated to be 1.3 percent. The total errors for the data of Paulsen were also given, the detectors for the measurement are NaI, telescope and solid state, the systematical error caused by NaI is about 1.5 percent and the one caused by telescope was estimated to be 1.25 percent according to Kudo's error analysis, so the systematical error was determined to be 2 percent. For Lu Hanlin's data, the standard error 0.5 percent was taken as the systematical error and the total error was corrected according to the standard. There is no error analysis in the information part of Swinhoe's data, but the detectors are scintilator and GeLi which can cause the systematical error about 1 percent respectively, the systematical error was determined to be 1.4 percent, the values of the error given along with data were taken for the total errors. The total errors were given for Raics' data, the systematical error was estimated to be 1.6 percent while the detector of fission chamber causing 1 percent，GeLi causing 1 percent，and the standard cross section causing 0.7 percent. No error information was given for Bulter's data, the systematical error was estimated to be 2 percent for the date is early and the standard cross section is not so good.

1.3 ^{27}Al (n,p)

After the first selection, there are eleven sets of data remained, namely the data sets of Grundl[21], Rubertson[22], Smith (three sets and their EXFOR entry are 10238020，10238021 and 10238022)[23], Gabbard[24], Ikeda[25], Filatenkov[19], Ryves[26], Kudo[27]and Ai[28]. Compared with Smith's data (10238021), the date of Rubertson's data is earlier and the data points are fewer while they are in the same energy range, so the data of Rubertson were abandoned. Similarly, Smith's data (10238020) and Grundl's data were given up while Ai's data were adopted in the low energy range. Then the left eight data sets were adopted. The ratio data of Smith are relative data using the cross section ^{238}U(n,f) as standard, the latest standard[20] were used to correct them, the data were also corrected for the γ branching ratio using the data evaluated by CNDC. Gabbard's data were normalized to 50 mb at the energy point of 14.4 MeV while ENDF/B-6 gives it to be 70 mb, the data were corrected with 70 mb as new standard and then the six datum points which are obviously not right in trend were abandoned. Filatenkov's data were also measured relatively, but the monitor wasn't given, because the cross section Al(n,α) which is used as standard is reliable, correction is not obligatory. The standard cross section used for Ryves' relative measurement is ^{56}Fe(n,p), and the data from ENDF/B-6 were used as new standard to correct them. The γ branching ratio data were also corrected for the data sets of Ai[28], Ikeda[25] and Filatenkov[29].

From Ai's detailed error analysis, the systematical error can be known as 5.2 percent, but some of the total errors given along with data are smaller than this, then 1.8 percent was added as the statistical error.

The systematical error was given to be 5 percent for the two data sets of Smith, and the values of the statistical error were also given, then the total error can be calculated. Only the values of error were given for Gabbard's data, they can be considered as total errors for they are very large, and because the measured date is early, the systematical error was estimated to be 6 percent. Kudo, Ryves and Ikeda all gave detailed error analysis and the values of total error for their data, the systematical error can be determined in turn to be 2.29 percent, 3.4 percent and 4.5 percent according to the error analysis. The total errors were also given for Filatenkov's data, but there is no error analysis, Ikeda's error analysis can be taken as reference, and because the measured date is later, every part can be estimated to be smaller, finally the systematical error was determined to be 2 percent.

1.4 ^{27}Al (n,γ)

There are only three sets of data above 210 keV except the one-point data, they are the data sets of Henkel[29], Calvi[30] and Allen[31]. The data sets of Henkel and Calvi are all measured relatively with themselves as standard, but the monitors weren't given, and compared with the data from ENDF/B-6 and JENDL-3.3, there is systematical error obviously, besides, these two data sets can not agree with each other end to end, so they were corrected in the following way: firstly, the one-point datum measured by Colditz [32] was corrected exactly, with this data as standard, Henkel's data were corrected, then the average of each data set in their common energy range (the last seven data points of Henkel and the first six of Calvi) was calculated and Calvi's data were corrected with the average of Henkel as standard. It is to say that the data sets of Henkel and Calvi are all corrected with Colditz's data, so the total error of Colditz's data was taken for their systematical error, which is 5.2 percent after carefully analysized. According to Calvi's error analysis, the total error is 15 percent in the energy range from 3.44 MeV to 4.0 MeV, 18 percent from 4.0 MeV to 4.5 MeV and 20 percent from 4.5 MeV to 5.0 MeV. No error analysis was given for Henkel's data and the total error was estimated to be 15 percent. Allen's data was measured with the cross section Au(n,γ) as standard , while the cross section Au(n,γ) itself is an international standard one, this data set is reliable even not corrected. Besides, while Allen'data were given in the form of the average in some energy range, we took the middle energy point for each energy range. The statistical error of Allen's data was given as 10 percent and the systematical error was estimated as 5 percent according to the measurement, then the total error can be calculated which is about 11.2 percent.

1.5 ^{27}Al (n,el)

Abandoning the one-point data sets, only six sets of data can be used, namely the data of Chien[33], Towle[34], Holmqvist[35], Kinney[36], Whisnant[37] and Tsukada[38]. But because the date of Tsukada's data is early, and the data points are just at the bottom of the statistical error bar with ENDF/B-6 as reference, besides, there are other data sets in this energy range, so Tsukada's data were given up. The remained five sets of data were adopted.

According to Holmqvist's error analysis，the statistical error is 2.02 percent and the total error is 5 percent，then the systematical error can be get which is 4.57 percent. Kinney's data gave the systematical error which is 7 percent and the values of the total error. There is no error analysis for Chien's data，the statistical error was estimated to be 2 percent and systematical error to be 5 percent with Holmqvist' error analysis as reference，then the total error can be calculated which is 5.4 percent. Only the values of the statistical error were given for Towle's data, the systematical error was estimated to be 6 percent and then the total errors can be calculated. The values of error given along with data by Whisnant are not agree with the error analysis in the reference, as the values of error are different with each other greatly, it must be caused by the statistical error. According to the error analysis，the range of the statistical error is from 1 percent to 5 percent，then 5 percent was taken for the third point，for its total error is 7 percent，the systematical error can be calculated to be 4.9 percent, then 1 percent can be taken as the statistical error for the first point and the total error can be calculated, the total error for the second point wasn't corrected.

1.6 ^{27}Al (n,2n)

There are five sets of data above 210 keV except the one-point data, namely the data sets of Iwasaki[39], Arnold[40], Sasao[41], Nakamura[42] and Mani[43]. Iwasaki gave the total (n,2n) cross section，but Arnold and Mani only gave ^{27}Al(n,2n)^{26m}Al cross section while Sasao and Nakamura only gave ^{27}Al(n,2n)^{26g}Al cross section. What we need is the summation of the two. Plotting and comparing, it was found that the statistic fluctuation of Mani's data early is too large, so Arnold's data and several more points by linear fitting were taken for ^{27}Al(n,2n)^{26m}Al cross section. For ^{27}Al(n,2n)^{26g}Al cross section, the data sets of Sasao and Nakamura were fitted with spline function. Then the total (n,2n) cross section was got by summing them with Mani's data at the same energy point.

The statistical error of Iwasaki's data was given as from 1.3 percent to 3.2 percent and total error is

from 10.8 percent to 11.2 percent, 3.2 percent was taken as the statistical error for the total error of 11.2 percent, and the systematical error can be got, which is 10.7 percent. The total errors were all given for the data of Arnold, Sasao and Nakamura，then the total errors for the corrected total (n,2n) cross section can be got, and the systematical error was estimated as 15 percent.

2 Data Processing

Not only one set of data were selected for each reaction channel, so curve fitting was needed to give the smooth optimum values in mathematics as the recommended data, and the covariance matrix should also be constructed for each experimental data set and then be merged to get the covariance matrix for the recommended data. The program SPCC[44] was used for this work. The code has three input files. The first is for the parameters used in the fitting, like spline order, knot, width, output energy point etc. The second is for the experimental data to be fitted. The third is for the covariance matrix of each set of experimental data, which can be input in various formats. The parameters such as the order number, the knots and the "width" of each data set were mainly adjusted. The knot selection is the key, generally the knots are selected at the peaks and valleys or the certain structures. "Width" is a quantity correlated with every data set's weight, and the larger the "width" is, the smaller the weight is. Generally, the "width" should be smaller than the smallest value of the error. Usually the parameters need to be adjusted many times to get the expected curve. It should be pointed out that if there are large discrepancies among different data sets and strong correlation among data points, so called PPP problem may happen[44]. The iteration method[44] to deal with this problem was used in this work.

3 The Results and Discussion

The experimental data and the fitting values are shown in Figs.1~6(a), and the correlation coefficient matrix are shown in Figs.1~6(b). From the comparison of the fit values with the experimental data and the evaluated data from the evaluated libraries ENDF/B-6, JENDL-3.3 and CENDL-2.1, it was found that our fit values agree with the experimental data better, especially for (n,p), (n,γ) reactions, for which our data reproduce the structures well, but they were smoothed out by other evaluated data.

The correlation mainly comes from the transformation of the error, and the larger the systematical error or the proportion of the systematical error in the total error is, the larger the correlation coefficient is. For example, the values of the systematical error for the total cross section are all small and only small proportions in the total error, the correlation coefficients are small correspondingly, but for the cross section of（n,el）and（n,2n），the systematical error is large and is the main source of the total error, then the correlation coefficients are also large. Besides, the constraint Math condition to make the curve smooth during the fitting can also cause the correlation among data, the large correlation between the energy points nearby is caused by this.

4 Conclusion

Based on the latest experimental data and using exact mathematic data processing method, the cross sections and their covariance data for ^{27}Al's six reaction channels were evaluated. Compared with the existing evaluated data, not only the cross sections themselves are improved, the covariance data are also added. The data can be used for the evaluated library and as the basis of theoretical calculation concerned.

The key point to covariance data evaluation is the error analysis, especially the confirmation of the systematical error.

The method adopted in this work for the covariance data evaluation of the experimental data is feasible and also can be used for other nuclear species' covariance data evaluation.

So called PPP problem may happen during the correlated data processing, and this problem is still being studied in the world.

Table 1 Error scale of different measurement

Section	Error range	Method	Detector
(n,tot)	1%~2%	Time of Flight(TOF)	SCIN
(n,el)	5%~10%		
(n,2n)	3%~8%	Activation (ACTIV)	NaI(1975) GeLi
(n,α)			
(n,γ)	3%~8%(E_n<0.5 MeV)		
(n,p)			
(n,d)			

Table 2 The data sets adopted for the evaluation of ^{27}Al's neutron cross section and their covariance data

Section	EXFOR entry	Times	Author	Lab	Method	Energy/MeV	Points	Error	
								Systemat	Total
(n,tot)	21926003	1984	M.Ohkubo	JPNJAE	TOF	0.009 8~0.94	1 010	0.5%	1%~3.3%
	22331004	1994	G.Rohr	ZZZGEL	TOF	0.25~20	49 709	0.5%	1.2%~10.2%
	20010004	1968	S.Cierjacks	GERKFK	TOF	0.5~32	5 101	1%	2.5%
（n,α）	30590003	1980	Raics	HUNKOS	ACTIV	6.5~11	9	1.6%	2.69%~2.83%
	11457006	1963	Bulter	CANCRC	ACTIV	5.4~14	32	2%	3.0%~3.7%
	30523003	1989	Lu Hanlin	CPRAEP	ACTIV	12.0~18.0	10	0.5%	3.4%~8.4%
	20986003	1979	Swinhoe	UK HAR	ACTIV	7.5~12	3	1.4%	2.4%~3.2%
	21923002	1984	Kudo	JPNTSU	ACTIV, COINC	14~20	8	1.3%	1.3%~4.0%
	20378003	1965	Paulsen	ZZZGEL	ACTIV	13~20	23	2%	5.9%~6.1%
(n,p)	30457002	1977	Ai	CHFSHI	ACTIV	2.8~4.6	16	5.2%	5.3%~6.2%
	10238021	1975	Smith	USAANL	ACTIV	4.0~5.9	40	5%	6.7%~7.2%
	10238022	1975	Smith	USAANL	ACTIV	5.4~10	18	5%	7.0%~7.5%
	11494004	1962	Gabbard	USAKTY	ACTIV	12.0~18	15	6%	7%~12%
	22312003	1993	Ikeda	JPNJAE	ACTIV,ASSOP	13~15	8	3.4%	3.5%~9.2%
	41240005	1997	Filatenkov	RUSRT	ACTIV	13~15	8	2%	2.1%~2.3%
	22094003	1988	Kudo	JPNTSU	ACTIV	15~20	6	2.29%	2.36%~6.8%
	20867005	1978	Ryves	UK NPL	ACTIV	15~19	6	4.5%	6.3%~10%
(n,γ)	11518004	1953	Henkel	USALAS	ACTIV	0.4~3.8	65	5.2%	15%
	20924002	1962	Calvi	ITYCAT	ACTIV	3.4~5.0	30	5.2%	15%~20%
	30288002	1975	Allen	AULAUA	no information	0.005~0.5	7	5%	11.2%
(n,el)	11201008	1966	Chien	USAANL	TOF	3.0~1.5	27	5%	5.4%
	20958015	1962	Towle	UK ADL	TOF	0.98~4.0	4	6%	6.7%~6.76%
	20019002	1969	Holmqvist	SWDAE	TOF	2.5~8.1	8	4.57%	5%
	10106092	1970	Kinney	USAORL	TOF	5.4~8.6	4	7%	7.2%~7.6%
	12875004	1984	Whisnant	USATNL	TOF	11.0~17	3	4.9%	5%~7%

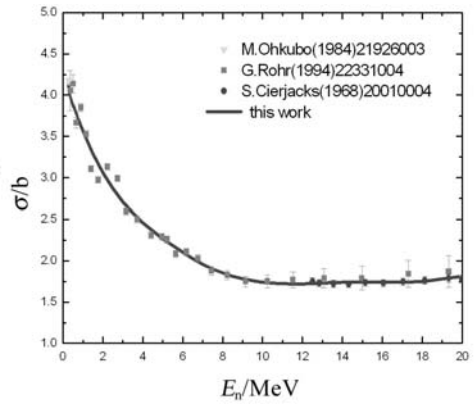

Fig.1 (a) The comparison of the fit values with the experimental data for ^{27}Al(n,tot)

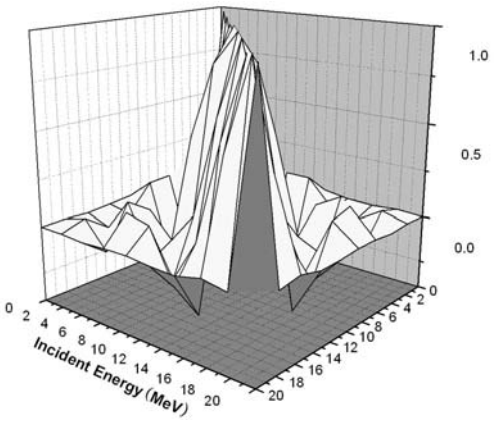

Fig.1 (b) Correlation coefficient matrix for ^{27}Al(n,tot)

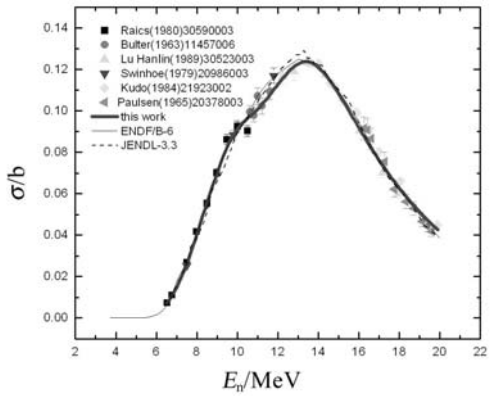

Fig.2 (a) The comparison of the fit values with the experimental data for ^{27}Al(n,α)

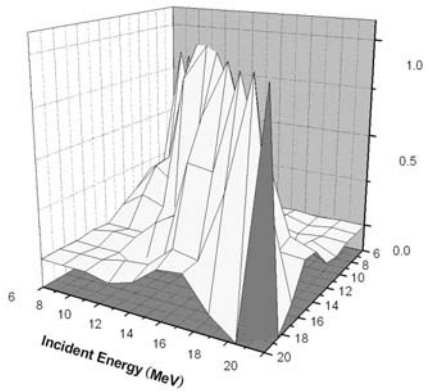

Fig.2 (b) Correlation coefficient matrix for ^{27}Al(n,α)

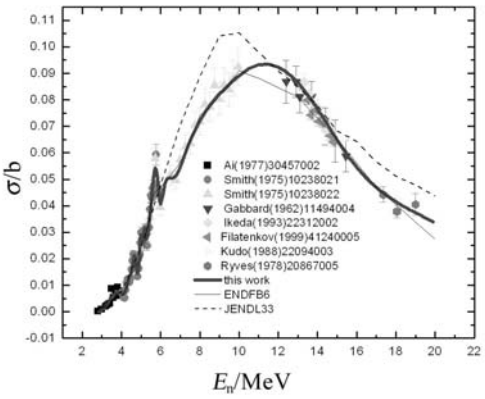

Fig.3 (a) The comparison of the fit values with the experimental data for ^{27}Al(n,p)

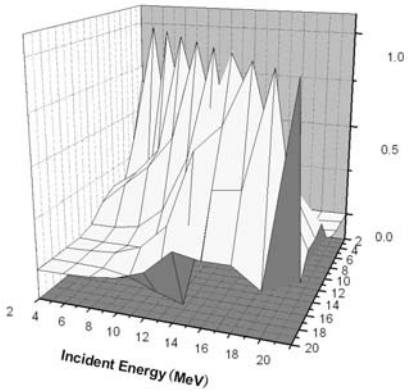

Fig.3 (b) Correlation coefficient matrix for ^{27}Al(n,p)

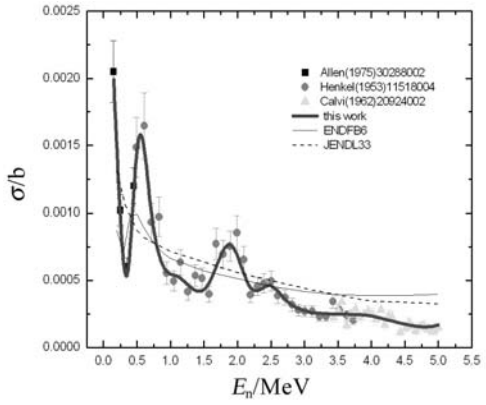

Fig.4 (a) The comparison of the fit values with the experimental data for ^{27}Al(n,γ)

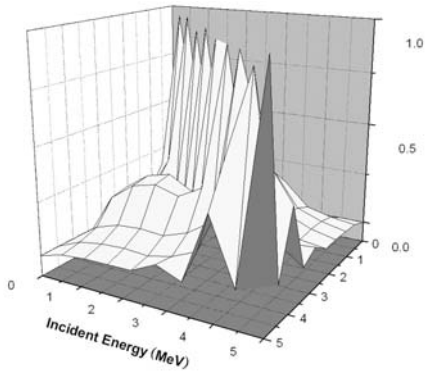

Fig.4 (b) Correlation coefficient matrix for ^{27}Al(n,γ)

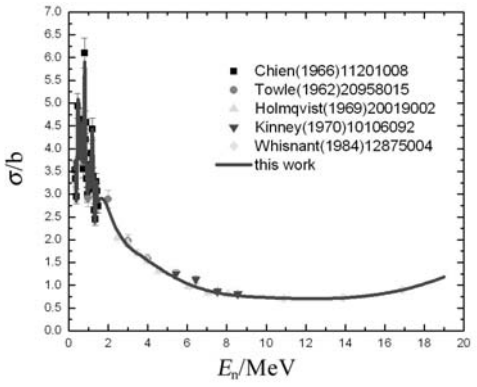

Fig.5 (a) The comparison of the fit values with the experimental data for ^{27}Al(n,el)

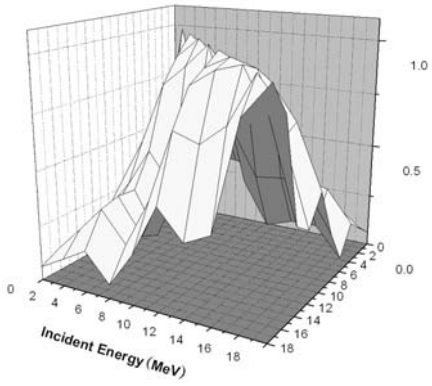

Fig.5 (b) Correlation coefficient matrix for ^{27}Al(n,el)

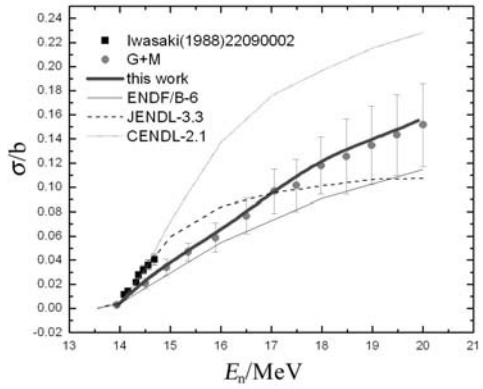

Fig.6 (a) The comparison of the fit values with the experimental data for ^{27}Al(n,2n)

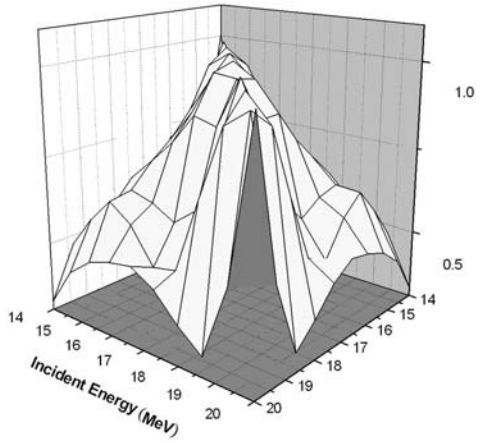

Fig.6 (b) Correlation coefficient matrix for ^{27}Al(n,2n)

References

[1] V.Mclane, EXFOR Data Library, IAEA-NDS-206,2000
[2] JIN Yongli, TT Code, inside reference,2002
[3] LIU Jianfeng, "Evaluation of Complete set of Neutron Data for Natural Zr and its Isotopes."(Internal report, in Chinese, 2002)
[4] WANG Fengge, The Code for Covariance Data Evaluation and Processing of Experimental Data and Neutron Covariance Data Evaluation of ^{58,60,61,62,64,Nat}NI" Master thesis, (In Chinese, 2003)
[5] R.B.Schwartz,et.al.,R,NBS-MONO-138,7401
[6] F.G.Perey,et.al.,R,ORNL-4823,7212
[7] S.Cierjacks,et.al.,R,KFK-1000,6806
[8] G.Rohr,et.al.,C,94GATLIN,,215,9405
[9] J.Cabe,et.al.,R,CEA-R-4524,7311
[10] M.Ohkubo,et.al.,W,OHKUBO,8412
[11] DIN Dazhao et al.，"Neutron Physics", p361, Published by Atomic Energy Press, 2001
[12] P.Raics,et.al.,C,80KIEV,1,236
[13] J.P.Butler,et.al.,J,CJP,41,372
[14] W.Enz,et.al.,J,ADP,42,(3),283,85
[15] W.T.Swinhoe,et.al.,P,AERE-PR/NP-26,39,7903
[16] LU Hanlin,et.al.,R,INDC(CRR)-16,8908
[17] A.Paulsen,et.al.,J,JNE/AB,19,907,6511
[18] K.Kudo,et.al.,W,KUDO,84
[19] A.A.Filatenkov,et.al.,R,INDC(CCP)-402,9701
[20] H.Conde, NEANDC-311"V",1992
[21] J.A.Grundl,et.al.,J,NSE,30,39,6710
[22] J.C.Robertson,et.al.,J,ANE,26,(1),1,72
[23] D.L.Smith,et.al.,J,NSE,58,314,7511
[24] F.Gabbard,et.al.,J,PR,128,1276,62
[25] Y.Ikeda,et.al.,J,NST,30,870,9309
[26] T.B.Ryves,et.al.,J,JP/G,4,(11),1783,78
[27] K.Kudo,et.al.,C,88MITO,1021,88
[28] C.E.Ai,et.al.,J,NSF,14,(4),1,7712
[29] R.L.Henkel,et.al.,W,HENKEL,5301
[30] G.Calvi,et.al.,J,NP,39,621,6212
[31] B.J.Allen,et.al.,C,75WASH,1,360,7503
[32] J.Colditz,et.al.,J,OSA,105,236,6806
[33] J.P.Chien,et.al.,J,NSE,26,500,66
[34] J.H.Towle,et.al.,J,NP,39,300,6212
[35] B.Holmqvist,et.al.,R,AE-366,6906
[36] W.E.Kinney,et.al.,R,ORNL-4516,7010
[37] C.S.Whisnant,et.al.,J,PR/C,30,1435,8411
[38] K.Tsukada,et.al.,C,61VIENNA,1,75(18/12),6108
[39] S.Iwasaki,et.al.,C,88MITO,295,88
[40] D.M.Arnold,et.al.,W,Arnold,6511
[41] M.Sasao,et.al.,J,PR/C,35,2327,8706
[42] T,Nakamura,et.al.,J,PR/C,43,(4),1831,910
[43] G.S.Mani,et.al.,J,NP,19,(5),535
[44] LIU Tingjin ect. The Spline Fitting for Multi-Sets of Correlative Data,INDC(CPR)-032/L,116,1994

Evaluation of Production Cross Sections of γ-Rays from Thermal-Neutron Captures

ZHOU Chunmei WU Zhendong

China Nuclear Data Center, CIAE, P.O.Box 275(41), Beijing 102413, P.R.China

【abstract】 *The evaluation and calculation of production cross sections of γ-rays from thermal-neutron captures are briefly presented. The check of intensity balance is made. The examples are given to illustrate their application.*

Introduction

The energies and production cross sections of γ-ray, and their decay schemes of thermal-neutron captures are one of the basic data of nuclear physics research, nuclear technology application and nuclear engineering design. The evaluation and calculation of production cross sections of γ-rays from thermal-neutron captures are presented. The check of intensity balance is made. Some examples are given to illustrate its application.

1 Main Evaluation Program

Main codes of production cross section evaluation of γ-rays from thermal-neutron captures and their functions are listed in Table 1. These codes are mainly from International Network[1] of Nuclear Structure and Decay Data Evaluation, the ENSDF data format is adopted in data evaluation.

2 Flow Chart of Production Cross Section Evaluation of γ-rays from Thermal-neutron Captures

The main flow chart of production cross section evaluation of γ-rays from thermal-neutron captures is given in Fig.1. The basic characters are as follows:

a. Measured data collection

Evaluator retrieves related references from Nuclear Science References File, NSRF. On the basis of the retrieval, all measured data are collected from journals, reports, and private communications.

b. Measured data evaluation and recommendation of the best measured data

All related-data gathered are analyzed and compared and treated by mathematical method (for example, limit-weighted or un-weighted average of measured data). And then, the best-measured relative intensities of γ-rays and thermal-neutron capture cross section, and decay scheme can be recommended on the basis of the measured data evaluation.

c. Establishment of temporary data file

After recommendation of the best-measured data, the evaluated data are in put into computer by hand, the temporary data file can be set up in ENSDF data format.

d. Theoretical calculation

Format checking must be done for temporary data file, and correction to old one should be done if necessary. Then, physical analysis and theoretical calculation are done and calculated results will be put into the gapes without measured data, so that without recommended data become a self-consistent and complete data set.

e. Recommendation of complete data set

A complete data set of thermal-neutron capture prompt γ-ray data and its decay scheme is recommended as evaluated data set.

3 Production Cross Section Calculations of γ-Rays from Thermal -neutron Captures

In the experimental measurements, relative γ-ray intensities are measured. In the practical applications, production cross sections of γ-rays from thermal-neutron captures should be known. The basic principle of the production cross section calculation of γ-rays from thermal-neutron captures is the γ transition intensity balance for each level.

Table 1 Main codes of production cross section evaluation of γ-rays from neutron captures and their functions

Code name	Main functions
GTOL	Level energy calculation by fitting to γ-energies
	Intensities balance calculation & checking
LWA	Limit-weighted and un-weighted average of measured data
HSICC	Internal conversion coefficients calculation
RADLST	Energy balance calculation & checking
FMTCHK	ENSDF data format checking
PANDOR	ENSDF physics checking
ENSDAT	Drawing decay schemes & listing data tables

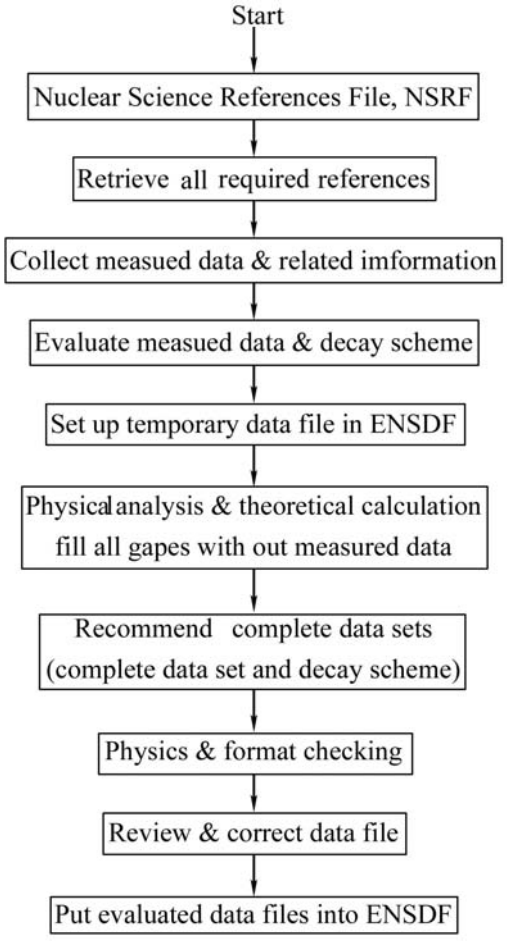

Fig. 1 Flow chart of production cross section evaluation of γ-rays from thermal-neutron captures

Main and general methods of the production cross section calculation of γ-rays from thermal-neutron captures are summarized as follows:

3.1 Calculation from γ-ray Decaying to Ground State

When a nuclide captures a thermal-neutron, the γ-rays decay into its ground state, as shown in Fig. 2. If there are m γ-rays decaying to ground state, I_k is the relative intensity for the k-th γ-ray, α_k is its total internal conversion coefficient, the equation can be written as follows

$$N_\gamma \sum_{k=1}^{m} I_k (1+\alpha_k) = \sigma_{n,\gamma} \qquad (1)$$

were N_γ is normalization factor for γ-ray production

cross sections per one thermal-neutron capture, $\sigma_{n,\gamma}$ is (n,γ) reaction cross section per thermal -neutron capture.

$$N_\gamma = \frac{\sigma_{n,\gamma}}{\sum_{k=1}^{m} I_k(1+\alpha_k)} \quad (2)$$

For light nuclides, the each internal conversion coefficient α_k is quite small and can be neglected, so

$$N_\gamma = \frac{\sigma_{n,\gamma}}{\sum_{k=1}^{m} I_k} \quad (3)$$

From Eq. (2) or (3), the normalization factor N_γ can be calculated, and then, γ-ray production cross sections for thermal-neutron capture can be calculated by using Eq. (4).

$$\sigma_{n,\gamma}(E_{\gamma k}) = N_\gamma I_{\gamma k} \quad (4)$$

where $\sigma_{n,\gamma}(E_{\gamma k})$ is γ-ray production cross section of k-th γ-ray of the energy $E_{\gamma k}$, $I_{\gamma k}$ is γ-ray relative intensity of k-th γ-ray of the energy $E_{\gamma k}$.

Fig. 2 Skeleton scheme of γ-ray decaying to ground state from high excitation state

The relative γ-ray data[2] for ^{26}Mg(n,γ) of thermal-neutron are given in Table 2 and its decay scheme is shown in Fig. 3, where the γ-ray relative intensities are given. The capture cross section, $\sigma_{n,\gamma}$=38.2±0.8 mb, for ^{26}Mg(n,γ) of thermal-neutron has been evaluated[3]. In Table 1, the γ-ray energies, their relative intensities and levels are given, from which, using Eq. (3) formula, N_γ=0.382±0.008 mb is calculated, and the γ-ray production cross sections can also be calculated from formula (4), as shown in Table 1.

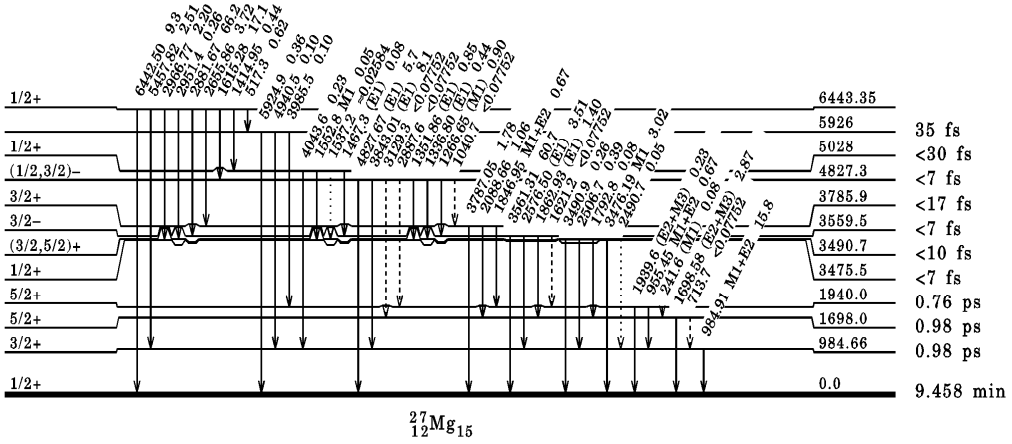

Fig. 3 Decay scheme and γ-ray intensity from ^{26}Mg(n,γ) thermal neutron reaction

Table 2 γ-ray data and production cross sections from ^{26}Mg(n,γ) thermal neutron reaction

E_γ/keV	E(level)/keV	I_γ ②	Mult.③	δ ③	$\sigma_{n,\gamma}(E_\gamma)$ / mb ④
241.6① 4	1 940.0 1	0.08 3	(M1)		0.03 1
517.3 3	6 443.35 4	0.62 8			0.24 3
713.7	1 698.0 1	<0.08			<0.03
955.45 8	1 940.0 1	0.67 8	M1+E2	–0.08 6	0.26 3
984.91 3	984.92	15.8 8	M1+E2	+0.22 2	6.0 3
1 040.7	4 827.3 4	<0.08			<0.03
1 266.65 18	4 827.3 4	0.90 8	(M1)		0.34 3
1 336.80 20	4 827.3 4	0.44 6	(E1)		0.17 2
1 351.86 8	4 827.3 4	0.85 8	(E1)		0.32 3
1 414.95 18	6 443.35 4	0.44 6			0.17 2

Cont. Table 2

E_γ/keV	E(level)/keV	I_γ ②	Mult.③	δ ③	$\sigma_{n,\gamma}(E_\gamma)$ / mb ④
1 467.3 5	5 028 1	0.08 3	(E1)		0.03 1
(1 537.2)	5 028 1	≈0.025 84			≈0. 01
1 552.8 7	5 028 1	0.05 3	M1		0.02 1
1 615.28 5	6 443.35 4	17.1 8			6.5 3
1 621.2	3 559.5 1	<0.08			<0.03
1 698.58 5	1 698.0 1	2.87 18	(E2+M3)	≈0.0	1.10 7
1 792.8 3	3 490.7 7	0.08 3			0.03 1
1 846.95 18	3 785.9 4	0.67 8	M1+E2	−0.0 3	0.26 3
1 862.93 10	3 559.5 1	1.40 11	(E1)		0.53 5
1 939.6 4	1 940.0 1	0.23 6	(E2+M3)	≈0.0	0.09 2
2 088.66 11	3 785.9 4	1.06 8			0.40 3
(2 490.7)	3 475.5 2	0.05 3			0.02 1
2 506.7 23	3 490.7 7	0.39 6			0.15 2
2 576.50 6	3 559.5 1	3.51 21	(E1)		1.34 8
2 655.86 6	6 443.35 4	3.72 18			1.42 7
2 881.67 4	6 443.35 4	66.2 21			25.3 8
2 887.6	4 827.3 4	<0.08			<0.03
2 951.4 4	6 443.35 4	0.26 6			0.10 2
2 966.77 22	6 443.35 4	2.20 16			0.84 6
3 129.3	4 827.3 4	<0.08			<0.03
3 476.19 9	3 475.5 2	3.02 16	M1		1.15 6
3 490.9 6	3 490.7 7	0.26 5			0.10 2
3 561.31 4	3 559.5 1	60.7 18			23.2 7
3 787.05 15	3 785.9 4	1.78 16			0.68 6
3 843.01 8	4 827.3 4	8.1 5	(E1)		3.10 16
3 985.5 6	5 926.2	0.10 3			0.04 1
4 043.6 3	5 028.1	0.23 6			0.09 2
4 827.67 6	4 827.3 4	5.7 4	(E1)		2.18 13
4 940.5 3	5 926.2	0.10 3			0.04 1
5 457.82 15	6 443.35 4	2.51 18			0.96 7
5 924.9 4	5 926.2	0.36 6			0.14 2
6 442.50 6	6 443.35 4	9.3 5			3.55 17

① uncertainty (error):the uncertainty in any number is given space after the number itself; for example, 241.6 4 means 241.6±0.4. ② Relative intensity. ③ Multipolarity and its mixture ratio for γ-ray. ④ γ-ray production cross section

3.2 Calculation from Primary γ-ray Decaying from Captured State

When a nuclide captures a thermal-neutron, the nuclide is de-excited from its capture state by mean of decaying primary γ-rays, as shown in Fig. 4. Suppose that there is n primary γ-rays, I_i is the relative intensity of i-th primary γ-ray and α_i is its total internal conversion coefficient of i-th primary γ-ray, then,

$$N_\gamma \sum_{i=1}^{n} I_i(1+\alpha_i) = \sigma_{n,\gamma} \tag{5}$$

$$N_{n,\gamma} = \frac{\sigma_{n,\gamma}}{\sum_{i=1}^{n} I_i(1+\alpha_i)} \tag{6}$$

And for light nuclide, Eq. (6) becomes

$$N_\gamma = \frac{\sigma_{n,\gamma}}{\sum_{i=1}^{n} I_i} \tag{7}$$

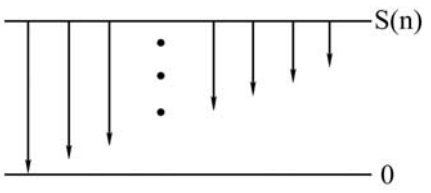

Fig. 4 Skeleton scheme of primary γ-rays from captured state

The primary γ-ray data[2] for ^{28}Si(n,γ) of thermal-neutron are listed in Table 3, and their decay

scheme is shown in the Fig. 5, where the γ-ray relative intensities are given. The capture cross section, $\sigma_{n,\gamma}$=177±5 mb, for ^{28}Si(n,γ) of thermal -neutron has been evaluated[3]. From Table 2, the γ-ray energies, their relative intensities and levels are given, from which, using Eq. (3) formula, N_γ=1.77±0.05 mb is calculated, and the γ-ray production cross sections can also be calculated from formula (4), as shown in Table 3.

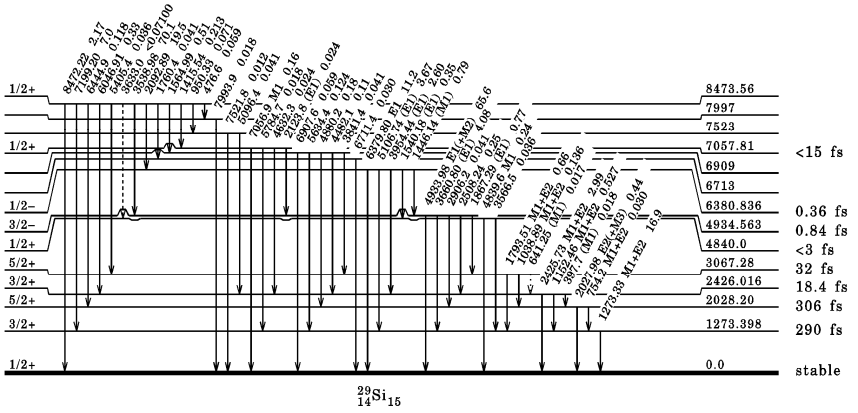

Fig. 5 Decay scheme and γ-ray intensity from ^{28}Si(n,γ) thermal neutron reaction

Table 3 γ-ray data and production cross sections from ^{28}Si(n,γ) thermal neutron reaction

E_γ/keV	E(level)/keV	I_γ ①	Mult.②	δ②	$\sigma_{n,\gamma}(E_\gamma)$ / mb③
397.7 4	2 426.016 15	0.018 6	(M1)		0.03 1
476.6 3	8 473.56 3	0.059 12			0.10 2
(641.25)	3 067.28 8	0.017 9	(M1)		0.030 15
754.2 4	2 028.20 6	0.030 12	M1+E2	–0.03 3	0.05 2
950.33 13	8 473.56 3	0.071 12			0.13 2
1 038.89 10	3 067.28 8	0.136 18	M1+E2	+0.04 2	0.24 3
④1 071.0 5		0.047 12			0.08 2
1 152.46 6	2 426.016 15	0.528 24	M1+E2	+0.09 8	0.93 4
1 273.33 3	1 273.398 11	16.9 9	M1+E2	+0.197 9	29.9 14
1 415.54 9	8 473.56 3	0.213 24			0.37 4
1 446.14 4	6 380.836 13	0.79 3	(M1)		1.40 5
1 540.18 6	6 380.836 13	0.35 3	(E1)		0.62 5
1 564.99 5	8 473.56 3	0.52 4			0.92 7
1 760.4 5	8 473.56 3	0.042 12			0.07 2
1 793.51 4	3 067.28 8	0.66 4	M1+E2	+0.26 2	1.18 6
1 867.29 5	4 934.563 13	0.77 4	(E1)		1.36 6
2 027.98 9	2 028.20 6	0.44 5	E2(+M3)	0.0	0.78 7
2 092.89 3	8 473.56 3	19.6 8			34.7 12
2 123.8 6	7 057.81 17	0.024 6	(E1)		0.04 1
2 425.73 4	2 426.016 15	3.00 12	M1+E2	–0.32 7	5.31 20
2 508.24 13	4 934.563 13	0.25 3			0.44 5
2 906.2 5	4 934.563 13	0.042 12			0.07 2
3 538.98 4	8 473.56 3	70.3 22			124.4 38
3 566.5 5	4 840.0 4	0.036 12			0.06 2
3 633.0	8 473.56 3	<0.071			<0.12
3 660.80 6	4 934.563 13	4.09 18	(E1)		7.2 3
3 841.4 6	6 909	0.042 12			0.07 2

Cont. Table 2

E_γ/keV		E(level)/keV		I_γ ①		Mult.②	δ②		$\sigma_{n,\gamma}(E_\gamma)$ / mb③	
3 954.44	5	6 380.836	13	2.61	18	(E1)			4.6	3
4 482.1	4	6 909		0.11	3				0.19	5
4 632.3	7	7 057.81	17	0.024	12				0.04	2
4 839.6	4	4 840.0	4	0.24	3	M1			0.42	5
4 880.2	5	6 909		0.18	3				0.31	5
4 933.98	3	4 934.563	13	65.7	21	E1(+M2)	–0.05	10	116.3	34
5 096.4	7	7 523		0.042	12				0.07	2
5 106.74	6	6 380.836	13	3.68	18	(E1)			6.5	3
5 405.4	9	8 473.56	3	0.036	12				0.06	2
5 634.4	4	6 909		0.125	18				0.22	3
5 784.7	7	7 057.81	17	0.018	6				0.03	1
6 046.91	16	8 473.56	3	0.33	4				0.58	6
6 379.80	4	6 380.836	13	11.3	6	E1			20.0	11
6 444.9	5	8 473.56	3	0.119	24				0.21	4
6 711.4	9	6 713		0.030	12				0.05	2
6 907.6	7	6 909		0.059	18				0.10	3
7 056.9	4	7 057.81	17	0.16	3	M1			0.28	5
7 199.20	5	8 473.56	3	7.1	3				12.6	5
7 521.8	9	7 523		0.012	6				0.02	1
7 993.9	9	7 997		0.018	6				0.03	1
8 472.22	7	8 473.56	3	2.17	12				3.84	21

① Relative intensity. ② Multipolarity and its mixture ratio for γ-ray. ③ γ-ray production cross section. ④ Unplaced in level scheme.

4 Intensity Balance Check

The most important is the physical consistent check of intensity balance for each levels.

For decay γ-ray to ground state, the Eq. (1) becomes

$$N_\gamma(b)\sum_{k=1}^{m} I_k(1+\alpha_k) = \sigma_{n,\gamma} \tag{8}$$

where N_γ(b) is normalization factor for γ-ray production cross sections of thermal-neutron captures.

For primary γ-ray from captured state, the Eq. (5) becomes as follows,

$$N_\gamma(p)\sum_{i=1}^{n} I_i(1+\alpha_i) = \sigma_{n,\gamma} \tag{9}$$

where N_γ(p) is normalization factor for γ-ray production cross sections of thermal-neutron captures. from Eq. (8) and (9), Eq.(10) can be got as,

$$N_\gamma(p)\sum_{i=1}^{n} I_i(1+\alpha_i) = N_\gamma(b)\sum_{k=1}^{m} I_k(1+\alpha_k) \tag{10}$$

or,

$$\frac{N_\gamma(p)}{N_\gamma(b)} = \frac{\sum_{k=1}^{m} I_k(1+\alpha_k)}{\sum_{i=1}^{n} I_i(1+\alpha_i)} \tag{11}$$

The normalization factors N_γ(p) and N_γ(b) for γ-ray production cross sections of thermal-neutron captures are not equal because the measurement uncertainty exists. Therefore,

$$\frac{N_\gamma(p)}{N_\gamma(b)} \approx 1 \tag{12}$$

within their uncertainty range .The Eq.(11) can be changed into

$$\frac{\sum_{i=1}^{n} I_i(1+\alpha_i)}{\sum_{k=1}^{m} I_k(1+\alpha_k)} \approx 1 \tag{13}$$

or,

$$\sum_{i=1}^{n} I_i(1+\alpha_i) \approx \sum_{k=1}^{m} I_k(1+\alpha_k) \tag{14}$$

The Eq. (14) is correct within their uncertainty range. For other levels, in addition to captured state and ground state, the intensities coming into and going out the level j are the same within their uncertainty range, as shown in Fig. 6.

$$\sum_{k=1}^{m} I_{jik}(1+\alpha_{jik}) - \sum_{i=1}^{n} I_{joi}(1+\alpha_{joi}) \approx 0 \tag{15}$$

In formula (15), I_{jik}, α_{jik} and I_{joi}, α_{joi} are γ-ray relative intensities and their internal conversion

coefficients for coming into and going out level J respectively.

In Table 4, the calculation and checking results of intensity balance for each levels from ^{28}Si(n,γ) reaction are given. From Table 4 it can be seen that the capture cross sections of thermal-neutron captures for each levels are consistent within their uncertainties.

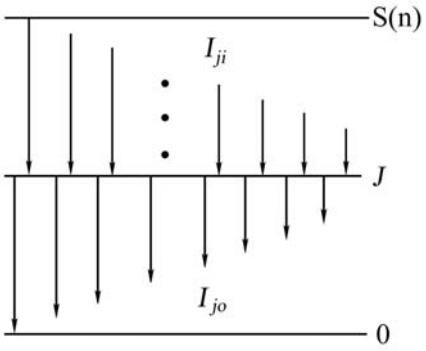

Fig. 6 Skeleton scheme of intensity balance calculation for excitation level

Table 4 Calculation and checking results of intensity balance from ^{28}Si(n,γ) reaction at E_n=thermal

		RI①			TI②		$\sigma_{n,\gamma}$/mb ③
Level	(OUT)	(IN)	(NET)	(OUT)	(IN)	(NET)	(CALC)
0	0.0	100 3	−100 3	0.0	100 3	−100 3	0.4 41
1 273.398 11	16.9 8	16.2 4	0.7 10	16.9 4	16.2 4	0.7 10	1.2 18
2 028.20 6	0.47 5	0.49 5	−0.02 10	0.47 5	0.49 5	−0.02 10	−0.04 12
2 426.016 15	3.54 12	3.4 2	0.14 24	3.54 12	3.4 2	0.14 24	0.30 41
3 067.28 8	0.82 4	0.85 4	−0.03 6	0.82 4	0.85 4	−0.03 6	−0.05 11
4 840.0 4	0.27 4	0.35 3	−0.08 5	0.27 4	0.35 3	−0.08 5	−0.14 9
4 934.563 13	70.9 2	71.0 3	−0.1 3	70.9 2	71.0 3	−0.1 3	−0.17 54
6 380.836 13	18.6 7	19.5 7	−0.9 10	18.6 7	19.5 7	−0.9 10	−1.5 18
6 713	0.030 12	0.041 12	−0.011 17	0.030 12	0.041 12	−0.011 17	−0.021 30
6 909	0.51 5	0.51 4	−0.00 6	0.51 5	0.51 4	−0.00 6	−0.02 12
7 057.81 17	0.22 4	0.21 3	0.010 6	0.22 4	0.21 3	0.010 6	0.02 7
7 523	0.053 14	0.071 12	−0.018 18	0.053 14	0.071 12	−0.018 18	−0.032 32
7 997	0.018 6	0.059 12	−0.041 14	0.018 6	0.059 12	−0.041 14	−0.073 25
473.56 3	100 3	0.000	100 3	100 3	0.000	100 3	177 5

① relative intensity. ② relative intensity including internal conversion. ③ intensity balance of capture cross section.

5 Summary

The calculation formulas of γ-ray production cross sections and intensity balance check from thermal-neutron captures have been introduced on the basis of decay scheme of captured state and its capture cross section. In general, the higher the neutron binding energy is, in the higher excitation state the captured state is, and more complex its decay scheme is. Sometimes, a lot of weak-intensity γ-ray are unable to be measured experimentally. Besides, measured uncertainties from background deducting and γ-spectra analysis lead to γ-ray intensity uncertainties. Strictly speaking, intensities of coming into and going out a level are unable to be exactly same, only can be consistent within their uncertainties. The normalization factors from primary γ-rays from captured state and decay γ-rays to ground state are different since above reasons. The normalization factor of γ-ray production cross sections in thermal-neutron capture reaction is usually calculated from the γ-rays of decaying to ground state.

References

[1] Burrows TW. ENSDF Physics Analysis Codes. Private Communication (1998)

[2] ZHOU Chunmei, Firestone RB. Thermal-neutron capture data for *A*=26~35. INDC(CPR)-054,Vienna: IAEA Nuclear Data Section, 2001, 1~79.

[3] Mughabghab SF. Thermal-neutron capture cross sections, resonance integrals and G-factors. INDC(NDS) -440,Vienna: IAEA Nuclear Data Section, 2003, 1~32.

CINDA INDEX

Nuclide	Quantity	Energy/ eV		Lab	Type	Documentation				Author, Comments
		Min	Max			Ref	Vol	Page	Date	
^{7}Be	Evaluation			APE	Eval	Jour CNDP	30	20	Apr 2006	WANG Baosong+ , Decay Data, HL
^{31}P	Calculation	1.0+2	2.0+7	APE	Theo	Jour CNDP	30	29	Apr 2006	LI Jiangting+, SIG, DA, DE
^{27}Al	Evaluation	2.1+5	2.0+7	ZHN	Eval	Jour CNDP	30	63	Apr 2006	LI Chunjuan+ , SIG, COV
^{59}Co	Calculation	1.0+3	2.0+7	APE	Theo	Jour CNDP	30	34	Apr 2006	WANG Shunuan, SIG, DA, DA/DE
^{92}Mo	Calculation	1.0+3	2.0+7	NKU	Theo	Jour CNDP	30	40	Apr 2006	CAI Chonghai+ , SIG, DA, DA/DE OR DE
^{94}Mo	Calculation	1.0+3	2.0+7	NKU	Theo	Jour CNDP	30	40	Apr 2006	CAI Chonghai+ , SIG, DA, DA/DE OR DE
^{96}Mo	Calculation	1.0+3	2.0+7	NKU	Theo	Jour CNDP	30	40	Apr 2006	CAI Chonghai +, SIG, DA, DA/DE OR DE
^{102}Mo	Calculation	1.0+3	2.0+7	APE	Theo	Jour CNDP	30	48	Apr 2006	LIANG Chuntai+, SIG, DA,DE
^{104}Mo	Calculation	1.0+3	2.0+7	APE	Theo	Jour CNDP	30	48	Apr 2006	LIANG Chuntai+, SIG, DA,DE
^{106}Mo	Calculation	1.0+3	2.0+7	APE	Theo	Jour CNDP	30	48	Apr 2006	LIANG Chuntai+, SIG, DA,DE
^{106}Cd	Calculation	1.0+3	2.0+7	APE	Theo	Jour CNDP	30	52	Apr 2006	WANG Shunuan, SIG, DA, DA/DE
^{108}Cd	Calculation	1.0+3	2.0+7	APE	Theo	Jour CNDP	30	52	Apr 2006	WANG Shunuan, SIG, DA, DA/DE
^{110}Cd	Calculation	1.0+3	2.0+7	APE	Theo	Jour CNDP	30	52	Apr 2006	WANG Shunuan, SIG, DA, DA/DE
^{111}Cd	Calculation	1.0+3	2.0+7	APE	Theo	Jour CNDP	30	52	Apr 2006	WANG Shunuan, SIG, DA, DA/DE
^{112}Cd	Calculation	1.0+3	2.0+7	APE	Theo	Jour CNDP	30	52	Apr 2006	WANG Shunuan, SIG, DA, DA/DE
^{113}Cd	Calculation	1.0+3	2.0+7	APE	Theo	Jour CNDP	30	52	Apr 2006	WANG Shunuan, SIG, DA, DA/DE
^{114}Cd	Calculation	1.0+3	2.0+7	APE	Theo	Jour CNDP	30	52	Apr 2006	WANG Shunuan, SIG, DA, DA/DE
^{116}Cd	Calculation	1.0+3	2.0+7	APE	Theo	Jour CNDP	30	52	Apr 2006	WANG Shunuan, SIG, DA, DA/DE
^{nat}Cd	Calculation	1.0+3	2.0+7	APE	Theo	Jour CNDP	30	52	Apr 2006	WANG Shunuan, SIG, DA, DA/DE
^{137}Cs	Evaluation			APE	Eval	Jour CNDP	30	16	Apr 2006	WANG Baosong+ , Decay Data, HL
^{233}U	Evaluation	1.0–5	2.0+7	APE	Eval	Jour CNDP	30	58	Apr 2006	YU Baosheng +, SIG, DA, DE